Doctoral theses at NTNU, 2021:8

Christian Øyn Naversen

Modelling Approaches for Hydro-Dominated System Balancing

Doctoral thesis

NTNU
Norwegian University of Science and Technology
Thesis for the Degree of
Philosophiae Doctor
Faculty of Information Technology and Electrical Engineering
Department of Electric Power Engineering

NTNU
Norwegian University of
Science and Technology

Christian Øyn Naversen

Modelling Approaches for Hydro-Dominated System Balancing

Thesis for the Degree of Philosophiae Doctor

Trondheim, April 2021

Norwegian University of Science and Technology
Faculty of Information Technology and Electrical Engineering
Department of Electric Power Engineering

NTNU

Norwegian University of
Science and Technology

NTNU
Norwegian University of Science and Technology

Thesis for the Degree of Philosophiae Doctor

Faculty of Information Technology and Electrical Engineering
Department of Electric Power Engineering

ISBN 978-82-471-9645-8 (printed ver.)
ISBN 978-82-471-9760-8 (electronic ver.)
ISSN 1503-8181 (printed ver.)
ISSN 2703-8084 (online ver.)

Doctoral theses at NTNU, 2021:8

Printed by NTNU Grafisk senter

Preface

The presented research was carried out at the Department of Electric Power Engineering at the Norwegian University of Science and Technology (NTNU) and started in December 2017. My main supervisor has been Associate Professor Hossein Farahamnd from NTNU, and Dr Arild Helseth from SINTEF Energy Research has been by co-supervisor.

The work was done as part of the project "Pricing Balancing Services in the Future Nordic Power Market" by SINTEF Energy Research. The project was financed by the Norwegian Research Council as a Knowledge-building Project for Industry with several project partners from the Norwegian hydropower industry as well as the Norwegian and Swedish transmission system operators.

Acknowledgements

Someone once told me that writing a PhD is one long ego trip. I found it to be more like an emotional roller coaster, a time when feeling invincible and completely useless was never far apart. I'm not sure if my ego came out on top in the end, but it has certainly been three interesting years!

Though I can say that this work truly feels like my own, I could never have completed any of it alone. My team of supervisors, Hossein and Arild, have always pointed me in the right direction and encouraged me to find my own way. Thank you both for the interest and dedication you have shown throughout my time as a PhD. I would also like to thank Professor Masood Parvania and Dr Bosong Li at the University of Utah for great discussions and collaboration on the topic of continuous-time optimization. All of the great work my courageous master student Mari Lund Øvstebø did during the final year of her MSc is also much appreciated.

To all my colleagues and good friends at the institute, thank you for always making the office a fun place to be, even in times of work-related stress and frustration. My fellow PhD students in the EMESP group deserve a special thanks, especially the corner-office crew (in order of appearance): Kasper Emil Thorvaldsen, Sigurd Bjarghov, Linn Emelie Schäffer, Dimitri Pinel, and Emil Dimanchev[1]. I would also like to give a shoutout to Martin Hjelmeland, my original office roommate, for showing me the ropes when I first started. In addition, my other colleagues at SINTEF Energy Research have been cheering me on from the start, and I feel very fortunate to have a fun and challenging job to look forward to.

My friends and family have helped in their own way, mostly by making me forget about work for a blessed while. Lazy Sunday dinners at my parents' house, tossing rocks and chopping wood at our family cabin, and hiking in the mountains with Gutta På Tur™ have been crucial for recharging my proverbial batteries.

Then there is Antonia, the woman crazy enough to move all the way to cold and dark Norway and start a new life with me. While learning a new language and adapting to a new culture, she has let me complain about reviewers, writing papers, and many other silly things. You are the bravest person I know, thank you for believing in me and us.

[1] There was also a brief guest appearance by Uğur Halden in our office, so you end up here in a footnote!

Summary

The generation mix in many power systems across the world is rapidly shifting towards higher degrees of variable renewable power generation. Maintaining the continuous power balance of the system under higher levels of uncertainty and variability requires better planning and use of the available flexible resources. Norwegian hydropower is one such flexible resource, and the ongoing construction of substantial transmission capacity to neighboring areas with high penetration of wind and solar generation can enable the use of the hydropower as a balancing resource for the North European region. Understanding the interaction between hydropower, thermal generation, and variable renewable power sources under conditions of uncertainty is paramount in order to effectively and securely plan the operation of the system.

The work conducted in this thesis has investigated the modeling of the short-term production and reserve scheduling of systems with considerable amounts of hydropower. A fundamental approach to modeling the different power imbalances that create the need for reserve capacity and subsequent balancing energy has been adopted in all of the models. Representing large-scale cascaded hydropower in the models has been essential and has motivated the development and adaptation of several different optimization methodologies. The work has been disseminated in four scientific papers, three published and one submitted for review at the time of writing, which constitute the backbone of the thesis. The thesis includes a thorough discussion and literature review on the core topics considered in those papers. A summary of the different models created and the main results of the work performed during this PhD is provided below:

- Two-stage models based on stochastic, robust, and hybrid uncertainty formulations were developed to investigate the impact of reserved capacity on hydropower plants being activated due to forecast errors in the net-load. The hybrid stochastic-robust model was found to be a good compromise between cost optimality and protection from extreme events. The distribution of reserves among the different hydropower plants is noticeably different in a deterministic model that does not consider the delivery of balancing energy, which impacts the cost of balancing the system. This effect is due to the strong temporal and topological coupling between hydropower plants created by the cascaded hydropower topology.
- A hydrothermal model formulation using the continuous-time optimization framework was developed, where several modifications to the previously published continuous-time unit commitment problem were made to accommodate the inclusion of hydropower. The structural imbalances created by the discrete spot market clearing are not present in the continuous-time formulation since the power balance is kept at all times. The continuous-time

model can potentially be used to estimate the cost of removing structural imbalances when compared to a standard discrete-time model. The possibility of adding continuous ramping constraints for thermal units shows how Norwegian hydropower can be used to alleviate ramping scarcity in neighboring areas.

- Combining stochastic optimization and the continuous-time formulation creates a model that can capture imbalances created by both the market structure and forecast errors. The results from a stylized case study of Northern Europe with uncertain offshore wind power show that Norwegian hydropower is a principal provider of reserve capacity and balancing energy in the system. The cost increase compared to an analogous discrete-time model is roughly 0.4% of the total daily expected system cost, which stems from balancing sub-hourly wind and load variations and employing more accurate thermal ramping constraints and startup/shutdown procedures.

In addition to the research published in the papers, the thesis includes Appendix C, which is a valuable resource for anyone interested in understanding and implementing the continuous-time formulation. The material in the appendix is based on the published literature on the topic and personal experience, and was written because no other comprehensive introduction to continuous-time unit commitment exists at the time of writing.

Contents

1 Introduction

1.1 System and Market Description

In December 2019, the European Commission presented their plan for a European Green Deal intending to make the European Union (EU) climate-neutral by 2050 [1]. As an important milestone for this long-term goal, the Commission later proposed to increase the 2030 emission reduction target from 40% to 55% compared to the emission levels of 1990. The objective of the first European Climate Law is to turn the proposals in the European Green Deal into binding legislation and policy change [2]. This is ongoing work at the time of writing, and the proposal is scheduled to be revised in June 2021. Large and fundamental changes to many parts of society are required to reach the emission goals for 2030 and 2050. One of the most important sectors to decarbonize in the transition to a zero-emission society is the energy sector, which is responsible for 75% of greenhouse gas emissions in the EU [3]. Renewable energy production plays a major role in the sector, with existing binding targets of 20% and 32% renewable energy consumption in the EU by 2020 and 2030, respectively [4].

The green shift is introducing deep penetration of renewable electricity production into the European power system. This is also the case for the Nordic synchronous area, which includes the power systems of Norway, Sweden, Finland and Eastern Denmark. In addition to the wind power production within the synchronous area, the growing amount of high-voltage direct current (HVDC) transmission capacity to neighboring power systems will increase the penetration of variable renewable power production into the Nordic system. Figure 1.1 shows a map of current HVDC lines connecting the Nordic synchronous area to adjacent power systems, where several of the connected countries also border the North Sea. This is one of the most attractive areas for offshore wind development in Europe due to its shallow waters and excellent wind conditions. In particular, Germany, the Netherlands, the United Kingdom, and Western Denmark have high offshore wind power potential [5].

Efficient use of flexible resources is needed in order to cope with the fluctuations introduced by high shares of variable renewable electricity production. Utilizing the existing flexibility in the power system is especially important in the transition phase from a conventional to a fully renewable power system since new energy storage technologies such as batteries and hydrogen production are still in the early phases of system scale integration. There are already substantial flexible power sources in the Nordic power system in the form of hydropower production

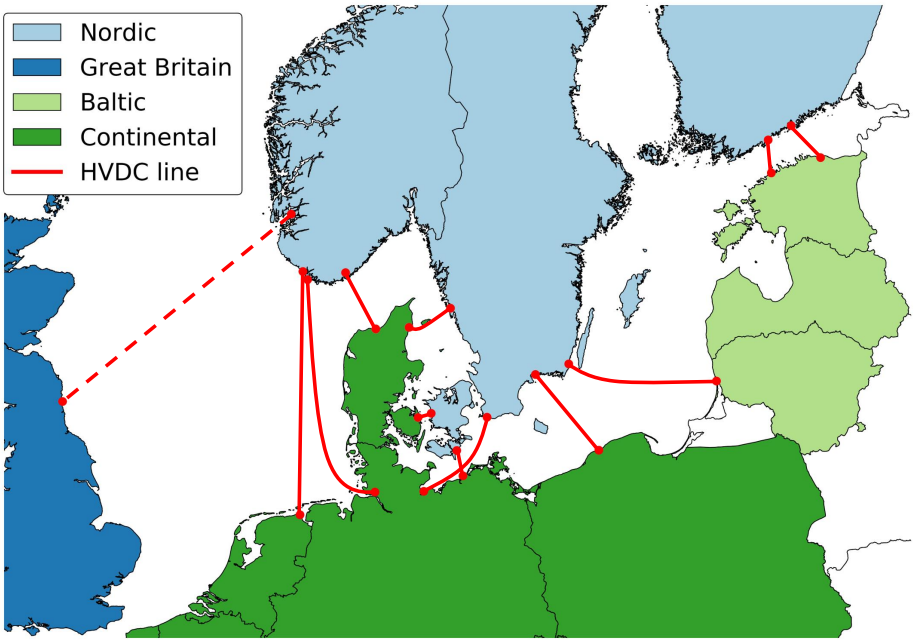

Figure 1.1: The current HVDC cables that create the interface between the Nordic synchronous area and the adjacent synchronous power systems. The cable between Norway and Great Britain is under construction at the time of writing, and is thus shown as a dashed line. The parallel lines between Norway and Denmark and Sweden and Denmark are represented as single lines. Based on the ENTSO-E grid map (`https://www.entsoe.eu/data/map/`) and the geographical shape file of Europe from [6].

in Norway, Sweden, and Finland. The Norwegian generation mix is particularly dominated by hydropower, with around 90% of the installed capacity and 91.5% of the average yearly production [7]. The Norwegian hydropower reservoir capacity of roughly 87 TWh [8] represents a significant potential for long-term energy storage of energy over the seasons. As hydropower turbines are fast-ramping and easily controllable, they can also provide short-term flexibility to balance sudden net-load variations. The flexible qualities of Norwegian hydropower are therefore of great interest to the larger North European power system interconnected with HVDC cables. The ongoing harmonization effort of electricity markets for balancing energy and capacity in the EU is therefore an essential enabler of efficient cooperation and coordination of flexible resources across country borders.

It is crucial to develop model tools that can aid decision-makers facing the future challenges of the interconnected North European power system. More uncertainty and variability in the power system must be addressed by improved cooperation

between countries and efficient coordination of the existing resources in the generation mix. Optimization models that can find the best way of operating the system as a whole serve as important benchmarks for analyzing the real world. An example of valuable knowledge that can be obtained from such models is how different generation technologies interact and complement each other. Finding ways of incorporating uncertainty and the fundamental causes for system imbalances into the models will be necessary in order to provide a better understanding of the complex issue of power system operation and planning in the future.

1.2 Power System Imbalances

As the power systems around the world undergo the transition from systems with conventional generation to hybrid, and finally fully renewable, power systems, several challenges arise for both the system operators and power producers. Increased variability from wind and solar power generation is one of the main challenges that must be tackled, as it potentially threatens system stability. In the Nordic power system and many other European countries, several successive electricity markets are used to plan the safe operation of the power system while ensuring competition between participants. The day-ahead energy market, also called the spot market, facilitates the matching of the planned energy production and consumption in each time interval (hourly in the Nordic system) of the following day. The intraday market allows for adjustments of commitments in the spot market closer to real-time. Both of these markets trade energy over a specified time interval, and are therefore unable to ensure a continuous matching of the injected and absorbed *power* in the system. Deviations between produced and consumed power must therefore be compensated in a different way in order to avoid large frequency deviations.

In order to maintain a continuous power balance, the responsible transmission system operators (TSOs) procure several different reserve capacity products from balancing service providers (BSPs) in advance of real-time energy delivery. The BSPs are subsequently called upon to increase or decrease their power production/consumption. The names and specifications of the different reserve capacity products have historically varied from country to country. To facilitate cooperation across countries, ENTSO-E has defined a set of common standards and basic requirements for reserve capacity products that are used in Europe [9]. Frequency containment reserves (FCR), automatic and manual frequency restoration reserves (aFRR, mFRR), and replacement reserves (RR) are the most common types of reserve capacity procured by European TSOs. FCR is the first line of defence against frequency disturbances as it is automatically activated and directly governed by the frequency signal. aFRR and mFRR are activated to alleviate the FCR response and restore the frequency to its nominal value before RR is potentially called upon for long-lasting disturbances. It is crucial for the TSO

to procure sufficient reserve capacity to respond to deviations in the power balance of the system, and the presence of flexible units with fast response time is therefore essential.

There are several reasons why power imbalances may occur. It is useful to categorize the imbalance types based on the fundamental phenomena that create them when looking at the problem from a modeling perspective. There are three primary sources of imbalances in power systems: contingency events, forecast errors, and the discrete nature of current electricity markets. In addition to handling the listed imbalance types, TSOs call upon the reserved production capacity to balance internal network congestion that is not considered in the market clearing.

Bottlenecks exist in every power grid, and the electricity markets in Europe do not consider grid constraints within the defined bidding zones. Situations where TSOs must use reserves to relieve internal congestion will therefore occur. The cost of this type of "special regulation" for the Norwegian TSO Statnett has been considerable in recent years, comparable to the cost of procuring FCR [10]. A detailed grid description with power flow constraints is the only way of accurately modeling the effects of grid bottlenecks on the reserve procurement process.

Contingency events encompass rare but very impactful incidents where major system components unexpectedly malfunction. A large power imbalance will occur if a large generator or transmission line suddenly fails, and reserve capacity on the remaining units in the system will need to be activated in response. Contingency event considerations are often the basis for determining the amount of reserves needed in a system [11]. These types of imbalances have been modeled in contingency-constrained unit commitment models such as [12], where the goal of the model is to ensure that the system balance can be kept after a contingency event occurs.

Forecasting the electricity demand and variable renewable power generation in the near future will never be completely accurate, but it is necessary for planning the operation of the system through the day-ahead electricity market. The forecast errors will cause imbalances between the scheduled production and consumption that have been cleared in the market based on the forecasted values. Figure 1.2 shows an example of the discrepancy between realized and forecasted wind power, which can be significant. Imbalances caused by forecast errors are stochastic in nature, as are the contingency imbalances described earlier. The major differences between these two types of stochastic imbalances are their probability of occurring and severity. Forecast errors are inevitable and will occur every single day to some extent, whereas contingency events rarely happen. Stochastic optimization techniques are often used to incorporate forecast errors into system planning models [13].

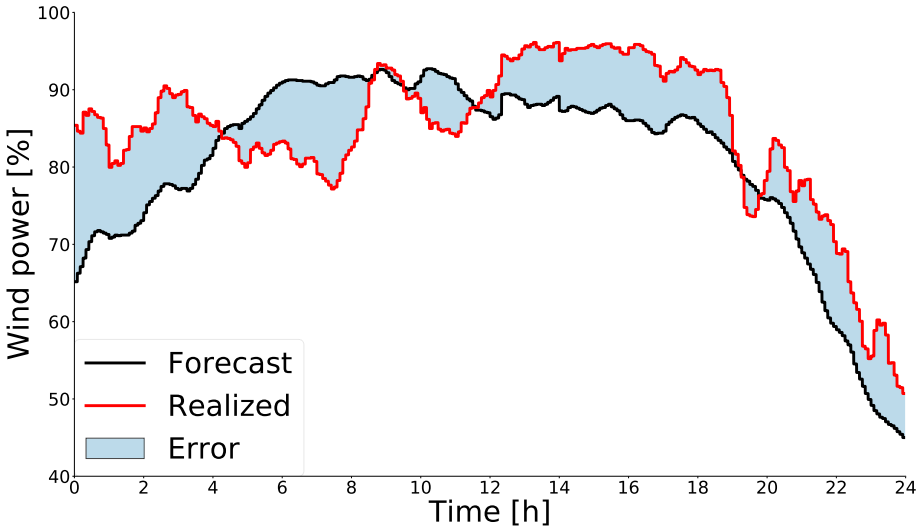

Figure 1.2: Forecasted and realized aggregated offshore wind power in Western Denmark on 12/10-2019, data with 5-minute resolution gathered from [14].

Imbalances caused by the market structure are referred to by different names, such as deterministic imbalances [15], structural imbalances [16], and schedule leaps [17]. They will be referred to as structural imbalances in this thesis as it is the most general term. The discrete structure of the electricity markets, which typically has a granularity of 15, 30, or 60 minutes in Europe, is the source of the structural imbalances. The day-ahead electricity market assumes a constant schedule through the bidding interval, but this is impossible to achieve in practice for both the consumer and producer side of the market. The deviations from the scheduled market-clearing manifest as imbalances, causing noticeable frequency deviations around the market's bidding interval shifts, as shown in Figure 1.3. The structural imbalances are predictable to a much larger extent than the imbalances caused by forecast errors and contingency events and are therefore sometimes referred to as deterministic imbalances. The net-load is typically decreasing during the night hours, which is shown in Figure 1.3 as under-frequency at the start, and over-frequency at the end, of the hour. When the net-load increases during the morning and evening peaks, the opposite phenomenon occurs. However, the exact size of the structural imbalances is not deterministic. Larger amounts of renewable power production can also worsen structural imbalances by increasing the net-load ramping. An example of this is the famous "duck curve" in California [18]. Even if a renewable power generator produces the forecasted amount of energy over a time interval, the sub-hourly power deviations around the average value will cause a type of stochastic structural imbalance. The ability to capture changes in power production and consumption within the market intervals is necessary to model structural imbalances.

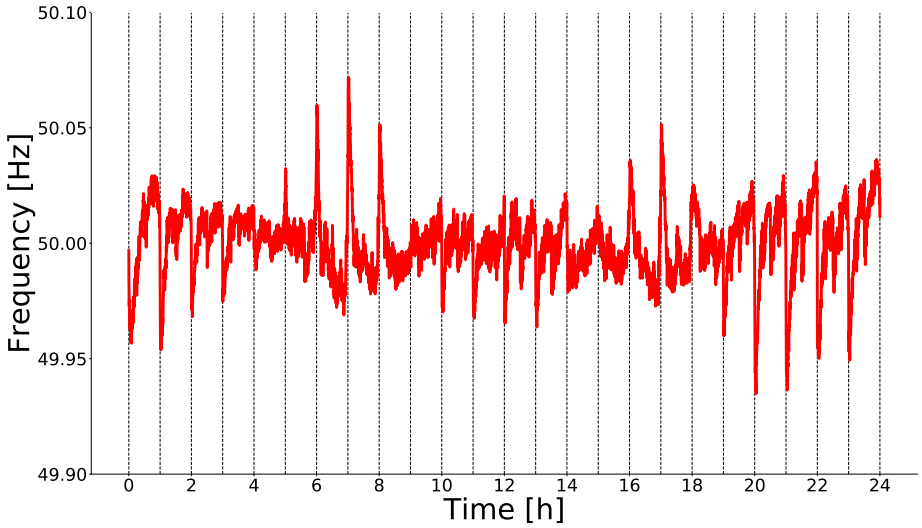

Figure 1.3: Median frequency in the Continental European power system in January 2019, data gathered from [19]. Clear frequency deviations around the hour shifts can be seen.

1.3 The PRIBAS Project

This PhD work is part of, and funded by, the research project "Pricing Balancing Services in the Future Nordic Power Market" (PRIBAS). In turn, the PRIBAS project is principally funded by the Research Council of Norway as a Knowledge-building Project for Industry (KPN) and led and organized by SINTEF Energy Research in Trondheim, Norway. Part of the funding is also provided by the industrial project partners, consisting of the Norwegian hydropower producers Statkraft, Hafslund E-CO, Lyse Produksjon, Agder Energi, and Hydro Energi, as well as the Norwegian and Swedish TSOs Statnett and Svenska Kraftnät. Industrial participation is a requirement for receiving financial backing from the Research Council of Norway in KPN projects, as it shows that the research topic is highly relevant and interesting for the industry.

The overall goal of the PRIBAS project is to develop model concepts to compute marginal prices for all physical electricity products in the Nordic power market. This includes day-ahead electricity prices as well as prices for balancing capacity and energy. The project's initial work focused on calculating prices for energy and reserve capacity in the Nordic power system [20], and the significance of using more detailed modeling of thermal units for the price signals [21]. A comprehensive list of the published work associated with the project is available online, see [22].

1.4 A Brief Overview of Hydro-Dominated System Scheduling

Optimal use of the water for electricity production in a cascaded hydropower system is a complicated problem with a long history. This section is written to help situate the work performed during the PhD and is not meant to provide a complete survey of the formulations and coupling techniques used in hydropower scheduling models. The changes and uncertainty in hydrology, weather, CO_2 prices, fuel costs, and net-load over the seasons are the major drivers that determine the optimal long-term strategy for operating the system. An accurate physical description and handling of operational constraints becomes more important from a short-term perspective. Solving a stochastic optimization problem with high physical detail and a long time horizon quickly becomes intractable. Therefore, the hydropower planning problem is usually split into a hierarchy of linked long-term, medium-term, and short-term problems [23]. Information about the uncertain future is condensed and passed on as input to the next model in the toolchain, which refines the result over a shorter time horizon but with more physical detail.

Long-term models take a fundamental approach to system planning, assuming that a system operator with perfect knowledge of the technical state of the system and topology performs a central dispatch to minimize the total system cost. The central dispatch point of view is equivalent to assuming a market setting where all participants behave as price takers under perfect competition. The fundamental approach means that long-term price forecasts can be generated from the long-term models, which can be used as input to the medium-term models in a liberalized market setting such as in the Nordic countries [24]. The long-term models handle the operation of the system over many seasons with a coarse time resolution and sometimes aggregated hydropower topology. The simplifications of the physical and temporal model aspects are made to preserve the complexity of the multi-stage uncertainty modeling. Solution strategies based on stochastic dynamic programming (SDP) and stochastic dual dynamic programming (SDDP) are often used in long-term models, see for instance [25] and [26]. Water values that describe the opportunity cost of using water now versus saving it for the future can be calculated by the long-term models as a result of the solution algorithm. SDP models usually aggregate the hydropower system into a single-reservoir system capable of coping with the exponential increase in complexity each state variable introduces. The resulting water values are therefore also aggregated. The SDDP formulation is better suited for including the hydropower topology, and the linear hyperplanes, often referred to as cuts, generated during the nested Benders decomposition scheme used to solve the SDDP problem, create a detailed water value description that couples all connected reservoirs. Water values provide an end valuation method for the reservoir contents in the

near future and propagate the long-term strategy to the lower levels of the model hierarchy. A water value description is not the only way to couple the models in time, but it is extensively used in the industry and considered as a flexible method for describing the long-term operational strategy.

The length of the planning horizon is not necessarily the best way to distinguish long-term from medium-term models, as it is heavily dependent on the size of the reservoirs in the system and their expected yearly inflow. A better distinction is the existence of an end valuation of the water in medium-term models, passed down from a long-term model. In a central dispatch system such as Brazil, the medium-term model has the same geographical scope and system cost minimization perspective as the long-term model [27]. Medium-term models in liberalized markets usually focus on a smaller geographical region and take into account the uncertainty in the spot price [28]. The fundamental medium-term models can calculate prices, while this is no longer the aim of the producer-focused medium-term models that use exogenous prices as input. A further refinement of the water values based on more details in the system description and a finer time resolution is the common factor between the two different perspectives. The medium-term models are primarily used as a linking tool between the long-term and short-term problems, and the refined water values are once again used as the coupling mechanism.

Due to tractability issues, the long-term and medium-term models are mostly linear programs. However, the hydropower scheduling problem is riddled with non-linear relationships that should be taken into account in the daily operations of a hydropower system. The short-term hydropower scheduling models therefore aim to include binary unit commitment constraints to model forbidden production zones, head loss due to friction, separate turbine and generator efficiency curves, and many other complicating constraints [29]. Short-term models such as [30] take on the perspective of a profit-maximizing producer in liberalized markets, where both the price and water value description are inputs to the model. The producer-centric short-term models only include the reservoirs and plants of a single producer, which significantly reduces the system size and makes it possible to incorporate many of the non-linear elements mentioned earlier. Fundamental short-term models that aim to minimize the total system cost and calculate the price, such as [31] and the models referred to in Section 1.3, still have to model the system as a whole. The large system boundary limits the number of physical complexities that can be added to the problem without rendering the model intractable.

1.5 Scope and Assumptions

How should the Nordic hydropower resources be used optimally in a future with a high penetration of variable renewable energy sources and tighter interconnection to the rest of Northern Europe? This broad question can certainly be explored in many different directions. The work conducted in this thesis has focused on developing new methodologies and formulations for the short-term scheduling and balancing problem for hydropower-dominated systems. The perspective taken in all of the presented models is that of a central system operator aiming to minimize the total system cost.

The choice of focusing more on the short-term variations and uncertainty in the power system means that no long-term effects are directly considered in any of the research presented. The long-term strategy of operating a cascaded hydropower system is primarily determined by uncertainty in inflow and net-load over several seasons, depending on the size of the reservoirs in the system. The water value description used as input to the models was calculated by the long-term hydropower model in [32] and is assumed to describe the long-term strategy in the short-term problem adequately.

The hydropower topology description used in the developed short-term models is shown in Appendix A. Reservoirs and power plants connected by the main tunnels, bypass gates, and spillage gates are modeled in the cascaded arrangement. Each hydropower plant in the system has been treated as a single production unit, ignoring the internal structure of the power plant. Therefore, the characteristics of the individual turbines and generators, possibly connected to different penstocks inside the power plant, are disregarded. An aggregated hydropower production function for the whole plant is used instead. Energy loss due to friction in the tunnels and head dependencies in the turbine efficiency curves have also not been considered.

Finding a unified way to model all the primary causes for power system imbalances described in Section 1.2 requires the combination of several modeling techniques and detailed system topology information. The imbalances from forecast errors and structural imbalances have been considered in the work of this thesis, and including contingency events in the models has been left for future work. Since special reserve regulation due to internal transmission constraints has not been considered, the AC transmission grid and power flow constraints have been omitted from the models. An aggregated zonal representation of the power system with HVDC interconnectors has been used instead, which still captures the interaction between zones dominated by different generation technologies such as hydropower, wind power, and thermal power.

Since the emphasis of the work has been the modeling techniques, large-scale and

realistic case studies for the Nordic power system and Northern Europe have not been conducted.

1.6 List of Publications

The papers listed below constitute the backbone of this PhD thesis and are reprinted in full in the "Publications" part of this document. In the remainder of the thesis, these papers will be referred to as Paper I, II, III, and IV. Paper III was first-authored by Mari Lund Øvstebø as part of her MSc thesis, where the candidate was her co-supervisor. Paper IV is currently in the first round of review, and modifications to the current manuscript should be anticipated in the final version.

I. C. Ø. Naversen, H. Farahmand, and A. Helseth, "Accounting for reserve capacity activation when scheduling a hydropower dominated system", in *Int. J. Electr. Power Energy Syst.*, vol. 119, p. 105864, Jul 2020. DOI: 10.1016/j.ijepes.2020.105864

II. C. Ø. Naversen, A. Helseth, B. Li, M. Parvania, H. Farahmand, and J. P. S. Catalão, "Hydrothermal scheduling in the continuous-time framework", in *Electr. Power Syst. Res.*, vol. 189, p. 106787, Dec 2020. DOI: 10.1016/j.epsr.2020.106787

III. M. L. Øvstebø, C. Ø. Naversen, A. Helseth, and H. Farahmand, "Continuous-time scheduling of a hydrothermal system with integration of offshore wind power", in *17th Int. Conf. Eur. Energy Mark. (EEM)*, Oct 2020. DOI: 10.1109/EEM49802.2020.9221980

IV. C. Ø. Naversen, B. Li, M. Parvania, A. Helseth, and H. Farahmand, "Stochastic Flexibility Coordination in Hybrid Hydro-Thermal-Wind Power Systems", under review in *IEEE Trans. Power Syst.*, submitted Sep 2020.

Several other publications that are either outside the scope of the thesis or only contain a minor contribution from the candidate have been published during the course of the PhD work:

- A. Helseth, M. Haugen, S. Jaehnert, B. Mo, H. Farahmand, and C. Ø. Naversen, "Multi-Market Price Forecasting in Hydro-Thermal Power Systems", in *15th Int. Conf. Eur. Energy Mark. (EEM)*, Jun 2018.
  DOI: 10.1109/EEM.2018.8469932

- C. Ø. Naversen, S. Bjarghov, and A. Helseth, "Operating a Battery in a Hydropower-Dominated System to Balance Net Load Deviations", in *16th Int. Conf. Eur. Energy Mark. (EEM)*, Sep 2019.
  DOI: 10.1109/EEM.2019.8916534

- H. O. Riddervold, E. K. Aasgard, H. I. Skjelbred, C. Ø. Naversen, and M. Korpås, "Rolling Horizon Simulator for Evaluation of Bidding Strategies for Reservoir Hydro", in *16th Int. Conf. Eur. Energy Mark. (EEM)*, Sep 2019.
  DOI: 10.1109/EEM.2019.8916227

- M. Haugen, A. Helseth, S. Jaehnert, B. Mo, H. Farahmand, and C. Ø. Naversen, "On the importance of detailed thermal modeling for price forecasting in hydro-thermal power systems", in *IEEE Electr. Power Energy Conf. (EPEC)*, Oct 2019.
  DOI: 10.1109/EPEC47565.2019.9074832

1.7 Thesis Structure

This thesis is split into three main parts. The first part includes Chapters 2 and 3, and contains an account of the methodologies and contributions of the thesis in addition to a discussion of future work and concluding remarks.

The second part of the thesis reprints the four papers listed in Section 1.6 in full. Each paper is marked in the thumb index of the printed version of the thesis.

Three appendices are included in the last part of the thesis as supplementary material to help the reader to understand the discussion in Chapters 2 and 3 and the papers themselves. Appendix A provides a brief description of the hydropower system that has been used in the research, while Appendix B goes through the necessary steps of reformulating and solving a two-stage robust optimization model. Appendix C gives detailed derivations and explanations of all fundamental properties of a continuous-time unit-commitment model.

2 Methodologies and Contributions

This chapter discusses the methodologies and contributions of the work performed during this PhD, based on the four papers listed in Section 1.6. Section 2.1 gives an overview of the research questions addressed in the thesis through the published papers. Sections 2.2 to 2.4 discuss the contributions and central modeling topics of each paper with accompanying surveys of the relevant scientific literature.

2.1 Research Questions and Paper Overview

Formulating new optimization model concepts to investigate how the flexibility of hydropower can be used in system balancing is the overarching objective of the work conducted in this thesis. To narrow the research focus, four more specific research questions have been examined within the scope of the work defined in Section 1.5:

RQ 1. How important is it to consider uncertainty of activation when procuring reserve capacity on cascaded hydropower units?

RQ 2. How can sub-hourly deviations be modeled to avoid structural imbalances?

RQ 3. To what extent can Norwegian hydropower be used for balancing of the North European interconnected system?

RQ 4. Is there a unified way of modeling both stochastic and structural imbalances?

The first question is central to the topic of efficiently balancing stochastic deviations caused by forecast errors with hydropower. There are several effects specific to energy storage units in general, and cascaded hydropower specifically, that indicate that considering the possibility of reserve activation could be important in the reserve procurement phase. This is investigated in Paper I and further discussed in Section 2.2. As implied in RQ 2, looking into structural imbalances requires a different approach than forecast imbalances. Paper II deals with this topic by formulating the standard hydrothermal unit commitment problem in a fundamentally different way by expressing it as a continuous-time problem. This is further expanded upon in Paper III, which also looks into RQ 3 by solving the model for a stylized North European system, see Section 2.3. The final research

question is tackled in Paper IV, described in Section 2.4, by combining the methods of the other papers. The paper also contributes to RQ 3 by also looking at a North European test system. Thus, the four papers presented in this thesis make a combined modeling effort towards a holistic approach for using hydropower to balance stochastic forecast errors and structural imbalances. Figure 2.1 shows a simple schematic of the connections between the papers.

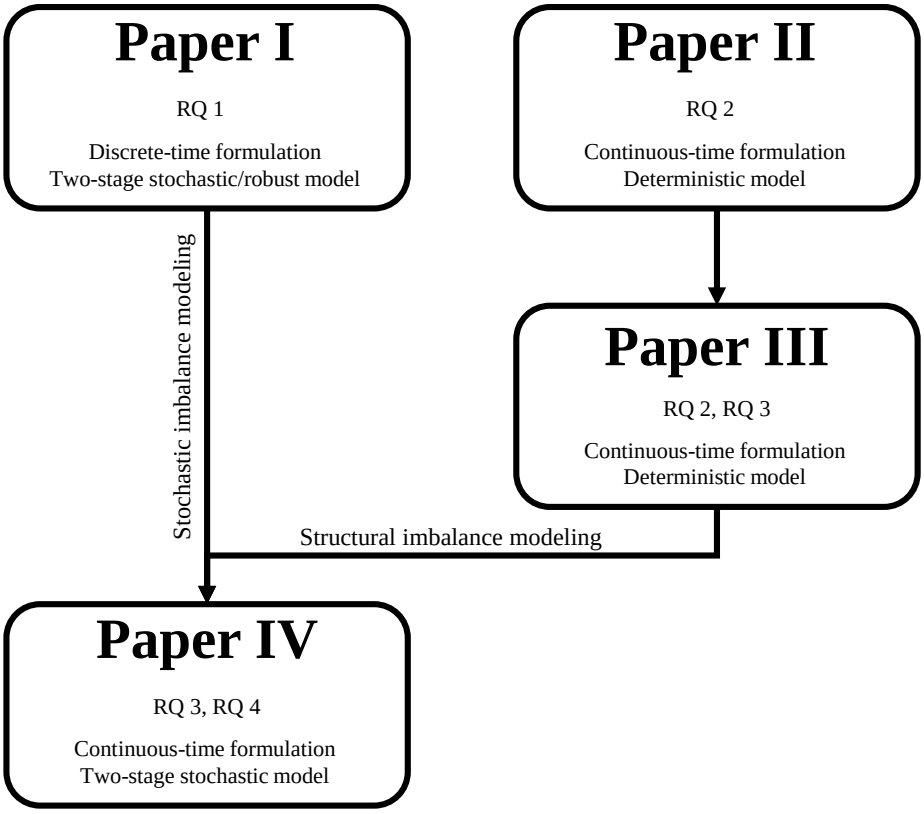

Figure 2.1: A sketch of the connection between the four papers included in the thesis. The boxes show which research questions each paper explores in addition to the methodologies used for describing time-dependent decisions and uncertainty.

The optimization problems described in all four papers are viewed from a central system operator's perspective who attempts to find the optimal schedule for dispatching the available power generation resources in terms of the system cost. The different approaches to this problem were formulated as linear programs (LPs) or mixed-integer linear programs (MILPs) that can be solved with standard optimization solvers. The commercial CPLEX solver [33] has been used in the solution procedure for all of the models described in the four papers, al-

though there are many alternative solvers that can solve such programs. The formulation of the optimization programs was performed in the open-source Pyomo framework [34, 35] for the Python programming language, which is flexible and can interface with most optimization solvers.

2.2 Contributions of Paper I

As mentioned in the previous section, Paper I studies the effect of considering uncertainty in the activation of reserved capacity when the day-ahead production and reserve schedules are optimized. There are two main aspects of uncertain reserve capacity activation that are explored in Paper I:

1. Considering the feasibility and economics of delivering the balancing energy that is expected to be available based on the reserved capacity.
2. Striking a balance between conservativeness and cost optimality when modeling the uncertain deviations in the net-load leading to reserve activation.

Both of these topics influence the production and reserve capacity decisions for a cascaded hydropower system in different ways. The first point addresses the question of having sufficient water stored in the reservoirs to meet real-time energy delivery corresponding to the reserved capacity, and is a deceptively subtle topic. The second point concerns the representation of uncertainty in the model, and resulted in the creation of a new hybrid uncertainty model based on both stochastic and robust optimization. The following subsections discuss the two questions in detail.

2.2.1 Feasibility of reserve capacity activation

The amount of scheduled power production (p_t) and spinning reserved capacity ($r_t^{\uparrow/\downarrow}$) for a running unit at time t is clearly constrained by the minimum and maximum production levels ($P^{min/max}$) of the unit:

$$p_t + r_t^{\uparrow} \leq P^{max} \tag{2.1}$$

$$p_t - r_t^{\downarrow} \geq P^{min}. \tag{2.2}$$

This is a *capacity* constraint that ensures that it is possible to fully activate the reserved capacity without violating the most fundamental operational limits of

the unit. However, the constraints do not take into account any *energy*-related concerns for activating the reserved capacity. Conventional thermal generators, such as gas-fired power plants, are usually assumed to have an infinite supply of fuel available, but this is not true for energy storage units. Let the scheduled energy content at the beginning of time interval t be denoted e_t, which is based on the production and consumption schedule for the energy storage device. Reserve capacity activated in time interval t must obey the energy constraints:

$$e_{t+1} + \eta^{\downarrow} r_t^{\downarrow} \Delta \leq E^{max} \tag{2.3}$$

$$e_{t+1} - \eta^{\uparrow} r_t^{\uparrow} \Delta \geq E^{min}. \tag{2.4}$$

In the constraints above, the reserves are assumed to be fully activated for a period of length Δ with constant efficiency $\eta^{\uparrow/\downarrow}$. The size of the energy storage, represented with the upper and lower energy limits $E^{max/min}$, with respect to the installed production/consumption capacity of the energy storage device, is an important factor in determining whether the capacity or energy reserve constraints will be binding. If the time it takes to fill or empty the energy storage is on the scale of a few hours, the energy constraints will likely be significant. Batteries are usually in the category of being able to fill and empty their energy storage quickly. In hydropower systems, the size of the reservoirs can vary greatly. The hydropower topology used in all of the papers presented in this PhD, see Appendix A and Figure A.1, has both large and tiny reservoirs. Without considering any inflow, it takes almost 98 days to empty reservoir M6 with maximal discharge, while it only takes 21 minutes to empty M2. In such cases, both the capacity and energy constraints for reserve capacity can be important for different reservoir-plant pairs.

Note that eqs. (2.3) and (2.4) are simplified in several respects. For instance, the efficiency is not necessarily constant for the whole production/consumption range, and therefore depends on the total net production after activation. However, the most important simplification is the time decoupling. The scheduled energy content e_t is based on the integral of the scheduled power production/consumption over time, which means that activating reserves at time interval t can be within the bounds set by eqs. (2.1) to (2.4) but still make the energy schedule infeasible at a later point. This is illustrated in Figure 2.2, where it is shown that the activation of reserve capacity can cause problems several time periods after it occurs. Time-linking constraints such as the energy balance therefore affect the reserve capacity procurement. Ramping constraints on conventional generators are also time-linking and result in similar issues about the feasibility of reserve capacity activation.

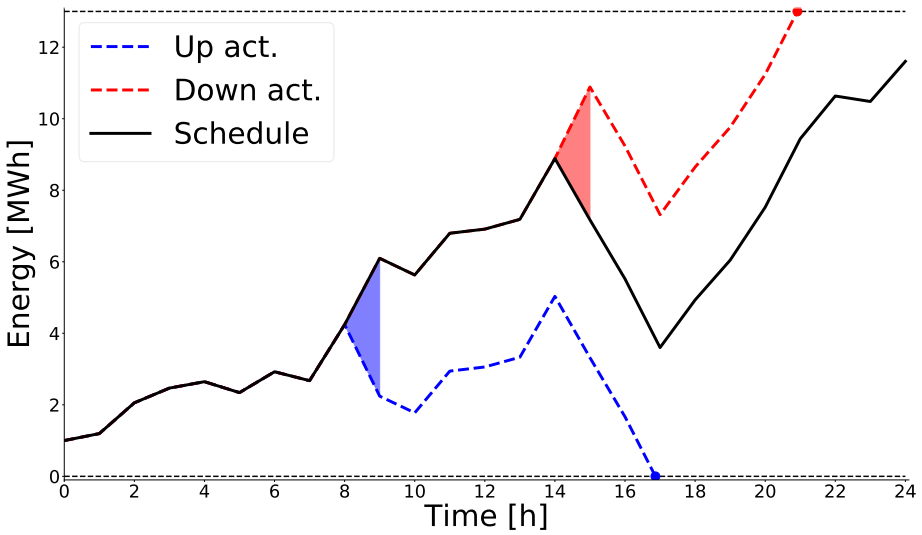

Figure 2.2: Shows the scheduled energy content of an energy storage device together with two possible trajectories after reserve capacity has been activated for a single hour. The activation does not cause immediate problems but makes the future production/consumption schedule infeasible as the energy content reaches either the upper or lower limit before the end of the horizon.

Although large-scale hydropower plants are less prone to reserve energy deployment scarcity than batteries, there are other challenges specific to cascaded hydropower systems. The cascaded topology that interconnects all hydropower plants in the system is one aspect that should be considered when reserve capacity is procured. When reserve capacity is activated, the amount of water discharged through the turbine of the hydropower plant must be increased or decreased to provide the reserve energy. This regulation will also affect the energy balance of the upstream and downstream reservoirs and could therefore cause problems of flooding or running dry. The tight coupling between different reservoirs drastically increases the complexity of the questions related to sufficient energy and storage capacity for balancing purposes. The future expected value of the stored water in the hydropower reservoirs significantly affects the optimal production decisions in short-term models. Due to the cascaded topology, this value depends on the end state of all reservoirs in the system. Reserving capacity on the wrong hydropower unit with respect to the water value could be costly if it leads to a poor system end state after activating the reserves.

The reasons discussed in this section show that considering the activation of reserved capacity in the scheduling and procurement phase of a hydropower model is important. The issues have been addressed in the literature to varying degrees. Table 2.1 lists 21 representative papers that have considered the topic

from different perspectives, and the papers have been selected to show the diversity in the modeling approaches. The taxonomy table labels the papers based on six different features deemed relevant. The first column separates the papers based on the energy technology modeled for reserve capacity provision, ranging from stand-alone batteries to large cascaded hydropower systems. As explained earlier in this section, the system dynamics can vary dramatically based on the energy storage technology. The model perspective, listed in the second column, distinguishes between models that aim to minimize the total system cost and models focused on individual producers maximizing their profit in the market(s). A characterization of the type of energy balance constraints for activated reserve capacity found in the model is listed in the third column. The uncertainty model type is shown in columns 4 and 5, and the end valuation for stored energy is included in the final column.

It is difficult to describe the modeling of reserve capacity activation and balancing energy constraints in only a few words, which is nonetheless attempted in column 3 of Table 2.1. Therefore, a more detailed description of this aspect is warranted. Papers [36–42] all consider batteries, or some similar form of general energy storage device, that deliver energy and reserve capacity. The models described in [36, 37] are strategic formulations allowing the battery to act as a price-maker, while the other listed papers on batteries assume perfect competition and aim at minimizing cost. The energy balance of the battery in [36] is only satisfied based on the expected reserve activation over all scenarios, while [37] adds single-period activation constraints similar to eqs. (2.3) and (2.4) based on a predefined duration of activation. Similar single-period activation constraints, in addition to an energy balance considering a predetermined fraction of activated reserves, are found in [39]. A more conservative approach is taken in [42], where extra energy balance constraints for maximal upward and downward activation are added to the problem formulation. The SDDP model in [38] explicitly considers reserve activation scenarios with a full energy balance for the balancing energy, although the energy limits of the battery are considered soft constraints. Both [40] and [41] are stochastic unit commitment models with complete energy balance constraints for all balancing scenarios. The same is true for the joint electricity and gas network model in [43] that considers a compressed air system with similar dynamics to a battery.

The papers in [44–47] consider pumped hydro (PH) plants that are not part of a larger cascaded hydropower system. Closed PH systems do not receive any natural inflow and are therefore modeled relatively similar to batteries, although some PH plants can discharge and pump simultaneously ("hydraulic short-circuit"). The energy balance of the PH storage is satisfied based on a predetermined probability of activation in [44], and the model in [45] also considers deterministic reserve activation. Several models are presented in [46], which include both single-period balancing energy constraints for extreme ramping scenarios and full energy balance for maximal activation in both the upward and downward direc-

tions. The work in [47] considers an open PH system with natural inflow into the reservoir. Activation of reserve capacity is not included directly into the deterministic optimization model, but the authors suggest reserving a portion of the reservoir content for balancing by tightening the upper and lower reservoir limits based on ex-post analysis of reservoir level deviations.

The remaining papers listed in the taxonomy table describe cascaded hydropower systems, except for [48, 49]. The model in [48] disregards the hydropower topology as it sequentially solves the scheduling and balancing problem of Northern Europe and only considers single-period energy constraints in the upward activation direction. A total energy limit for the seasonal reservoirs considering maximal upward regulation is considered in [49], although the energy balance constraints for these reservoirs are not considered. The physically detailed model in [50] distributes different reserve products between the generators in the system but does not consider any energy constraints related to the activation of the reserves. The medium-term model in [51] includes both energy and reserve capacity markets but also disregards reserve activation constraints. Multi-period energy constraints are added in [52] based on a fixed percentage of reserve activation, although a full reservoir energy balance for balancing energy is not kept. The upward reserve capacity sold in the market is constrained in each time interval by the amount of scheduled water available in [53], similar to eq. (2.4). The model in [54] accounts for maximal upward activation in the reservoir energy balance, while [55] and [56] employ single-period reservoir energy balances for balancing energy that accounts for the cascaded topology. A minimal reservoir content after balancing energy has been provided is also required in [55].

It is clear that reserve energy constraints are quite common to consider in models where batteries are used to provide reserve capacity. The models in [40, 41] fully model the reserve activation phase with energy balances for the batteries, which ensures deployment feasibility for the set of considered balancing scenarios. The robust model in [42] goes further by requiring feasibility for maximal activation in both directions. The listed hydropower models do not go as far in ensuring that the energy balance is preserved after activation. This gap in the literature was addressed in Paper I, listed at the bottom of Table 2.1, by incorporating full energy balances considering the cascaded topology for the activated reserve energy in all scenarios.

2.2.2 Reserve procurement and dealing with uncertainty modeling

The task of procuring reserves for system balancing should arguably be performed in a risk-averse way, as failing to balance the system is very costly. The TSOs in the Nordic countries procure a fixed amount of reserves in each category, and

Table 2.1: Taxonomy table for energy storage devices providing both energy and reserve capacity.

Ref	Storage type	Perspective	Balancing energy constraints added	Solution strategy	Uncertainty type	End valuation of stored energy
[36]	Battery	Producer	Energy balance in expectation	Bi-level stochastic	Net-load	None, fixed end level
[37]	Battery	Producer	Single-period activation per scenario	Bi-level stochastic	Load, wind, reserve requirement	None, minimum end level
[38]	Battery	Producer	Full energy balance	SDP/SDDP	PV and reserve activation	Cut description
[39]	Battery	System operator	Single-period activation	Multi-stage stochastic	Wind	None
[40]	Battery	System operator	Full energy balance per scenario	Two-stage stochastic	Load and wind	Constant value per MWh
[41]	Battery	System operator	Full energy balance per scenario	Two-stage stochastic	Load and wind	None
[42]	Battery	System operator	Full energy balance for worst-case activation	Two-stage robust	Wind	None
[43]	Compressed air	System operator	Full energy balance per scenario	Two-stage stochastic	Load and wind	None
[44]	Closed PH	Producer	Full energy balance for deterministic activation	Point estimate method	Wind, EV availability, prices, reserve activation	None
[45]	Closed PH	Producer	Full energy balance for deterministic activation	Single-stage stochastic	Prices	None, fixed end level
[46]	Closed PH	System operator	Single-period activation and worst-case activation	Two-stage stochastic	Wind	None
[47]	Open PH	Producer	Reservoir content reserved for balancing energy	Deterministic	None	None, fixed end level
[48]	Decoupled hydro	System operator	Single-period upward activation	Deterministic	None	Constant value per MWh
[49]	Decoupled hydro	System operator	Energy limit for worst-case upward activation	Two-stage stochastic	Inflow and contingencies	Constant value per m^3
[50]	Cascaded hydro	Producer	None	Deterministic	None	Several possible
[51]	Cascaded hydro	Producer	None	SDDP	Inflow and wind	Cut description
[52]	Cascaded hydro	Producer	Multi-period activation	Two-stage stochastic	Inflow and prices	None, fixed end level
[53]	Cascaded hydro	Producer	Single-period upward activation	Hybrid SDP/SDDP	Inflow and prices	Cut description
[54]	Cascaded hydro	Producer	Full energy balance for worst-case upward activation	SDP/SDDP	Inflow and price	Cut description
[55]	Cascaded hydro	System operator	Single-period energy balance and minimum energy level	Hybrid SDDP/Robust	Inflow and contingencies	Cut description
[56]	Cascaded hydro	System operator	Single-period energy balance	Two-stage stochastic	Wind and contingencies	None, fixed end level
Paper I	Cascaded hydro	System operator	Full energy balance per scenario	Two-stage stochastic/robust	Net-load	Constant value per m^3

simply setting this level high enough will lead to a safe procurement. However, this can easily lead to an overly conservative solution given the current state of the system and the nature of the short-term uncertainties. By modeling the fundamental drivers behind the need for reserve capacity, such as the variability in the net-load due to renewable generation, the model finds an endogenous and dynamic reserve capacity level. An example of this is the battery model in [40] listed in Table 2.1, which uses a two-stage stochastic formulation to model deviations in the demand and generation that must be balanced by activating reserved capacity. The uncertainty is only revealed after some of the decisions, e.g. production and reserve capacity schedules, have been made in a two-stage model. Two-stage stochastic models usually consider the expected value of the cost (or benefit) of the second stage, which usually involves generating a finite set of scenario realizations of the uncertainty with specified probabilities of occurring [57]. This is a risk-neutral method of incorporating the uncertainty, as the variance in the objective value over the scenarios is ignored. While risk-averse stochastic optimization techniques exist, a different point of view of uncertainty and risk is taken in robust optimization. Instead of finding the optimal solution given some known probability distribution, the solution is hedged against a

"worst-case" realization of the uncertain parameters, which naturally leads to a conservative and robust solution, hence the name. Defining what constitutes a worst-case realization is a critical part of constructing a sensible and tractable robust optimization model.

The precursor to robust optimization was proposed by Soyster in [58] from 1973 as a way of dealing with data uncertainty in optimization problems. The technique was expanded upon in the late 1990s by Ben-Tal and Nemirovski [59, 60] and El Ghaoui et al. [61, 62], where the conservatism of the solution could be tuned. This is achieved by constraining the uncertain parameters to be within an ellipsoidal uncertainty set, limiting the extremity of the realized worst-case situation. Bertsimas et al. refined and simplified the method in [63] with the introduction of the concept of linear uncertainty sets and a budget of uncertainty. This leads to robust models that are tractable due to their linearity and modest size. Two-stage or multi-stage robust model formulations, sometimes called adjustable robust optimization, can describe the same mechanisms as stochastic models when it comes to the revelation of uncertainty. However, the first-stage decisions will be influenced by the worst-case realizations of the uncertainty instead of the expected outcome.

Adjustable robust optimization has been employed in many research fields and has a large presence in power system operation and planning modeling. A fairly recent and comprehensive review is given in [64]. Especially worthy of mention is the seminal paper [65], which formulates a two-stage robust optimization problem for energy and reserve scheduling with unit commitment and uncertain net-load injections. The paper provides a detailed step-by-step procedure for formulating simple yet effective uncertainty sets as well as a solution procedure for the resulting robust model. Other important works include the introduction of dynamic uncertainty sets with correlations [66] and their extension to multi-stage robust models with affine policies [67]. Robust optimization has also been used in hydropower scheduling models, such as [68–72] and [55] listed in Table 2.1. Appendix B gives a brief comparison of stochastic and robust two-stage optimization and details the steps of reformulating and solving a two-stage robust model.

The work in Paper I revolves around how cost optimality under the expected imbalance conditions can be weighed against protecting the solution from extreme cases with high variability. A hybrid robust and stochastic model was formulated for this purpose in an effort to potentially temper the conservativeness of robust optimization while maintaining protection against worst-case situations. There have been many attempts to combine robust and stochastic optimization in order to get the benefits of both formulations. Several models combine robust and stochastic optimization to handle different sources of uncertainty. One example is [73], where the expected value over strategic uncertainties is optimized given that the worst-case realization of the operational uncertainties manifests.

The important paper [74] handles the same uncertainty by robust and stochastic optimization in the same model formulation. The expected value over a set of scenarios and the worst-case value based on a robust uncertainty set are both included in the objective function, but scaled with factors α and $1 - \alpha$, respectively. Setting $\alpha = 1$ results in an objective function that only includes the expected cost, while $\alpha = 0$ gives a robust objective function. The constraints for the stochastic and robust parts of the model are always included, meaning the solution will always be feasible in all scenarios and for the worst-case realization even though the cost might not be included in the objective. This model is solved iteratively by a Benders decomposition scheme to handle the robust min-max-min structure. Another solution procedure known as column-and-constraint generation (CCG) can also solve the two-stage robust problem. This technique was first described by Zeng and Zhao in [75,76], and can be described as a primal decomposition strategy compared to Benders decomposition. Instead of generating a single constraint for the master problem in each iteration, CCG finds the current worst-case uncertainty realization and adds all second-stage constraints for that "robust scenario" to the master problem. The size and complexity of solving the master problem increases rapidly when using CCG, but this is often rewarded by a rapid convergence. After solving a robust two-stage model with CCG, a set of worst-case realizations of the uncertainty contained within the defined uncertainty set has been generated. In our work in Paper I, these are viewed as robust scenarios that are then added to a regular two-stage stochastic model. The expected value of the robust scenarios, assuming they are equiprobable, is added to the objective function together with a set of scenarios generated in a standard way. The same scaling between the stochastic and robust objective parts is employed as in [74], and so the conservativeness of the hybrid model can be tuned by giving more or less weight to the robust scenarios.

2.3 Contributions of Papers II and III

While Paper I focused on modeling stochastic forecast imbalances, Paper II and Paper III look at the structural imbalances caused by the discrete market clearing in the Nordic energy markets for electricity. It is necessary to model the actual power balance over time instead of the average energy balance per time interval to investigate structural imbalances on a fundamental level. Perhaps the most straightforward way of attempting to model structural imbalances is to formulate a model with a very fine time resolution. However, going from an hourly resolution to minute or second resolution drastically increases the size and damages the tractability of the model. A fundamentally different approach to the problem is to express all time-varying data and decisions as continuous functions in time, which leads to arbitrarily fine time resolution and the possibility of asserting a true power balance. The challenge with continuous-time models is the reformulation to a convex, or mixed-integer, optimization program

that can be reliably solved in practice. It turns out that it is possible to find such a tractable reformulation by clever use of a set of basis functions called the Bernstein polynomials. Appendix C gives a detailed step-by-step description of how a continuous-time model can be formulated based on the properties of the Bernstein polynomials. The appendix includes derivations of all of the important features of the polynomials, a guide to how an analogous continuous-time model can be created based on a "normal" discrete-time formulation, and a thorough discussion on complicating constraints such as the binary unit commitment decisions. Therefore, mathematical details on the topic are omitted from this chapter, but the following subsection gives a detailed literature review of continuous-time modeling used in power system planning and operation.

2.3.1 Continuous-time optimization

The topic of continuous-time optimization is closely related to the field of control theory, which deals with the control of dynamic systems. Spectral decomposition methods to approximately solve non-linear optimal control problems have been used in many fields for some time [77]. They were first applied to the subject of optimal unit commitment in 2016 by Parvania and Scaglione in [78], which has formed the basis for the continuous-time formulations applied in the models described in this thesis. Note that similar techniques have been applied to related fields, such as [79–81] modeling the control of natural gas flow in transmission networks coupled with electricity generation. These works are non-linear models with most of the attention given to the dynamics of the gas flow and are more closely related to control theory compared to the unit-commitment model of [78]. The earliest work in [78] and [82] was motivated by ramping scarcity problems in the Californian power system with high ramping needs during startup and shutdown of solar power during the morning and evening. The continuous-time framework for the unit commitment problem established in these papers was used to more accurately model the ramping capabilities of the thermal generators in the system to lessen ramping scarcity events.

The later contributions to continuous-time optimization in power system planning have been focused on a few different directions. The topic is still new, and a relatively comprehensive overview of the papers published on the subject is attempted here. Twenty additional papers published after [78, 82] are included, not counting the papers related to this thesis. Either Parvania or Scaglione is part of the author list on most of these papers, showing that the research community working with continuous-time unit commitment is still small. Table 2.2 lists the papers categorized by the included power generation technologies, solution strategy with respect to uncertainty, and the overall goal of the model.

Calculating the continuous-time marginal price is one area that has seen some interest, as it turns out to be a challenging problem. Both [83] and [84] derive

the continuous-time marginal price for the economic dispatch problem with conventional generators including ramping constraints. This is done by applying methods of variational calculus and satisfying the Euler-Lagrange equations and the KKT conditions. The method was first expanded to include flexible loads in the form of electric vehicles (EVs) in [85], and then energy storage devices in [86]. The continuous-time pricing problem was further augmented in [87] by including transmission constraints based on unit shift factors and modeling energy storage devices and conventional generators.

The deterministic unit commitment problem of the original continuous-time formulation in [78] has also been expanded to incorporate uncertainty and other generation technologies. The work in [88] and [89] formulates continuous-time unit commitment models including EVs, which consider optimal queuing and service quality constraints for the EVs. A multi-stage stochastic unit commitment and reserve scheduling problem in continuous-time was formulated in [90]. The model was later extended in [91] to include energy storage devices, DC power flow constraints, and exact quadratic cost curves in the objective function. Energy storage devices and transmission network constraints under the DC power flow assumptions are also found in [92]. The two-stage stochastic unit commitment and reserve scheduling model in [41] includes energy storage units and uses Bernstein polynomials of different degrees in the two stages to model higher variability in the second stage. Another stochastic two-stage model is found in [93], which combines reserve capacity for ramping and energy in a single product.

It is also possible to incorporate the frequency dynamics of synchronous generators into a continuous-time scheduling problem, as shown in [94]. Continuous-time optimization has also been used in the closely related areas of optimizing a joint electricity and gas energy system in [95], and distribution network operation in [96].

Several continuous-time models have also investigated the very short-term operations in regulation markets by using receding horizon techniques. The model in [97] specifically looks at the use of energy storage devices in the regulation markets, and considers the day-ahead continuous-time schedules from conventional generators as fixed input to the model. The receding horizon look-ahead model in [98] has a similar structure, but unlike [97] the input day-ahead schedules and reserve capacity procurement are co-optimized in a separate model. The model also includes a flexible ramp product first described in [99]. However, it does not consider energy storage devices, only conventional generators. The model was extended to include energy storage in [100].

The continuous-time input data in the aforementioned models, e.g. load and wind power curves, are usually created based on a direct conversion from a discrete-time data series. Methods such as minimizing the square error between the continuous-time curve and the discrete-time data can be used to create the input

data, as in [90]. An alternative way is presented in [101], where forecasting a continuous and smooth electricity load is done by constructing a continuous-time Gaussian process, which was later employed in [93].

Paper II formulates a deterministic continuous-time unit commitment model for a system with hydropower and thermal generation, and shows how the hydropower scheduling constraints can be formulated in a continuous-time framework. As described in the paper, modifications to the usual continuous-time constraints and the standard hydropower scheduling constraints had to be made to accommodate the modeling of hydropower in continuous-time. Paper II is therefore primarily a modeling paper, but the topic of structural imbalances in relation to discrete-time markets and operation of large HVDC cables between countries is also discussed.

Paper III extends Paper II with a larger case study of a simplified North European system with offshore wind power in the North Sea. The thermal area is modeled by 104 units of different types based on generator data from the Netherlands and Northern Germany, while the offshore wind power is based on data from Western Denmark. The system is scaled so that the proportion of hydropower production capacity, thermal capacity, offshore wind capacity, and HVDC line transmission capacity is comparable to the current real system. The continuous-time model in Paper III was compared to a discrete-time model, and also used to show which hours are especially problematic in terms of structural imbalances by taking the discrete-time model unit commitment decisions as fixed input.

2.4 Contributions of Paper IV

It is important to include both stochastic forecast imbalances and structural imbalances to assess the total balancing need of the system in the short term. The structural imbalances can be significant in systems with considerable ramping in the net-load curve, as discussed in Paper II, and the increasing renewable generation profile in most power systems increases the potential for larger forecast errors. The cooperation of system operators across balancing regions, countries, and synchronous systems will be an essential element of system balancing in the future. Germany is an interesting case study in relation to cooperation. Despite the increase in variable renewable power generation in the German system over the last few decades, the amount of activated reserves has significantly diminished. This "German paradox" was described in [17], and later studies have shown that increased cooperation between TSOs and the introduction of shorter market intervals with trading around the clock have decreased the total balancing need despite increased imbalances from renewable generation [11, 102]. An accurate representation of the flexibility of the interconnected system is key to efficient cross-border cooperation, as well as a holistic approach to balancing all types of deviations. Investigating the hybrid system dynamic of different generation

technologies such as hydropower, thermal power, and wind power cooperating to balance the system is valuable as a benchmark for optimal operation. This is the goal of Paper IV, which develops an approach to incorporate both stochastic forecast imbalances and structural imbalances in the same model by combining the methodologies of Papers I, II, and III for a hybrid hydrothermal system with uncertain wind power connected by HVDC cables.

The two-stage method of modeling the activation of reserves due to forecast errors discussed in Section 2.2 was shown to give good results in terms of the stability of the system balancing cost in Paper I, including the pure stochastic two-stage model. Formulating the wind power scenarios in continuous-time gives a more realistic representation of the real-time variations with the possibility of modeling rapid sub-interval deviations. The structural imbalances can also be internalized in a two-stage continuous-time model as long as the first-stage decisions and net-load forecast are also expressed in the continuous-time format. According to Table 2.2, the combination of stochastic models with several stages and the continuous-time formulation has previously been performed in [41,90,91, 93], where [91] and [41] include energy storage devices. As briefly mentioned in Section 2.3.1, it is possible to use polynomial expansions of different degrees in the different stages of the model, typically to model faster variations in the data in the later stages. This is conducted in [41] and [93] and called multi-fidelity continuous-time modeling. Paper IV incorporates the multi-fidelity approach by formulating the wind power scenarios in the second-stage with polynomials of degree five, which gives the possibility of more rapid sub-hourly changes than the first-stage data modeled by third-degree polynomials. The second-stage recourse actions also have to be modeled with higher fidelity to ensure that it is possible to balance the deviations.

The continuous-time methodology allows for modeling rapid sub-interval deviations, but another important aspect is the stronger formulation of constraints derived from differential equations. Examples of important differential relationships in power system models include ramping limitations and the evolution of the energy storage content in a battery or reservoir, see Appendix C.3 for a more detailed discussion. The coupling in time for decisions made in a continuous-time model is generally much stronger than in a discrete-time model. In addition to applying constraints directly on the analytical derivative or integral of the continuous-time decision variables connected by differential relationships, the time-coupling is further tightened by including the continuity constraints derived in Appendix C.1.4. The consequences of strongly time-linked decisions are important to consider because of the reserve energy deployment scarcity issues discussed in Section 2.2.1.

Considering both activation of reserves due to forecast errors and enforcing a smooth and continuous operation makes the stochastic continuous-time model less likely to overestimate the overall system flexibility compared to a discrete-

time formulation. At the same time, hydropower units with considerable storage potential are very flexible and can rapidly change production. To preserve the flexibility of the hydropower, the continuity constraints are relaxed for the individual hydropower plants. The combination of continuous-time and a two-stage stochastic approach intrinsically highlights the importance of flexibility in the system. By using this modeling concept, Paper IV is able to demonstrate how hydropower can be used to relieve both ramping scarcity issues and wind power uncertainty in a hybrid system without overestimating the available flexibility.

Table 2.2: Taxonomy table for continuous-time models in power system operation. Note that [101] is not included in the table due to the different topic being explored.

Ref	Generation technologies	Solution strategy	Planning task
[78]	Thermal	Deterministic	Optimal unit commitment
[82]	Thermal	Deterministic	Optimal unit commitment
[83]	Thermal	Deterministic	Price calculation
[84]	Thermal	Deterministic	Price calculation
[85]	Thermal, flexible load	Deterministic	Price calculation
[86]	Thermal, battery	Deterministic	Price calculation
[87]	Thermal, battery	Deterministic	Price calculation with network
[88]	Thermal, flexible load	Deterministic	Optimal unit commitment and EV charging
[89]	Thermal, flexible load	Deterministic	Model predictive control of EV charging
[90]	Thermal	Multi-stage stochastic	Optimal unit commitment and reserve schedule
[91]	Thermal, battery	Multi-stage stochastic	Optimal unit commitment and reserve schedule
[93]	Thermal, renewables	Two-stage stochastic	Optimal unit commitment and reserve schedule
[41]	Thermal, solar, battery	Two-stage stochastic	Optimal unit commitment and reserve schedule
[92]	Thermal, battery	Deterministic	Optimal unit commitment
[99]	Thermal	Deterministic	Optimal unit commitment and flexibility reserve schedule
[94]	Thermal	Deterministic	Optimal dispatch under frequency dynamics
[95]	Thermal, wind, gas storage	Fuzzy information-gap decision theory	Joint electricity and gas network dispatch
[96]	Distributed generation, battery	Deterministic	Optimal scheduling of distribution network
[97]	Thermal, battery	Receding horizon look-ahead	Optimal reserve energy dispatch
[98]	Thermal	Receding horizon look-ahead	Optimal unit commitment / reserve energy dispatch
[100]	Thermal, battery	Receding horizon look-ahead	Optimal unit commitment / reserve energy dispatch
Paper II	Cascaded hydro, thermal	Deterministic	Optimal unit commitment
Paper III	Cascaded hydro, thermal, wind	Deterministic	Optimal unit commitment

3 Conclusion

This thesis has taken a model-technical optimization approach to the research questions formulated in Section 2.1, and has made contributions towards new modeling techniques and methodology for power imbalances in hydropower-dominated systems. The main findings and potential future work are discussed in the following sections.

3.1 Key Takeaways

The effect the activation of reserved capacity can have on a hydropower system is not a topic that has been investigated in the literature to a great extent. Allocating reserve capacity on hydropower plants without considering the implications that a call for activation may have can be a poor decision, as discussed in Paper I. The change in the amount of reserve capacity allocated on the different hydropower plants in the system is the tangible measure of the impact of considering uncertain activation, which is shown in Figure 7 of Paper I. The result is a shift from allocating the majority of the reserve capacity on a single large plant to distributing it among the different plants. This makes it possible to collectively regulate closely connected plants up and down, which ensures better use of the water according to the water values when the reserved hydropower capacity is activated. There is an increased cost for the day-ahead schedule, but Paper I shows that the cost increase is minor compared to the reduction in balancing costs in most cases. The method used to model the uncertainty has an influence on the day-ahead scheduling and procurement cost increase, where a robust optimization model was found to be overly conservative in the case study of Paper I. The proposed hybrid stochastic-robust model was shown to be a good compromise between the low average cost of a stochastic model and the protection from extreme balancing events found by the robust model. In relation to RQ 1 posed in Section 2.1, it seems pertinent to include full energy balance constraints for activated reserve capacity in hydropower systems due to the strong time-coupling between hydropower plants in cascaded watercourses.

The continuous-time formulation for hydropower scheduling developed in Paper II gives an opportunity to model the responsiveness and flexibility of hydropower while imposing a more accurate physical model on the time-dependent operation of the whole system. Both the hydropower plants and thermal units are less flexible when modeled in continuous-time because of the increased time-coupling effects inherent to the formulation, although the thermal units are affected to

a greater extent due to the thermal ramping and unit commitment constraints. The continuous-time formulation is stricter overall and will generally increase the cost of covering the net-load compared to an analogous discrete-time model. The total cost increase for the single day seen in Paper III and IV is roughly 0.5% and 0.4%, respectively. The higher cost can be interpreted as the price of removing structural imbalances from the system, assuming that the continuous-time net-load is the actual net-load and that the physical model imposed by the continuous-time formulation is accurate. The accuracy of these assumptions improves as the degree of the polynomial expansion used in the continuous-time formulation increases. However, using third-degree polynomials often results in a good fit of the underlying data when it is on an aggregated level. Therefore, continuous-time modeling is a useful tool for investigating structural imbalances, which is one possible answer to RQ 2.

The results presented in Paper III and Paper IV both indicate that the overall flexibility of the system is perceived quite differently in the continuous-time and discrete-time models, which has an impact on how the hydropower assets are utilized. The discrete-time models are able to incorporate more hydropower and less thermal generation in the day-ahead schedule to achieve an overall lower cost, as mentioned earlier. The continuous-time models use more constraining ramping bounds on the thermal units and impose smooth and continuous flow on the HVDC lines between the areas. The hydropower usage is shifted towards alleviating ramping scarcity in the thermal area, which is not seen in the discrete-time models. Abrupt changes in the HVDC line flow from one interval to the next can be seen in the discrete-time models, which is challenging for the TSOs to handle in the Nordic system. Avoiding this problem in the continuous-time models as an integrated part of the formulation is therefore beneficial. When structural imbalances in the system are considered through continuous-time optimization, the hydropower is used for ramping flexibility to a greater extent. The specific hours where the discrete-time model underestimates the ramping scarcity in the system are pinpointed in Paper III by using the unit commitment solution from the discrete-time model as fixed input to the continuous-time model. Hours with high ramping in the net-load are easily underestimated by the discrete-time model. When both forecast errors and structural imbalances are considered in Paper IV to address RQ 4, the hydropower is responsible for providing more than 50% of the necessary reserve capacity despite representing only a third of the power generation capacity in the system. The hydropower is responsible for most of the system regulation during the steep ramping hours before and after the thermal area experiences peak load. The results from the case studies presented in Paper III and Paper IV are partial answers to RQ 3 and indicates how Norwegian hydropower could be used for balancing in a larger European setting.

A drawback of the continuous-time formulation is the increase in model size and solution time seen in Papers II, III, and IV. The deterministic continuous-time

model in Paper II uses polynomials of degree 3, and the number of binary variables, continuous variables, and constraints are respectively increased by a factor of 1.5, 3.4, and 5.7 compared to the analogous discrete-time model. These numbers are based on the reduced model size after the automatic presolve routine in the CPLEX solver. The extra binary variables are primarily due to the formulation of the hydropower production function, which has to be modeled using binary variables[1]. The piece-wise linear formulation needs the additional binary variables to ensure that each discharge segment is used in the correct order in the continuous-time model. The number of regular variables is expected to increase by roughly $n + 1$ times for a continuous-time model using polynomials of degree n, while the number of constraints increases more due to the complicated ramping and reservoir storage constraints in addition to the continuity constraints. Comparing the solution times of two different mixed-integer linear problems in a fair way is difficult. There are many parameters available for tuning the performance and solution strategy of MILP problems in commercial solvers, and they can impact the solution time. However, the MIP gap is the most critical setting, as it determines the numerical tolerance for considering a feasible integer solution optimal. In order to be certain that the optimal solution has been found, the MIP gap must be set to zero. As seen in Paper III, demanding a MIP gap of 0% results in the continuous-time model taking almost 30 times longer to solve than the analogous discrete-time model. The requirement of absolute optimality is rarely vital in operational settings, and quickly finding a feasible solution with a reasonable MIP gap is often more valuable. The experience from testing the different continuous-time models presented in Papers II, III, and IV has been that a good solution can be found relatively quickly and that it is the small remaining MIP gap that takes a long time to close. However, it is unquestionable that the continuous-time formulation increases the complexity, size, and solution time for all the hydrothermal models created during this PhD work.

The key takeaways from the work conducted in this PhD can be summarized as follows:

- To avoid inefficient use of water when providing balancing energy, constraints related to activation of reserves should be considered when procuring reserve capacity from hydropower plants in a cascaded topology.
- Robust optimization can be used to generate extreme scenarios for a stochastic optimization model, which leads to a hybrid stochastic-robust formulation that maintains some of the risk-averse properties of robust optimization. The conservativeness of the hybrid model can be tuned by changing the weight given to the robust scenarios compared to the regular scenarios.

[1] Variables part of a special ordered set (SOS) could be used instead to potentially improve tractability.

- The enforcement of a continuous power balance constraint in the continuous-time formulation removes the structural imbalances that are typically left behind in discrete-time models. The difference in objective function values between a continuous-time and a discrete-time model is a measure of the cost of the structural imbalances.

- The stochastic hydrothermal continuous-time formulation is well suited for assessing the ability of hydropower to deliver short-term ramping flexibility to thermal zones in periods of local ramping scarcity.

- Computational difficulty and solution time is significantly increased in the formulated continuous-time hydrothermal models compared to their analogous discrete-time formulations.

3.2 Future Work

The scope of this PhD thesis, defined in Section 1.5, leaves several directions for expanding the work on modeling short-term balancing in hydropower-dominated systems. Some of the most interesting and critical topics for future research are discussed in the following sections.

3.2.1 Reserve dimensioning

As mentioned in Section 1.2, contingency events are important for reserve dimensioning and should be considered in a model that tries to determine the total system balancing need dynamically. Portraying contingency events through stochastic or robust optimization as seen in contingency-constrained unit commitment models is possible, although incorporating it into the methodology used in Paper IV is not straightforward. The exact way in which the uncertain contingency events should be integrated into the model in relation to the forecast error scenarios is an open question, and the increased complexity of another source of uncertainty will damage the tractability of the model. However, it is worth pursuing a holistic approach that considers all major sources of system imbalances to ensure a fundamental modeling level. Representing the AC transmission grid to capture internal congestion problems within bidding zones is another crucial aspect that should be included in a complete model for reserve dimensioning. Adding a power flow description for the AC transmission network can be smoothly incorporated into linear models by using the DC power flow approximation. However, this requires detailed data and further complicates the model by introducing tighter coupling in space and time.

3.2.2 Computational performance

The papers comprising this thesis are focused on developing and verifying new methodologies. To make it easier to compare results and isolate specific behaviors and effects of the modeling, simplified test systems have been used in the different case studies performed in the papers. It is natural to move towards applying the models on larger and more realistic cases in the future, as this is a necessary and important step towards adopting the techniques in practice. In addition to preparing the extra data needed, solution time and computational efficiency are vital for running an extensive analysis. Solution time is already an issue for continuous-time models, as discussed in Section 3.1, and developing decomposition schemes that are tailored for efficiently solving continuous-time models may become necessary. Preliminary testing of the models in Papers II, III, and IV indicates that the continuity constraints are to blame for a significant part of the slow calculation time and are good candidates for relaxation within the applied decomposition method. Appendix C.2.5 shows that the continuity constraints fundamentally change the linear problem structure, and removing them would remove much of the linking between time intervals. The unit commitment constraint formulations derived in Appendix C.3.2 also heavily contribute to the stronger time-coupling in continuous-time models. A Lagrange relaxation procedure targeting these constraints would be a good initial attempt at decomposing the problem. Note that the extensive form of the two-stage stochastic continuous-time model presented in Paper IV was solved directly, and that standard decomposition techniques for stochastic problems such as Benders decomposition could be applied directly without the need for special modifications.

Other means of reducing the difficulty of solving a large-scale continuous-time model should also be investigated. Clustering techniques for the standard unit commitment problem aggregate units into clusters that can be represented with a single integer variable instead of many binary variables, which can drastically reduce the solution time [103]. Adapting the clustering method for the continuous-time formulation should be possible. However, care must be taken when formulating the ramping and reserve constraints to avoid overestimating the flexibility of the cluster compared to the sum of the individual units [104,105]. Aggregation of the hydropower plants and reservoirs is also possible, although this removes the interesting dynamics of the cascaded hydropower topology in short-term operations.

3.2.3 Pricing in continuous-time models

The dual value of the load balance constraint is the marginal cost of providing energy to the system in a linear discrete-time model because it is the cost of incrementally increasing the load. The price cannot be found in such a simple

way for continuous-time models due to the spectral reformulation that creates one load balance per Bernstein polynomial used in the expansion. Calculating the price in a continuous-time model is important for understanding the value of providing the flexibility needed to keep the sub-interval power balance, especially during periods of ramping scarcity. Several papers have been published on the subject of calculating the marginal continuous-time price; these are listed in Section 2.3. The procedure relies on complex variational calculus, and an extension to include hydropower producers with implicit marginal costs defined by a water value description does not seem straightforward. A possible way around the complicated ex-post price calculation explored in the literature is to formulate the continuous-time model as a mixed complementarity problem (MCP). The MCP formulation can smoothly incorporate the system price into the problem by using a bi-level structure where the market is cleared in the upper level and the producers maximize their profit at the lower level. Replacing the lower-level optimization problems with their KKT conditions transforms the bi-level structure to a single MCP. A good reference for the use of MCP models in energy markets can be found in [106]. The price is directly calculated by solving the MCP, and it is possible to model both perfect competition and strategic bidding behavior. Solving MCPs is not straightforward due to the nonlinearities that arise from the KKT conditions, although specialized solvers such as the PATH solver [107] can still find a solution relatively efficiently. Exploring MCP formulations of hydrothermal continuous-time models to calculate the price appears to be an intriguing avenue of future research. It is essential to bridge the gap between the theoretical continuous-time formulation and a market design that is implementable in practice, and MCP modeling could be part of the solution.

Bibliography

[1] The European Commission, "The European Green Deal," URL: https://ec.europa.eu/commission/presscorner/detail/e%20n/ip_19_6691, accessed dec 2020.

[2] The European Commission, "European Climate Law," URL: https://ec.europa.eu/clima/policies/eu-climate-action/law_en, accessed dec 2020.

[3] The European Commission, "What is the European Green Deal?" DOI: 10.2775/275924.

[4] F. Capizzi, A. Das, T. Dauwe, I. Moorkens, R. J. Saarikivi, and M. Tomescu, "Renewable energy in Europe 2019: Recent growth and knock-on effects," European Topic Centre on Climate Change Mitigation and Energy, Tech. Rep., 2019, https://www.eionet.europa.eu/etcs/etc-cme/products/etc-cme-reports/renewable-energy-in-europe-2019-recent-growth-and-knock-on-effects.

[5] IEA, "Offshore Wind Outlook 2019," IEA, Tech. Rep., 2019, https://www.iea.org/reports/offshore-wind-outlook-2019.

[6] C. E. P. Tapiquén, "Europe," Orogénesis Soluciones Geográficas. Based on shapes from Enviromental Systems Research Institute (ESRI). Free Distribution. URL: http://tapiquen-sig.jimdo.com, in Spanish, accessed dec 2020.

[7] The Norwegian Water Resources and Energy Directorate, "Kraftproduksjon," URL: https://www.nve.no/energiforsyning/kraftproduksjon, in Norwegian, accessed dec 2020.

[8] The Norwegian Water Resources and Energy Directorate, "Magasinstatistikk," URL: https://www.nve.no/energiforsyning/kraftmarkedsdata-og-analyser/magasinstatistikk/, in Norwegian, accessed dec 2020.

[9] ENTSO-E, "Electricity Balancing in Europe," URL: https://www.entsoe.eu/news/2018/12/12/electricity-balancing-in-europe-entso-e-releases-an-overview-of-the-european-electricity-balancing-market-and-guideline/, accessed dec 2020.

[10] Statnett, "Rapport fra systemansvarlig 2019," URL: https://www.statnett.no/contentassets/e95b00b70ca646dda684137722467466/rapport-fra-systemansvarlig-2019-.pdf, in Norwegian, accessed dec 2020.

[11] C. Koch and L. Hirth, "Short-term electricity trading for system balancing: An empirical analysis of the role of intraday trading in balancing Germany's electricity system," *Renew. Sustain. Energy Rev.*, vol. 113, p. 109275, oct 2019.

[12] A. Street, F. Oliveira, and J. M. Arroyo, "Contingency-Constrained Unit Commitment With n - K Security Criterion: A Robust Optimization Approach," *IEEE Trans. Power Syst.*, vol. 26, no. 3, pp. 1581–1590, aug 2011.

[13] Q. P. Zheng, J. Wang, and A. L. Liu, "Stochastic Optimization for Unit Commitment - A Review," *IEEE Trans. Power Syst.*, vol. 30, no. 4, pp. 1913–1924, jul 2015.

[14] Energinet, "Power system data published by Energinet," URL: https://www.energidataservice.dk/search, accessed dec 2020.

[15] T. Weißbach, S. Remppis, and H. Lens, "Impact of Current Market Developments in Europe on Deterministic Grid Frequency Deviations and Frequency Restauration Reserve Demand," in *15th Int. Conf. Eur. Energy Mark. (EEM)*, jun 2018.

[16] T. Haugland, G. Doorman, and J. Hystad, "Structural imbalances in the Nordic power system - Causes, future expectations and remedies," in *11th Int. Conf. Eur. Energy Mark. (EEM)*, may 2014.

[17] L. Hirth and I. Ziegenhagen, "Balancing power and variable renewables: Three links," *Renew. Sustain. Energy Rev.*, vol. 50, pp. 1035–1051, oct 2015.

[18] P. Denholm, M. O'Connell, G. Brinkman, and J. Jorgenson, "Overgeneration from Solar Energy in California: A Field Guide to the Duck Chart," National Renewable Energy Laboratory, Tech. Rep., 2015, https://www.nrel.gov/docs/fy16osti/65023.pdf.

[19] RTE, "Frequency data published by RTE," URL: https://www.services-rte.com/en/download-data-published-by-rte.html, accessed dec 2020.

[20] A. Helseth, M. Haugen, S. Jaehnert, B. Mo, H. Farahmand, and C. Ø. Naversen, "Multi-Market Price Forecasting in Hydro-Thermal Power Systems," in *15th Int. Conf. Eur. Energy Mark. (EEM)*, jun 2018.

[21] M. Haugen, A. Helseth, S. Jaehnert, B. Mo, H. Farahmand, and C. Ø. Naversen, "On the Importance of Detailed Thermal Modeling for Price Forecasting in Hydro-Thermal Power Systems," in *IEEE Electr. Power Energy Conf. (EPEC)*, oct 2019.

[22] Arild Helseth, "PRIBAS - Pricing Balancing Services in the Future Nordic Power Market," URL: https://www.researchgate.net/project/PRIBAS-Pricing-Balancing-Services-in-the-Future-Nordic-Power-Market, accessed dec 2020.

[23] A. Helseth and A. C. Geber de Melo, "Scheduling Toolchains in Hydro-Dominated Systems: Evolution, Current Status and Future Challenges for Norway and Brazil," SINTEF Energy Research, Tech. Rep., 2020, https://sintef.brage.unit.no/sintef-xmlui/handle/11250/2672581.

[24] O. B. Fosso, A. Gjelsvik, A. Haugstad, B. Mo, and I. Wangensteen, "Generation scheduling in a deregulated system. The Norwegian case," *IEEE Trans. Power Syst.*, vol. 14, no. 1, pp. 75–80, 1999.

[25] O. Wolfgang, A. Haugstad, B. Mo, A. Gjelsvik, I. Wangensteen, and G. Doorman, "Hydro reservoir handling in Norway before and after deregulation," *Energy*, vol. 34, no. 10, pp. 1642–1651, oct 2009.

[26] M. E. P. Maceiral, D. D. J. Penna, A. L. Diniz, R. J. Pinto, A. C. G. Melo, C. V. Vasconcellos, and C. B. Cruz, "Twenty Years of Application of Stochastic Dual Dynamic Programming in Official and Agent Studies in Brazil-Main Features and Improvements on the NEWAVE Model," in *20th Power Syst. Comput. Conf. (PSCC)*, jun 2018.

[27] A. L. Diniz, F. D. S. Costa, M. E. Maceira, T. N. Dos Santos, L. C. B. Dos Santos, and R. N. Cabral, "Short/Mid-term hydrothermal dispatch and spot pricing for large-scale systems-The case of Brazil," in *20th Power Syst. Comput. Conf. (PSCC)*, jun 2018.

[28] A. Gjelsvik, M. M. Belsnes, and A. Haugstad, "An algorithm for stochastic medium-term hydrothermal scheduling under spot price uncertainty," in *13th Power Syst. Comput. Conf. (PSCC)*, jun 1999.

[29] J. Kong, H. I. Skjelbred, and O. B. Fosso, "An overview on formulations and optimization methods for the unit-based short-term hydro scheduling problem," *Electr. Power Syst. Res.*, vol. 178, p. 106027, jan 2020.

[30] H. I. Skjelbred, J. Kong, and O. B. Fosso, "Dynamic incorporation of non-linearity into MILP formulation for short-term hydro scheduling," *Int. J. Electr. Power Energy Syst.*, vol. 116, p. 105530, mar 2020.

[31] T. N. Santos, A. L. Diniz, C. H. Saboia, R. N. Cabral, and L. F. Cerqueira, "Hourly pricing and day-ahead dispatch setting in Brazil: The dessem model," *Electr. Power Syst. Res.*, vol. 189, p. 106709, dec 2020.

[32] A. Helseth, B. Mo, A. Lote Henden, and G. Warland, "Detailed long-term hydro-thermal scheduling for expansion planning in the Nordic power system," *IET Gener. Transm. Distrib.*, vol. 12, no. 2, pp. 441–447, 2018.

[33] IBM, "IBM CPLEX Optimizer," URL: https://www.ibm.com/analytics/cplex-optimizer, accessed dec 2020.

[34] W. E. Hart, C. D. Laird, J.-P. Watson, D. L. Woodruff, G. A. Hackebeil, B. L. Nicholson, and J. D. Siirola, *Pyomo–optimization modeling in python*, 2nd ed. Springer Science & Business Media, 2017, vol. 67.

[35] W. E. Hart, J.-P. Watson, and D. L. Woodruff, "Pyomo: modeling and solving mathematical programs in python," *Mathematical Programming Computation*, vol. 3, no. 3, pp. 219–260, 2011.

[36] E. Nasrolahpour, J. Kazempour, H. Zareipour, and W. D. Rosehart, "A Bilevel Model for Participation of a Storage System in Energy and Reserve Markets," *IEEE Trans. Sustain. Energy*, vol. 9, no. 2, pp. 582–598, apr 2018.

[37] H. Pandžić, Y. Dvorkin, and M. Carrión, "Investments in merchant energy storage: Trading-off between energy and reserve markets," *Appl. Energy*, vol. 230, pp. 277–286, nov 2018.

[38] O. Megel, J. L. Mathieu, and G. Andersson, "Stochastic Dual Dynamic Programming to schedule energy storage units providing multiple services," in *IEEE Eindhoven PowerTech*, aug 2015.

[39] N. Li, C. Uckun, E. M. Constantinescu, J. R. Birge, K. W. Hedman, and A. Botterud, "Flexible Operation of Batteries in Power System Scheduling with Renewable Energy," *IEEE Trans. Sustain. Energy*, vol. 7, no. 2, pp. 685–696, apr 2016.

[40] D. Pozo, J. Contreras, and E. E. Sauma, "Unit commitment with ideal and generic energy storage units," *IEEE Trans. Power Syst.*, vol. 29, no. 6, pp. 2974–2984, nov 2014.

[41] R. Khatami and M. Parvania, "Stochastic Multi-Fidelity Scheduling of Flexibility Reserve for Energy Storage," *IEEE Trans. Sustain. Energy*, pp. 1–1, 2019.

[42] N. G. Cobos, J. M. Arroyo, N. Alguacil, and J. Wang, "Robust Energy and Reserve Scheduling Considering Bulk Energy Storage Units and Wind Uncertainty," *IEEE Trans. Power Syst.*, vol. 33, no. 5, pp. 5206–5216, sep 2018.

[43] M. A. Mirzaei, A. S. Yazdankhah, B. Mohammadi-Ivatloo, M. Marzband, M. Shafie-khah, and J. P. Catalão, "Stochastic network-constrained co-optimization of energy and reserve products in renewable energy integrated power and gas networks with energy storage system," *J. Clean. Prod.*, vol. 223, pp. 747–758, jun 2019.

[44] A. Shayegan-Rad, A. Badri, and A. Zangeneh, "Day-ahead scheduling of virtual power plant in joint energy and regulation reserve markets under uncertainties," *Energy*, vol. 121, pp. 114–125, feb 2017.

[45] M. Chazarra, J. I. Pérez-Díaz, and J. García-González, "Optimal joint energy and secondary regulation reserve hourly scheduling of variable speed pumped storage hydropower plants," *IEEE Trans. Power Syst.*, vol. 33, no. 1, pp. 103–115, jan 2018.

[46] K. Bruninx, Y. Dvorkin, E. Delarue, H. Pandžić, W. D'haeseleer, and D. S. Kirschen, "Coupling Pumped Hydro Energy Storage with Unit Commitment," *IEEE Trans. Sustain. Energy*, vol. 7, no. 2, pp. 786–796, apr 2016.

[47] J. Filipe, R. J. Bessa, C. Moreira, and B. Silva, "Optimal bidding strategy for variable-speed pump storage in day-ahead and frequency restoration reserve markets," *Energy Syst.*, vol. 10, no. 2, pp. 273–297, may 2019.

[48] H. Farahmand and G. Doorman, "Balancing market integration in the Northern European continent," *Appl. Energy*, vol. 96, pp. 316–326, aug 2012.

[49] C. J. López-Salgado, O. Añó, and D. M. Ojeda-Esteybar, "Energy and reserve co-optimization within the Short Term Hydrothermal Scheduling under uncertainty: A proposed model and decomposition strategy," *Electr. Power Syst. Res.*, vol. 140, pp. 539–551, nov 2016.

[50] J. Kong and H. I. Skjelbred, "Operational hydropower scheduling with post-spot distribution of reserve obligations," in *14th Int. Conf. Eur. Energy Mark. (EEM)*, jun 2017.

[51] M. N. Hjelmeland, C. T. Larsen, M. Korpås, and A. Helseth, "Provision of rotating reserves from wind power in a hydro-dominated power system," in *Int. Conf. Probabilistic Methods Appl. to Power Syst. (PMAPS)*, oct 2016.

[52] M. Chazarra, J. García-González, J. I. Pérez-Díaz, and M. Arteseros, "Stochastic optimization model for the weekly scheduling of a hydropower system in day-ahead and secondary regulation reserve markets," *Electr. Power Syst. Res.*, vol. 130, pp. 67–77, jan 2016.

[53] A. Helseth, M. Fodstad, and B. Mo, "Optimal Medium-Term Hydropower Scheduling Considering Energy and Reserve Capacity Markets," *IEEE Trans. Sustain. Energy*, vol. 7, no. 3, pp. 934–942, jul 2016.

[54] H. Abgottspon, K. Njálsson, M. A. Bucher, and G. Andersson, "Risk-averse medium-term hydro optimization considering provision of spinning reserves," in *Int. Conf. Probabilistic Methods Appl. to Power Syst. (PMAPS)*, jul 2014.

[55] A. Street, A. Brigatto, and D. M. Valladão, "Co-Optimization of Energy and Ancillary Services for Hydrothermal Operation Planning Under a General Security Criterion," *IEEE Trans. Power Syst.*, vol. 32, no. 6, pp. 4914–4923, nov 2017.

[56] C. J. López-Salgado, A. Helseth, O. Añó, and D. M. Ojeda-Esteybar, "Stochastic daily hydrothermal scheduling based on decomposition and parallelization," *Int. J. Electr. Power Energy Syst.*, vol. 118, p. 105700, jun 2020.

[57] J. R. Birge and F. Louveaux, *Introduction to Stochastic Programming*, ser. Springer Series in Operations Research and Financial Engineering. New York, NY: Springer New York, 2011.

[58] A. L. Soyster, "Technical Note—Convex Programming with Set-Inclusive Constraints and Applications to Inexact Linear Programming," *Oper. Res.*, vol. 21, no. 5, pp. 1154–1157, oct 1973.

[59] A. Ben-Tal and A. Nemirovski, "Robust Convex Optimization," *Math. Oper. Res.*, vol. 23, no. 4, pp. 769–805, nov 1998.

[60] A. Ben-Tal and A. Nemirovski, "Robust solutions of uncertain linear programs," *Oper. Res. Lett.*, vol. 25, no. 1, pp. 1–13, aug 1999.

[61] L. El Ghaoui and H. Lebret, "Robust solutions to least-squares problems with uncertain data," *SIAM J. Matrix Anal. Appl.*, vol. 18, no. 4, pp. 1035–1064, jul 1997.

[62] L. El Ghaoui, F. Oustry, and H. Lebret, "Robust solutions to uncertain semidefinite programs," *SIAM J. Optim.*, vol. 9, no. 1, pp. 33–52, jul 1998.

[63] D. Bertsimas and M. Sim, "The Price of Robustness," *Oper. Res.*, vol. 52, no. 1, pp. 35–53, feb 2004.

[64] İ. Yanıkoğlu, B. L. Gorissen, and D. den Hertog, "A survey of adjustable robust optimization," *Eur. J. Oper. Res.*, vol. 277, no. 3, pp. 799–813, sep 2019.

[65] D. Bertsimas, E. Litvinov, X. A. Sun, J. Zhao, and T. Zheng, "Adaptive Robust Optimization for the Security Constrained Unit Commitment Problem," *IEEE Trans. Power Syst.*, vol. 28, no. 1, pp. 52–63, feb 2013.

[66] Á. Lorca, X. A. Sun, E. Litvinov, and T. Zheng, "Multistage Adaptive Robust Optimization for the Unit Commitment Problem," *Oper. Res.*, vol. 64, no. 1, pp. 32–51, feb 2016.

[67] Á. Lorca and X. A. Sun, "Multistage Robust Unit Commitment With Dynamic Uncertainty Sets and Energy Storage," *IEEE Trans. Power Syst.*, vol. 32, no. 3, pp. 1678–1688, may 2017.

[68] R. Jiang, J. Wang, and Y. Guan, "Robust Unit Commitment With Wind Power and Pumped Storage Hydro," *IEEE Trans. Power Syst.*, vol. 27, no. 2, pp. 800–810, may 2012.

[69] A. Soroudi, "Robust optimization based self scheduling of hydro-thermal Genco in smart grids," *Energy*, vol. 61, pp. 262–271, nov 2013.

[70] D. Mejia-Giraldo, J. Villarreal-Marimon, and H. Lopez-Mejia, "Adjustable Robust long-term energy planning under hydrological uncertainty," in *IEEE Power Energy Soc. Gen. Meet.*, oct 2014.

[71] H. Dashti, A. J. Conejo, R. Jiang, and J. Wang, "Weekly Two-Stage Robust Generation Scheduling for Hydrothermal Power Systems," *IEEE Trans. Power Syst.*, vol. 31, no. 6, pp. 4554–4564, nov 2016.

[72] D. Apostolopoulou, Z. De Greve, and M. McCulloch, "Robust Optimization for Hydroelectric System Operation Under Uncertainty," *IEEE Trans. Power Syst.*, vol. 33, no. 3, pp. 3337–3348, may 2018.

[73] D. Yue and F. You, "Optimal supply chain design and operations under multi-scale uncertainties: Nested stochastic robust optimization modeling framework and solution algorithm," *AIChE J.*, vol. 62, no. 9, pp. 3041–3055, sep 2016.

[74] C. Zhao and Y. Guan, "Unified Stochastic and Robust Unit Commitment," *IEEE Trans. Power Syst.*, vol. 28, no. 3, pp. 3353–3361, aug 2013.

[75] L. Zhao and B. Zeng, "Robust unit commitment problem with demand response and wind energy," in *IEEE Power Energy Soc. Gen. Meet.*, jul 2012.

[76] B. Zeng and L. Zhao, "Solving two-stage robust optimization problems using a column-and- constraint generation method," *Oper. Res. Lett.*, vol. 41, no. 5, pp. 457–461, sep 2013.

[77] J. Ruths, A. Zlotnik, and S. Li, "Convergence of a pseudospectral method for optimal control of complex dynamical systems," in *Proc. IEEE Conf. Decis. Control*, 2011.

[78] M. Parvania and A. Scaglione, "Unit Commitment With Continuous-Time Generation and Ramping Trajectory Models," *IEEE Trans. Power Syst.*, vol. 31, no. 4, pp. 3169–3178, jul 2016.

[79] A. Zlotnik, M. Chertkov, and S. Backhaus, "Optimal control of transient flow in natural gas networks," in *54th IEEE Conf. Decis. Control*, dec 2015.

[80] A. Zlotnik, L. Roald, S. Backhaus, M. Chertkov, and G. Andersson, "Control policies for operational coordination of electric power and natural gas transmission systems," in *Proc. Am. Control Conf.*, jul 2016.

[81] A. Zlotnik, L. Roald, S. Backhaus, M. Chertkov, and G. Andersson, "Coordinated Scheduling for Interdependent Electric Power and Natural Gas Infrastructures," *IEEE Trans. Power Syst.*, vol. 32, no. 1, pp. 600–610, jan 2017.

[82] M. Parvania and A. Scaglione, "Generation ramping valuation in day-ahead electricity markets," in *Proc. Annu. Hawaii Int. Conf. Syst. Sci.*, mar 2016.

[83] A. Scaglione, "Continuous-time Marginal Pricing of Power Trajectories in Power Systems," *Inf. Theory Appl. Work. ITA 2016*, jul 2016.

[84] M. Parvania and R. Khatami, "Continuous-Time Marginal Pricing of Electricity," *IEEE Trans. Power Syst.*, vol. 32, no. 3, pp. 1960–1969, may 2017.

[85] R. Khatami, M. Heidarifar, M. Parvania, and P. Khargonekar, "Scheduling and Pricing of Load Flexibility in Power Systems," *IEEE J. Sel. Top. Signal Process.*, vol. 12, no. 4, pp. 645–656, aug 2018.

[86] R. Khatami, M. Parvania, and P. P. Khargonekar, "Scheduling and Pricing of Energy Generation and Storage in Power Systems," *IEEE Trans. Power Syst.*, vol. 33, no. 4, pp. 4308–4322, jul 2018.

[87] R. Khatami and M. Parvania, "Spatio-Temporal Value of Energy Storage in Transmission Networks," *IEEE Syst. J.*, vol. 14, no. 3, pp. 3855–3864, sep 2020.

[88] R. Khatami, M. Parvania, and K. Oikonomou, "Continuous-time optimal charging control of plug-in Electric Vehicles," in *IEEE Power Energy Soc. Innov. Smart Grid Technol. Conf.*, feb 2018.

[89] R. Khatami, M. Parvania, and A. Bagherinezhad, "Continuous-time Model Predictive Control for Real-time Flexibility Scheduling of Plugin Electric Vehicles," *IFAC-PapersOnLine*, vol. 51, no. 28, pp. 498–503, jan 2018.

[90] K. Hreinsson, B. Analui, and A. Scaglione, "Continuous Time Multi-Stage Stochastic Reserve and Unit Commitment," in *20th Power Syst. Comput. Conf. (PSCC)*, jun 2018.

[91] K. Hreinsson, A. Scaglione, and B. Analui, "Continuous Time Multi-Stage Stochastic Unit Commitment With Storage," *IEEE Trans. Power Syst.*, vol. 34, no. 6, pp. 4476–4489, nov 2019.

[92] R. Khatami and M. Parvania, "Optimal Coordination of Energy Storage and Generation Flexibility in Transmission Networks," in *IEEE Power Energy Soc. Gen. Meet.*, aug 2019.

[93] R. Khatami, M. Parvania, and A. Narayan, "Flexibility Reserve in Power Systems: Definition and Stochastic Multi-Fidelity Optimization," *IEEE Trans. Smart Grid*, vol. 11, no. 1, pp. 644–654, jan 2020.

[94] P. Chakraborty, S. Dhople, Y. C. Chen, and M. Parvania, "Dynamics-aware Continuous-time Economic Dispatch and Optimal Automatic Generation Control," in *Proc. Am. Control Conf.*, jul 2020.

[95] A. Nikoobakht, J. Aghaei, M. Shafie-Khah, and J. P. S. Catalão, "Continuous-Time Co-Operation of Integrated Electricity and Natural Gas Systems with Responsive Demands under Wind Power Generation Uncertainty," *IEEE Trans. Smart Grid*, vol. 11, no. 4, pp. 3156–3170, jul 2020.

[96] Z. Deng, M. Liu, H. Chen, W. Lu, and P. Dong, "Optimal Scheduling of Active Distribution Networks With Limited Switching Operations Using Mixed-Integer Dynamic Optimization," *IEEE Trans. Smart Grid*, vol. 10, no. 4, pp. 4221–4234, jul 2019.

[97] R. Khatami, M. Parvania, and P. Khargonekar, "Continuous-time Look-Ahead Scheduling of Energy Storage in Regulation Markets," in *Proc. 52nd Hawaii Int. Conf. Syst. Sci.*, jan 2019.

[98] A. Bagherinezhad, R. Khatami, and M. Parvania, "Continuous-time look-ahead flexible ramp scheduling in real-time operation," *Int. J. Electr. Power Energy Syst.*, vol. 119, p. 105895, jul 2020.

[99] A. Bagherinezhad and M. Parvania, "Continuous-time Flexible Ramp Scheduling in Forward Power Systems Operation," in *IEEE Power Energy Soc. Gen. Meet.*, aug 2019.

[100] B. Li, A. Bagherinezhad, R. Khatami, and M. Parvania, "Continuous-Time Look-Ahead Optimization of Energy Storage in Real-Time Balancing and Regulation Markets," *IEEE Syst. J.*, pp. 1–8, jul 2020.

[101] R. Khatami, M. Parvania, P. Khargonekar, and A. Narayan, "Continuous-Time Stochastic Modeling and Estimation of Electricity Load," in *IEEE Conf. Decis. Control*, dec 2018.

[102] F. Ocker and K.-M. Ehrhart, "The 'German Paradox' in the balancing power markets," *Renew. Sustain. Energy Rev.*, vol. 67, pp. 892–898, jan 2017.

[103] B. S. Palmintier and M. D. Webster, "Heterogeneous Unit Clustering for Efficient Operational Flexibility Modeling," *IEEE Trans. Power Syst.*, vol. 29, no. 3, pp. 1089–1098, may 2014.

[104] J. Meus, K. Poncelet, and E. Delarue, "Applicability of a Clustered Unit Commitment Model in Power System Modeling," *IEEE Trans. Power Syst.*, vol. 33, no. 2, pp. 2195–2204, mar 2018.

[105] G. Morales-Espana and D. A. Tejada-Arango, "Modeling the Hidden Flexibility of Clustered Unit Commitment," *IEEE Trans. Power Syst.*, vol. 34, no. 4, pp. 3294–3296, jul 2019.

[106] S. A. Gabriel, A. J. Conejo, J. D. Fuller, B. F. Hobbs, and C. Ruiz, *Complementarity Modeling in Energy Markets*, ser. International Series in Operations Research & Management Science. Springer, 2013, vol. 180.

[107] S. P. Dirkse and M. C. Ferris, "The path solver: A nonmonotone stabilization scheme for mixed complementarity problems," *Optim. Methods Softw.*, vol. 5, no. 2, pp. 123–156, 1995.

[108] C. Ø. Naversen, H. Farahmand, and A. Helseth, "Accounting for reserve capacity activation when scheduling a hydropower dominated system," *Int. J. Electr. Power Energy Syst.*, vol. 119, p. 105864, jul 2020.

[109] F. S. Hiller and G. J. Lieberman, *Introduction to Operations Research, Ninth Edition*, ser. Industrial engineering series. McGraw-Hill, 2010.

[110] G. G. Lorentz, *Bernstein Polynomials*, ser. Mathematical expositions. University of Toronto Press, 1953.

[111] S. M. Lozinskii, "On the hundredth anniversary of the birth of S. N. Bernstein," *Russ. Math. Surv.*, vol. 38, no. 3, pp. 163–178, jun 1983.

[112] E. W. Weisstein, "Binomial theorem," from MathWorld - A Wolfram Web Resource, URL: https://mathworld.wolfram.com/BinomialTheorem.html.

Publications

Paper I

The paper **"Accounting for Reserve Capacity Activation when Scheduling a Hydropower Dominated System"** is published by **Elsevier** in the **International Journal of Electrical Power & Energy Systems (IJEPES)**. The final published paper is reprinted here without changes in compliance with the CC-BY 4.0 license[2] it is published under.

Cite as:
C. Ø. Naversen, H. Farahmand, and A. Helseth
"Accounting for reserve capacity activation when scheduling a hydropower dominated system"
Int. J. Electr. Power Energy Syst., vol. 119, p. 105864, Jul 2020
DOI: 10.1016/j.ijepes.2020.105864
URL: `https://doi.org/10.1016/j.ijepes.2020.105864`

[2]For licence details, see: `https://creativecommons.org/licenses/by/4.0/`.

Electrical Power and Energy Systems 119 (2020) 105864

Contents lists available at ScienceDirect

Electrical Power and Energy Systems

journal homepage: www.elsevier.com/locate/ijepes

Accounting for reserve capacity activation when scheduling a hydropower dominated system

Christian Øyn Naversen[a,*], Hossein Farahmand[a], Arild Helseth[b]

[a] Department of Electric Power Engineering, Norwegian University of Science and Technology, 7491 Trondheim, Norway
[b] Department of Energy Systems, SINTEF Energy Research, Sem Sælands vei 11, 7034 Trondheim, Norway

ARTICLE INFO

Keyword:
Activation of reserved capacity
Hydropower scheduling
Hybrid stochastic-robust optimization

ABSTRACT

As the penetration of variable renewable power generation increases in power systems around the world, system security is challenged. It is crucial to coordinate the available flexible generating resources, such as hydropower, to meet the need for system balancing. However, reserved capacity on hydropower plants should only be activated if there is sufficient energy or storage capacity to either increase or decrease production. The potential change in production will also affect all reservoirs and plants connected by the cascaded topology. These issues are largely ignored or simplified in hydropower reserve scheduling models. To properly account for the possible activation of reserved capacity, several two-stage model formulations based on stochastic and robust optimization are presented and compared in this paper. The uncertainty in net load deviations due to forecasting errors in renewable power generation is considered the source of reserve capacity activation. The case study based on a real Norwegian watercourse clearly shows the benefit of using any of the two-stage model solutions over the standard deterministic reserve procurement. A novel hybrid stochastic-robust model formulation is presented and shown to efficiently increase the robustness of the solution without notably increasing the reserve procurement cost compared to the stochastic and robust models.

1. Introduction

Hydropower is a valuable asset for any power system, as it is flexible and fast to regulate compared to thermal generation technologies. As the share of variable renewable energy sources in power systems across the world increases, so does the need for balancing capacity and energy. Although hydropower is well suited to help balance the system, the technical constraints and cascaded topology must be considered to realistically estimate this balancing capability. A watercourse connects hydropower plants in space and time. Thus, the balancing actions of a single plant will impact the operation of the whole system, which is a challenge when considering spinning reserve capacity allocation. A hydropower plant delivering spinning reserve capacity in both directions must have sufficient stored water upstream to increase its production, and simultaneously it is beneficial to keep enough upstream storage capacity available to save unused water, in case the reserved capacity is activated upward or downward. The same is valid for the plants connected downstream of the activated plant since the water released has changed from its scheduled value. Another complicating aspect is the implicitly defined marginal cost of operating a hydropower plant. The stored water in each reservoir has an associated opportunity cost or water value, which in general depends on the stored water volumes. This makes the cost of procuring reserve capacity on a specific hydropower plant dependent on the capacity procured on the surrounding plants. Activating poorly coordinated reserve capacity in complex hydropower systems could lead to needless loss of potential energy and increased risk of load shedding.

Reserve capacity procurement and system balancing have been incorporated into hydropower scheduling models in several ways. These features can be found in both long-term planning models [21,13,14,1,18,20,28] and short-term operational models [24,23,9,15]. The fundamental models in [21,13,14] sequentially clear the day-ahead market, reserve procurement and system balancing steps for Northern Europe. The activation of reserve capacity is based on the marginal cost of the hydropower plants in their day-ahead position, but does not include hydrological constraints nor account for available energy in the reservoirs. The methods presented in [1] and [18] consider a producer participating in day-ahead energy and spinning reserve capacity markets under uncertainty in inflow and market prices within modified stochastic dual dynamic programming (SDDP) frameworks. Both methods ensure that enough water is stored in the reservoir to produce the allocated reserve capacity, although activation is not directly

* Corresponding author.
E-mail address: christian.naversen@ntnu.no (C.Ø. Naversen).

https://doi.org/10.1016/j.ijepes.2020.105864
Received 5 September 2019; Received in revised form 20 November 2019; Accepted 15 January 2020
Available online 08 February 2020

Nomenclature

$\mathcal{L}$	robust uncertainty set
$\mathcal{I}_m^{d/b/o}$	modules that discharge/bypass/spill water into module m, index i
$\mathcal{J}$	robust worst-case scenarios, index j
$\mathcal{M}$	hydropower modules, index m
$\mathcal{N}_m$	discharge segments in module m, index n [A]
$\mathcal{S}$	balancing scenarios, index s
$\mathcal{T}$	time periods, index$t$
Ω	dual feasibility constraints for the balancing stage
$\mathcal{X}$	scheduling-stage feasibility constraints
$\mathcal{Y}$	balancing-stage feasibility constraints

Parameters

Δ^{max}	maximal net load deviation [MW]
Γ	budget of uncertainty
Λ_t	maximal hourly net load deviation in $\mathcal{L}$ [MW]
π_s	scenario probability
C^+	penalty for shedding load [mu/MW]
C^-	penalty for dumping power [mu/MW]
C^b	penalty for bypassing water [mu/m^3]
C^o	penalty for spilling water [mu/m^3]
E_{mn}	energy conversion factor [MWs/m^3]
F_t	length of time period [s]
I_{mt}	natural inflow [m^3/s]
L_t	forecasted system net load [MW]
P_m	maximal production capacity [MW]
Q_m^b	maximal flow through bypass gate [m^3/s]
Q_{mn}^d	maximal flow through discharge segment [m^3/s]
Q_m^o	maximal flow through spill gate [m^3/s]
R_t	system reserve requirement [MW]
T	number of time periods in $\mathcal{T}$
V_m^0	initial reservoir volume [m^3]
V_m	maximal reservoir capacity [m^3]
WV_m	end value of water [mu/m^3]

Variables

$\alpha^{\pm}$	auxiliary variables used in "big-M" formulation
Δ_t	net load deviation [MW]
λ_t	dual value of the power balance constraint in the balancing stage [mu/WMh]
θ	auxiliary variable approximating the value of the second-stage problem [mu]
ϕ	vector of all dual balancing-stage variables
$\mathbf{x}$	vector of all scheduling-stage variables
$\mathbf{y}$	vector of all balancing-stage variables
B	normalized system balancing cost [mu]
K	procurement cost of reserves [mu]
p_{mt}	generated hydropower [MW]
q_{mt}^b	flow through bypass gate [m^3/s]
q_{mnt}^d	flow through discharge segment [m^3/s]
q_{mt}^{in}	total controlled flow into reservoir [m^3/s]
q_{mt}^{out}	total controlled flow out of reservoir [m^3/s]
q_{mt}^o	flow through spill gate [m^3/s]
r_{mt}	symmetric spinning reserved capacity [MW]
s_t^+	load shedded [MW]
s_t^-	power dumped [MW]
U	normalized total system cost [mu]
u_t^+	load deviation in upward direction
u_t^-	load deviation in downward direction
v_{mt}	volume at the beginning of the time period [m^3]
W^{bal}	dual of second-stage objective function [mu]
Z^{bal}	second-stage objective function [mu]
Z^{da}	first-stage objective function [mu]

modelled. In [20], it is investigated how wind power can contribute to the provision of rotating reserves in a hydropower-dominated system by using the SDDP algorithm, but without considering reserve activation. The deterministic model presented in [24] has a high degree of physical detail and can model the reservation of all the different reserve capacity products in Norway. The total amount of reserve capacity to be allocated in the system is exogenously given to the model and is distributed among the hydropower plants while optimizing the day-ahead market position. The probability of activation in the balancing markets modifies the expected income in the deterministic model in [23], and the work in [9] is based on the assumption that a certain percentage of the reserve capacity sold to the market is activated by the system operator in every inflow and price scenario. The models in [28] and [15] do not explicitly model the reserve capacity procurement, but consider system balancing through bidding into the day-ahead, intraday and real-time energy markets.

This paper addresses the importance of explicitly representing the activation of reserved production capacity in the reserve procurement phase of a hydropower scheduling model. To the best of the authors' knowledge, this has not been addressed in detail in the literature before, and so emerges as a gap in the existing research. Related work on general energy storage devices exists to some degree. The stochastic unit commitment model with ideal energy storage in [36] balances load deviations by activating reserve capacity on thermal generators and energy storage devices. The model in [8] considers individual pumped storage plants coupled with thermal units, and energy constraints are applied to the reserve capacity procurement for extreme ramping scenarios that are decoupled in time. Bi-level complementarity models can be used to study the participation of an energy storage unit in day-ahead and reserve markets [33,35]. The work in [33] considers energy delivery in both the day-ahead and the real-time markets, but only satisfies the energy constraints of the storage units on average over a set of net load deviation scenarios. The bi-level energy storage investment model in [35] requires that there is sufficient storage and energy available to activate the reserved capacity at maximum for a single hour. The model presented in this paper differs from the general energy storage models in the representation of realistic and large-scale cascaded hydropower systems. To this end, note that short-term hydropower and hydrothermal scheduling is an active field of research, see for instance [25] and [12] for recent descriptions of state-of-the-art formulations.

The uncertain nature of variable renewable power generation and consumption contributes to the need for balancing services. Forecast errors in the net load of a power system force the system operator to activate reserved production capacity to meet the actual net load. There are several ways of modelling the uncertainty in net load deviations that cause the system to be unbalanced, such as stochastic and robust optimization. Stochastic optimization typically yields models which are risk neutral, while robust optimization hedges the solution against the worst-case realization of the uncertainty [6]. Robust optimization has been widely and successfully applied to power system planning and operation problems in recent years [32]. A large portion of the published scientific material has been related to the unit commitment problem under uncertainty, where the goal typically is to commit a sufficient number of thermal units to be able to balance real-time deviations [39]. These types of models are usually formulated as two-stage models [22,5,41,2,7], though single-stage [37] and multistage models [31,30] also exist. Robust optimization has also been used in the

context of hydropower scheduling under uncertainty, as in [3], where the energy content of the hydropower system is maximized while accounting for uncertain net load and inflow. In this paper, a combination of both the stochastic and robust modelling approaches are used to construct two-stage models that account for the effect of activation of reserve capacity in a hydropower system.

The combination of robust and stochastic optimization has been proposed in different ways. Stochastic and robust optimization may handle separate sources of uncertainty, such as generator availability and power prices in [11] and variable power generation and power prices in [27]. Moreover, it is possible to create hybrid models by taking a stochastic or a robust model and introducing some characteristics from the other approach. The work in [7] partitions the scenarios in a stochastic model into bundles where robust optimization is applied within each bundle, while [2] introduces several robust uncertainty sets to a robust model by weighting them in the objective function akin to scenario probabilities. The medium-term hydrothermal model presented in [38] procures reserve capacity to ensure system security in the face of a $N-k$ security criterion, which is done by incorporating robust optimization into the SDDP framework itself. The unified stochastic-robust model presented in [41] models the same source of uncertainty by both stochastic and robust optimization. This is done by introducing weight β of the average scenario cost and $1-\beta$ of the robust worst-case cost in the objective function, which represents a direct integration of both the stochastic and the robust optimization methods in a single problem. A novel hybrid model stochastic-robust model is presented in this paper, which leverages the popular column-and-constraint generation (CCG) solution technique (see [40,42]) as a scenario generator. The CCG provides robust scenarios for the mixed stochastic-robust model, which can be considered as extreme scenarios generated based on a robust uncertainty set. By tuning the probability given to these extreme scenarios, a model that is more robust without being overly conservative compared to its deterministic, robust, and stochastic counterparts is achieved. The complexity of the mixed stochastic-robust model is manageable, as the calculation of the robust scenarios is done before solving the complete model. In short, the contributions of this paper are considered twofold:

1. A new hybrid mixed stochastic-robust optimization model which is less complex in construction compared to other hybrid models is presented. In the numerical case study the new hybrid model improves the robustness of the solution without drastically increasing the cost compared to the pure robust and pure stochastic models.
2. The impact of considering activation of reserve capacity in complex and cascaded hydropower systems has been quantified.

The rest of the paper is organized into three parts: Section 2 details the modelling of the optimization problem formulations, a case study is presented in Section 3, and concluding remarks are found in Section 4. Section 2 is split into subsections describing the deterministic day-ahead scheduling problem (Section 2.1), the system balancing problem (Section 2.2), the stochastic and robust two-stage problems (Section 2.3), and the new mixed stochastic-robust problem (Section 2.4). The case study in Section 3 presents results from tuning the mixed stochastic-robust model (Section 3.2) and how the different model formulations compare (Section 3.3).

2. Modelling

The perspective taken in this paper is that of a system operator aiming at optimally scheduling and balancing a completely renewable system dominated by hydropower. The system is scheduled to be in balance according to the net load forecast in the day-ahead planning stage, and symmetric spinning reserve capacity is procured to ensure the balancing capabilities of the system. The existence of variable generation components in the system, such as wind and solar generation, is not modelled explicitly, but manifests as uncertainty in the net load. The forecast errors are seen as the main factors of this uncertainty, and are therefore the drivers behind the need for balancing services. The forecast errors in the net load become known after the scheduling step, and so the operator must use the procured reserve capacity to balance the system in the most efficient way possible.

2.1. Deterministic day-ahead scheduling problem

The deterministic short-term scheduling problem for the system operator,

$$\min_{\mathbf{x}} Z^{da}(\mathbf{x})$$
$$\mathbf{x} \in \mathcal{X}, \tag{1}$$

aims to minimize the cost of using water to cover the required net load and spinning reserve requirements while respecting the physical constraints of the system. A standard linear definition of the hydropower scheduling problem, see for instance [19], is formulated as

$$\min_{\substack{v,p,r,\\ q^d,q^b,q^o,\\ q^{in},q^{out}}} -\sum_{m\in\mathcal{M}} WV_m v_{m,T+1} + \sum_{m\in\mathcal{M},t\in\mathcal{T}} F_t(C^b q^b_{mt} + C^o q^o_{mt}) \tag{2}$$

s.t.

$$v_{m0} = V^0_m \quad \forall\, m \in \mathcal{M} \tag{3}$$

$$q^{in}_{mt} = \sum_{i\in I^d_m, n\in\mathcal{N}_i} q^d_{int} + \sum_{i\in I^b_m} q^b_{it} + \sum_{i\in I^o_m} q^o_{it} \quad \forall\, m, t \in \mathcal{M}, \mathcal{T} \tag{4}$$

$$q^{out}_{mt} = \sum_{n\in\mathcal{N}_m} q^d_{mnt} + q^b_{mt} + q^o_{mt} \quad \forall\, m, t \in \mathcal{M}, \mathcal{T} \tag{5}$$

$$\frac{v_{m,t+1} - v_{mt}}{F_t} = I_{mt} + q^{in}_{mt} - q^{out}_{mt} \quad \forall\, m, t \in \mathcal{M}, \mathcal{T} \tag{6}$$

$$p_{mt} = \sum_{n\in\mathcal{N}_m} E_{mn} q^d_{mnt} \quad \forall\, m, t \in \mathcal{M}, \mathcal{T} \tag{7}$$

$$\sum_{m\in\mathcal{M}} p_{mt} = L_t \quad \forall\, t \in \mathcal{T} \tag{8}$$

$$p_{mt} + r_{mt} \le P_m \quad \forall\, m, t \in \mathcal{M}, \mathcal{T} \tag{9}$$

$$p_{mt} - r_{mt} \ge 0 \quad \forall\, m, t \in \mathcal{M}, \mathcal{T} \tag{10}$$

$$\sum_{m\in\mathcal{M}} r_{mt} \ge R_t \quad \forall\, t \in \mathcal{T} \tag{11}$$

$$0 \le v_{mt} \le V_m \quad \forall\, m, t \in \mathcal{M}, \mathcal{T}\cup\{T+1\} \tag{12}$$

$$0 \le q^d_{mnt} \le Q^d_{mn} \quad \forall\, m, n, t \in \mathcal{M}, \mathcal{N}_m, \mathcal{T} \tag{13}$$

$$0 \le q^b_{mt} \le Q^b_m \quad \forall\, m, t \in \mathcal{M}, \mathcal{T} \tag{14}$$

$$0 \le q^o_{mt} \le Q^o_m \quad \forall\, m, t \in \mathcal{M}, \mathcal{T} \tag{15}$$

$$0 \le p_{mt} \le P_m \quad \forall\, m, t \in \mathcal{M}, \mathcal{T} \tag{16}$$

All symbols in uppercase are input parameters to the model, while lowercase symbols represent the decision variables $\mathbf{x}$. The model is defined for the hydropower modules $m \in \mathcal{M}$ over the time periods $t \in \mathcal{T}$, where the terminology "hydropower module" is used to describe the combined unit of a reservoir connected to a power plant. The water may be moved between reservoirs through three different waterways: flow through the turbine, bypass gate, and spillage, see Fig. 1. The objective (2) of the model is to minimize the total cost of using water according to the water value and end volume of all reservoirs, as well as the small penalties for using the alternative bypass and spillage waterways. These penalties are applied to encourage the use of the main waterway through the plant. Water values represent the opportunity

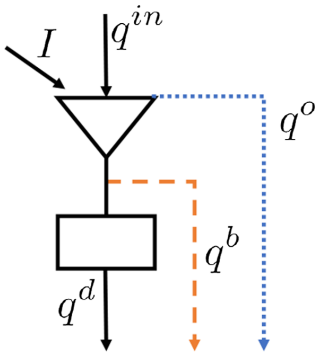

Fig. 1. Depiction of a hydropower module (reservoir and power plant) with different waterways for discharging, bypassing and spilling water.

cost of using water now versus storing it for later use, and are calculated by long-term models such as [19]. The end value of the water generally depends on the end volume in all reservoirs in the system, typically described by linear cutting planes. Constant water values are used in this model formulation for simplicity. Eqs. (3)–(6) preserve the water balance and topology between the modules in the system. The relation between water discharged through the turbine and the power produced by the generator is modelled as a piece-wise linear constraint in Eq. (7), where the efficiency is decreasing for increasing discharge segment number to ensure convexity of the problem. The power balance is kept by Eq. (8), while Eqs. (9) and (10) bound the available symmetric spinning reserve capacity of the plants. Note that the model is linear, which allows production down to 0 MW. To make sure the reserved capacity is spinning, the symmetric requirement is imposed. Enough reserve capacity must be allocated to satisfy the static reserve requirement in Eq. (11). Eqs. (12)–(16) are the bounds of the variables based on the physical capacities of the hydropower modules.

2.2. The balancing problem

Balancing the system in real time after a net load deviation Δ has occurred is necessary to maintain system stability. The decisions $\mathbf{x}$ made in the day-ahead scheduling stage will affect the system's ability to perform the balancing actions, and so the balancing problem

$$\begin{aligned} &\min_{\mathbf{y}} Z^{bal}(\mathbf{y}) \\ &\mathbf{y} \in \mathcal{Y}(\mathbf{x}, \Delta), \end{aligned} \tag{17}$$

depends on both $\mathbf{x}$ and Δ. The formulation is near identical to the day-ahead scheduling problem described by Eqs. (2) and (16) except for changes to Eqs. (2) and (8)–(10). All of the variable types found in Eqs. (2) and (16), except for the reserved capacity r, are found in $\mathbf{y}$ and have an analogous meaning. Let these variables be marked by an overline, so that $\bar{p}$ represents the power produced by a plant in the balancing stage and so on. The power balance constraint in Eq. (8) is augmented to include the net load deviation Δ as well as non-negative penalty variables for shedding load and dumping power:

$$\sum_{m \in \mathcal{M}} \bar{p}_{mt} + s_t^+ - s_t^- = L_t + \Delta_t. \quad \forall\, t \in \mathcal{T} \tag{18}$$

The penalty costs for using these penalty variables are added to the objective function formulation of Eq. (2),

$$\begin{aligned} &Z^{bal}(\mathbf{y}) \\ &= -\sum_{m \in \mathcal{M}} WV_m \bar{v}_{m,T+1} + \sum_{m \in \mathcal{M}, t \in \mathcal{T}} F_t (C^b \bar{q}^b_{mt} + C^o \bar{q}^o_{mt}) + \\ &\sum_{t \in \mathcal{T}} (C^+ s_t^+ + C^- s_t^-), \end{aligned} \tag{19}$$

and the production limits, Eqs. (9) and (10), are based on the procured spinning reserve capacity and production schedule in the day-ahead stage:

$$\bar{p}_{mt} \le p_{mt} + r_{mt} \quad \forall\, m, t \in \mathcal{M}, \mathcal{T} \tag{20}$$

$$\bar{p}_{mt} \ge p_{mt} - r_{mt} \quad \forall\, m, t \in \mathcal{M}, \mathcal{T} \tag{21}$$

The constraints defined in the day-ahead scheduling problem, Eqs. (3)–(7) and (12)–(16), are also included in the balancing problem constraints $\mathbf{y} \in \mathcal{Y}(\mathbf{x}, \Delta)$, but now pertaining to the balancing variables $\mathbf{y}$. The only connection to the decisions made in the day-ahead scheduling stage is through Eqs. (20) and (21).

2.3. Two-stage stochastic and robust problems

To account for the potential cost of activating the procured reserves in the scheduling phase, a two-stage model combining the day-ahead scheduling problem described in Section 2.1 with the system balancing problem in Sectin 2.2 is needed. In this section, two-stage problems based on traditional stochastic and robust optimization are formulated. The scheduling of production and procurement of reserve capacity is the first-stage problem, while balancing the system based on the first-stage solution and realized net load deviation Δ_t is considered as the second stage.

A stochastic problem is formulated by constructing a set $\mathcal{S}$ of balancing scenarios with net load deviations Δ_{st} and probabilities π_s, and then introducing a copy of the balancing problem (17) for each scenario into the deterministic scheduling problem (1). This leads to the extensive form of the classical two-stage stochastic problem formulation [32]:

$$\begin{aligned} &\min_{\mathbf{x}, \mathbf{y}_s} Z^{da}(\mathbf{x}) + \textstyle\sum_{s \in \mathcal{S}} \pi_s Z^{bal}(\mathbf{y}_s) \\ &\mathbf{x} \in \mathcal{X} \\ &\mathbf{y}_s \in \mathcal{Y}(\mathbf{x}, \Delta_s) \quad \forall\, s \in \mathcal{S}. \end{aligned} \tag{22}$$

The expected cost of balancing the system in all scenarios $s \in \mathcal{S}$ by activating the procured reserve capacity is minimized in this formulation, while also minimizing the cost of scheduling the system to meet the net load forecast and procuring the reserve capacity. The effect of activating the reserved capacity is properly captured in this model formulation, as constraints describing the cascaded hydropower topology and the energy usage of balancing the system are present in the balancing constraints. Note that the reserve capacity is activated for the whole time period t, which means the model does not distinguish between different types of reserves with different activation times.

The two-stage robust optimization formulation represents a more conservative approach than the stochastic formulation in Eq. (22). Robustness of the solution is of interest to the system operator, as keeping the system in balance, also in extreme situations, is a priority. The robust two-stage counterpart to the stochastic formulation is the tri-level problem

$$\begin{aligned} &\min_{\mathbf{x}} Z^{da}(\mathbf{x}) + \max_{\Delta} \min_{\mathbf{y}} Z^{bal}(\mathbf{y}) \\ &\mathbf{x} \in \mathcal{X} \\ &\Delta \in \mathcal{L} \\ &\mathbf{y} \in \mathcal{Y}(\mathbf{x}, \Delta), \end{aligned} \tag{23}$$

where the net load deviation Δ is constrained to be part of the uncertainty set $\mathcal{L}$. The robust problem aims to minimize the first-stage cost and the worst-case balancing cost. In this paper, the simple formulation first proposed in [4] will be used to define:

$$\mathcal{L}: =\{\Delta_t | \Delta_t = \Lambda_t \cdot (u_t^+ - u_t^-); \\ \sum_{t\in\mathcal{T}} (u_t^+ + u_t^-) \le \Gamma;\ u_t^\pm \in \{0, 1\}\}, \tag{24}$$

where the parameters Λ_t and Γ are the maximal net load deviation and the budget of uncertainty, respectively. The binary variables $u_t^\pm$ signify if a deviation in positive or negative direction has occurred. Note that it is possible to include both spatial and temporal correlations in the uncertainty set [29,30]. Since the distribution used to generate the scenarios for the stochastic model does not include any temporal correlations in the case study presented in Section 3, correlations are not included in the uncertainty set.

The min-max-min formulation of the robust optimization problem in Eq. (23) cannot be solved directly. The column-and-constraint generation (CCG) procedure, first proposed in [40,42], is a popular primal decomposition scheme to remedy this. Other solution techniques such as Benders decomposition (see for instance [5]) and affine policy approximation [31,30] are not considered in this work because the model presented in Section 2.4 depends on the CCG approach. CCG first requires the inner minimization problem of Eq. (23) to be transformed to its dual maximization form, so that the maximization steps may be combined:

$$\max_{\Delta\in\mathcal{L}} \min_{\mathbf{y}} Z^{bal}(\mathbf{y}) \ \Leftrightarrow \ \max_{\Delta\in\mathcal{L},\phi} W^{bal}(\mathbf{x}, \Delta, \phi) \\ \mathbf{y} \in \mathcal{Y}(\mathbf{x}, \Delta) \quad \phi \in \Omega. \tag{25}$$

Let the dual variables of the power balance constraints in the balancing stage, Eq. (18), be denoted as λ_t. Bi-linear terms $\Delta_t\lambda_t = \Lambda_t \cdot (u_t^+\lambda_t - u_t^-\lambda_t)$ appear in the objective function W^{bal} when Eq. (18) is dualized. The binary definition of Δ_t in Eq. (24) allows for an exact reformulation of the bi-linear problem to a mixed integer linear program (MILP) by using a "big-M" approach. This is done in for instance [22], though other options are available for solving the problem. An alternating direction method was used in [29], while a cutting plane outer approximation was implemented in [5]. In this paper the exact MILP reformulation will be used, as it can be solved directly with a standard MILP solver. With the introduction of the penalty costs $C^\pm$ for shedding load and dumping power in Eq. (19) through the non-negative variables $s_t^\pm$, the dual variables λ_t will be constrained by these values:

$$-C^- \le \lambda_t \le C^+ \quad \forall\, t \in \mathcal{T}. \tag{26}$$

Using the bounds on λ_t in the big-M expansion allows the bi-linear terms $\pm u_t^\pm\lambda_t$ to be replaced by the new variables $\alpha_t^\pm$ and the additional constraints

$$\alpha_t^+ \le \lambda_t + C^-(1 - u_t^+) \quad \forall\, t \in \mathcal{T} \tag{27}$$

$$\alpha_t^+ \le C^+ u_t^+ \quad \forall\, t \in \mathcal{T} \tag{28}$$

$$\alpha_t^- \le -\lambda_t + C^+(1 - u_t^-) \quad \forall\, t \in \mathcal{T} \tag{29}$$

$$\alpha_t^- \le C^- u_t^- \quad \forall\, t \in \mathcal{T}. \tag{30}$$

The CCG technique is based on repeatedly solving the dual form of Eq. (25) for iteratively updated first-stage solutions $\mathbf{x} \in \mathcal{X}$. The solution yields the realization of the worst-case net load deviation Δ_j, which is iteratively added to the master problem

$$\min_{\mathbf{x},\mathbf{y}_j,\theta} Z^{da}(\mathbf{x}) + \theta \\ \mathbf{x} \in \mathcal{X} \\ \theta \ge Z^{bal}(\mathbf{y}_j) \quad \forall\, j \in \mathcal{J} \\ \mathbf{y}_j \in \mathcal{Y}(\mathbf{x}, \Delta_j) \quad \forall\, j \in \mathcal{J}. \tag{31}$$

The set $\mathcal{J}$ represents the worst-case net load deviation scenarios that have been identified by the inner maximization problem, and the auxiliary variable θ is an outer approximation of Eq. (25). Solving the master problem results in an updated first-stage solution $\mathbf{x}$, which is used to solve Eq. (25) in the next iteration. When the current value of θ and W^{bal} have converged within a specified tolerance, the procedure is complete as the optimal solution of Eq. (23) has been found.

2.4. Mixed stochastic-robust problem

In an effort to combine the advantages of the stochastic and the robust problem formulations presented in Section 2.3, a novel mixed stochastic-robust formulation that utilizes the solution of the pure robust problem formulated in Eq. (23) is proposed here. Solving the robust problem with the CCG algorithm results in a set of worst-case net load deviations $\mathcal{J}$, as explained in Section 2.3. These deviations are realizations of the net load that maximizes the cost of balancing the system in the robust formulation. Therefore, the CCG algorithm can be seen as a generator of extreme scenarios that are contained within the uncertainty set $\mathcal{L}$. The mixed stochastic-robust model is formed in Eq. (32) by extending the stochastic problem formulation in Eq. (22) with the set of robust scenarios:

$$\min_{\mathbf{x},\mathbf{y}_s,\mathbf{y}_j} Z^{da}(\mathbf{x}) + \sum_{s\in\mathcal{S}} \pi_s^* Z^{bal}(\mathbf{y}_s) + \sum_{j\in\mathcal{J}} \pi_j Z^{bal}(\mathbf{y}_j) \\ \mathbf{x} \in \mathcal{X} \\ \mathbf{y}_s \in \mathcal{Y}(\mathbf{x}, \Delta_s) \quad \forall\, s \in \mathcal{S} \\ \mathbf{y}_j \in \mathcal{Y}(\mathbf{x}, \Delta_j) \quad \forall\, j \in \mathcal{J}. \tag{32}$$

Note that the probabilities of the original scenarios $s \in \mathcal{S}$ have been scaled so that

$$\sum_{s\in\mathcal{S}} \pi_s^* + \sum_{j\in\mathcal{J}} \pi_j = 1. \tag{33}$$

All original scenarios are scaled down with the same factor $0 \le \beta \le 1$,

$$\pi_s^* = \beta\pi_s \quad \forall\, s \in \mathcal{S}. \tag{34}$$

The robust scenarios are considered to be equiprobable, which results in the robust probabilities

$$\pi_j = (1 - \beta)/|\mathcal{J}| \quad \forall\, j \in \mathcal{J}. \tag{35}$$

Choosing a scaling of $\beta = 1$ will put zero weight on the robust scenario balancing costs, and similarly $\beta = 0$ removes the cost of balancing the original scenarios. The constraints $\mathcal{Y}(\mathbf{x}, \Delta)$ associated with the original and robust scenarios will persist regardless of the choice of β. The formulation in Eq. (32) is similar to the unified stochastic-robust model in [41], as the robust and stochastic components of the problem is weighted in the objective function in both models. However, there are two main differences between Eq. (32) and other hybrid models;

Firstly, the robust scenarios $\mathcal{J}$ are computed by solving the robust model in Eq. (23) before the mixed model is solved. In contrast, the unified stochastic-robust model must be solved in an iterative way with the presence of the scenarios $\mathcal{S}$ in every iteration, which can be problematic regarding the tractability of the problem. The mixed model presented here may be solved directly in its extensive form, or by any other suitable decomposition technique for stochastic optimization problems. The reusability of the robust scenarios $\mathcal{J}$ are also higher in the mixed model formulation since they are completely independent of the original scenarios $\mathcal{S}$. For instance, if the mixed model is solved for successive days, the scenarios $\mathcal{J}$ can be used as a good initial set of constraints in the solution of the robust model. This sharing of contingency events between time periods has also been proposed for the long-term hydrothermal planning model in [38], which incorporates CCG in a SDDP framework.

The second important difference is that the expected value of the robust scenarios is added to the objective function in Eq. (32) instead of the max-min robust formulation. If only the maximal cost of the robust scenarios was minimized, the mixed model would be little more than an approximation of the unified model of [41] with pre-generated robust scenarios. As pointed out in Section 2.2, the only direct connections between the first and second stages are the production limits Eqs. (20) and (21). For the hydropower scheduling problem, this turns out to be a

very weak coupling in the sense that including the constraints $\mathbf{y} \in \mathcal{Y}(\mathbf{x}, \Delta)$ alone do not have a big impact on the first-stage decisions. It is important to include the balancing cost $Z^{bal}(\mathbf{y})$ of a scenario to the objective function to actually influence the scheduling decisions. This effect is clear in the numerical calculations in Section 3.2 for the edge case $\beta = 1$. Directly including all robust scenarios in the objective function through their expected cost instead of only minimizing the maximal balancing cost leads to a tighter connection between the stages, and a more efficient way of propagating the conservative nature of the robust scenarios to the reserve capacity procurement decision. The coupled model proposed in [26] also minimizes the expected value of robust scenarios, but in their case the robust scenarios are iteratively added to the set $\mathcal{S}$ through the CCG procedure. The approach still has the potential tractability issues of the unified problem formulation, especially since the convergence of the CCG algorithm is unproven in their proposed framework.

3. Case study

The focus of this case study is on the quality of the solution of the deterministic, stochastic, robust, and mixed model formulations presented in Section 2. The solution quality is measured in terms of the cost of procuring the reserve capacity and the subsequent cost of activating the reserves to balance the system. The topic of solution times of the different models is not discussed directly, as this will be heavily dependent on the solution parameters and techniques used to solve the models, especially the robust and, by extension, the mixed models. All optimization models have been implemented in the Pyomo modelling package for Python [16,17] using the MILP solver CPLEX 12.8 [10].

The hydropower system used in the study is shown in Fig. 2. It is based on a real watercourse in Norway, and consists of 12 modules with a total production capacity of 537.4 MW. The initial reservoir volume of every module is set to 65% of its maximal storage capacity, which represents a normal hydrological situation during the winter in Norway. Water values are calculated by the long-term hydropower scheduling model described in [19], and are measured in monetary units (mu) per Mm^3 in the range of 1200–9000 mu/Mm^3. The penalty for shedding load and dumping power is chosen to be 3000 mu/MW and 1000 mu/MW, respectively. Note that the results in the case study is not overly affected by the choice of these values due to the way the net load deviation scenarios are generated. The time horizon is set to 24 h with hourly resolution, and the forecasted net load profile is shown in Fig. 3. The profile is based on the amount of energy sold in the day-ahead market in the Norwegian NO3 bidding zone on 1/1-2019 [34], with values scaled down to get a peak of 420 MW. The maximal forecast error possible is considered to be $\Delta^{max} = 42$ MW, 10% of the peak load, in either direction in every hour. No temporal correlations between net load forecast errors are assumed for simplicity.

To generate scenarios for the stochastic and mixed models, the forecast errors Δ_t are chosen to be normally distributed with $\mu_t = 0$ and $\sigma_t = \Delta^{max}/2.5 = 16.8$ MW. However, to ensure that the values drawn to generate the scenarios are within the postulated maximal forecast error band, any values outside this band are truncated to its outer limits. In other words, $|\Delta_{st}| \leq \Delta^{max}$ is enforced for all scenarios.

There are two measures that are used to quantify the quality of a production and reserve capacity procurement schedule; The cost of procuring the reserves K and the following cost of balancing the system B. The cost of procuring reserves is defined as the increase in the first-stage objective function Z^{da} relative to the cost of the deterministic model in Eq. (1) solved without any reserve requirement, Z_0^{da}:

$$K = Z^{da} - Z_0^{da}. \tag{36}$$

This cost represents the opportunity cost of procuring the reserves. For a given realization of the net load deviation Δ_i, the cost B_i of balancing this deviation is calculated by solving the primal balancing problem in Eq. (17) for the given production schedules p and allocated reserve capacity r. This yields the objective function Z_i^{bal}, which is normalized by the objective function given perfect foresight, Z_i^{PF}, to produce the balancing cost:

$$B_i = Z_i^{bal} - Z_i^{PF}. \tag{37}$$

The perfect foresight cost is found by relaxing the production limit constraints of the balancing problem, Eqs. (20) and (21), to let every plant produce between zero and maximum capacity. The sum of the procurement cost and the normalized balancing cost is the total system cost,

$$U_i = K + B_i. \tag{38}$$

K is easily found by direct calculation, whereas the balancing costs B_i must be estimated by simulation. In this case study, 5000 different sampled net load deviations were used to measure the balancing cost of the given schedule. The robustness of the different model solutions was tested by generating two different batches of 5000 balancing scenarios. The first batch, from now on referred to as "the normal scenario batch", was generated based on the same truncated normal distribution used when generating scenarios for the stochastic and mixed models. A different seed for the random number generator was used when generating the normal scenario batch to avoid redrawing the same scenarios generated for the solution of the stochastic and mixed models. The second batch of scenarios was generated from a uniform distribution drawing values in the range $|\Delta_t| \leq \Delta^{max}$. This uniform scenario batch gives balancing scenarios that are more extreme compared to the normal scenario batch. The system is guaranteed not to experience any net load deviation larger than Δ^{max} in any of the scenarios in the two batches, and so penalties for load shedding and dumping power can be avoided given that enough energy and storage capacity is available when the reserves are activated.

3.1. Sensitivity analysis of the budget of uncertainty in the robust model

The parameters of the robust uncertainty set $\mathcal{L}$ are chosen to be comparable to the scenarios generated from the truncated normal distribution. The maximal deviation is set to $\Lambda_t = \Delta^{max}$ so that the worst-case deviation contained in $\mathcal{L}$ does not exceed the maximal hourly net load deviation. The budget of uncertainty Γ heavily influences the solution of the robust model. According to the formulation in Eq. (24), Γ limits the maximal number of hours with a worst-case deviation. To gauge the robustness of the solution of the robust model in Eq. (23), a sensitivity analysis of Γ in the range from 1 to 24 was performed. The robust model was solved for the 24 different values of Γ to an absolute

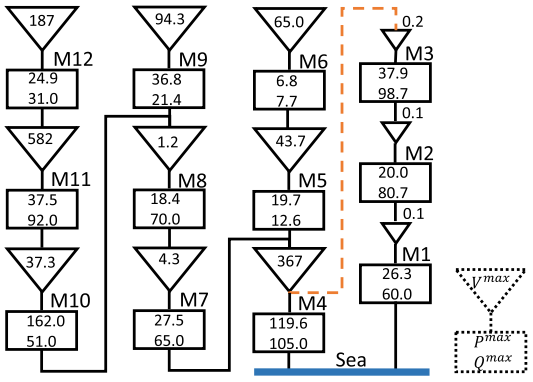

Fig. 2. Sketch of the hydropower topology. Reservoirs (triangles), power plants (rectangles), and water routes for discharge (solid lines) and bypass (dashed line) are shown together with maximal values for discharge (m^3/s), production (MW) and reservoir volumes (Mm^3).

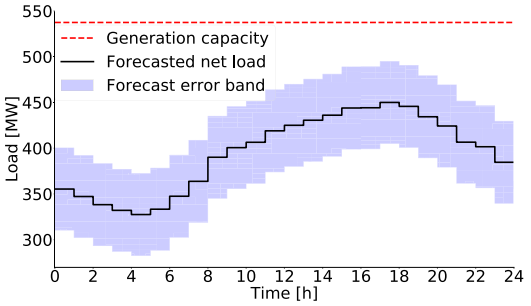

Fig. 3. Forecasted system net load with the region of possible deviations and the total generation capacity of the system.

convergence tolerance of 5 mu, with an absolute MIP gap of 5 mu and integer tolerance of 10^{-9} for the second-stage problem. The CCG algorithm on average converged in 15 iterations, and always within 29 iterations. The procurement cost K was determined based on Eq. (36) and balancing cost B_i was then calculated for all of the scenarios in the normal and uniform scenario batches according to Eq. (37). The numerical results are shown in Fig. 4.

The sensitivity analysis shows that the value of Γ has a big impact on both the procurement cost and simulated balancing cost of the robust model. As expected, K increases almost monotonically as a function of Γ. The balancing cost is generally higher for low values of Γ for both batches of simulation scenarios, but the trend is not monotone. There is a distinct drop in the variability of B_i for $\Gamma > 10$, but the variability starts to increase again when close to the maximal value of $\Gamma = 24$. This shows that simply choosing a high budget of uncertainty does not necessarily result in a more robust solution. Fig. 4 shows that choosing $\Gamma = 1$ results in the lowest average total cost U^{mean} when simulating with the normal scenario batch but the highest U^{mean} in the uniform scenario batch. In terms of robustness, the best choice is arguably $\Gamma = 15$. The 95th percentile of the total cost is lowest for this value of Γ for both simulation scenario batches, and its average total cost is also the lowest in the uniform scenario batch.

3.2. Sensitivity analysis of the robust weight βb in the mixed stochastic-robust model

The scaling factor β of the mixed stochastic-robust model in Eq. (32) is considered a tuning parameter in this case study, and its optimal value is estimated in this section based on a similar type of sensitivity analysis as in Section 3.1. It was determined that $\Gamma = 15$ gave the most robust solution when the pure robust model was considered, which was reached after 12 iterations of the CCG algorithm. The corresponding 12 robust scenarios form the set $\mathcal{J}$ for the mixed model. An additional 50 equiprobable scenarios were generated to form the set $\mathcal{S}$ of balancing scenarios based on the truncated normal distribution described in Section 3. The mixed model was solved for a range of different values of β to find the procurement cost K before the balancing cost B_i was simulated based on the 5000 scenarios in the normal and the uniform scenario batches. The numerical results are visualized in Fig. 5. When determining the range of β to consider in the mixed model, it is useful to calculate the value of β that results in equal weights for the scenarios in $\mathcal{S}$ and $\mathcal{J}$. Based on Eqs. (34) and (35), this value is

$$\beta_0 = \frac{|\mathcal{S}|}{|\mathcal{S}| + |\mathcal{J}|} \approx 0.806 \tag{39}$$

given the number of robust and regular scenarios used. A value of $\beta < \beta_0$ will result in a mixed model where the individual robust scenarios are given a higher weight than the scenarios in $\mathcal{S}$, which is likely to give an overly conservative solution. This turned out to be true in this case study, so only values in the range $0.8 \leq \beta \leq 1.0$ are presented in this analysis.

The results show that a lower value of β gives a lower standard deviation $\sigma(U_i)$ at the expense of a higher base procurement cost K. Interestingly, the standard deviation increases noticeably for the edge case $\beta = 1$. Only adding the constraints related to the balancing problem without considering the associated balancing cost in the objective causes this effect, and the balancing constraints alone do not impact the model sufficiently to increase its robustness. The value of β that achieves the lowest average total cost is 0.99 and 0.91 when using the normal and uniform simulation scenario batches, respectively. The most robust solutions occur at $\beta = 0.93$ and $\beta = 0.84$ in the two simulation cases when the 95th percentile of the total cost as a measure for robustness. This finding shows that it is possible to gain both robustness and lower average costs at the same time by adding robust scenarios to a stochastic optimization problem. The "best" choice of β depends on the preferences of the system operator, and most choices in the region $0.84 \leq \beta \leq 0.99$ can be justified based on a trade-off between robustness and low average cost. However, it is clear that giving zero weight to the robust scenarios ($\beta = 1$) is a sub-optimal choice either way.

3.3. Model comparison

To compare the mixed model and the robust model with the deterministic (Eq. (1)) and stochastic (Eq. (22)) formulations, the same simulation run of 5000 balancing scenarios drawn from the truncated normal distribution and the uniform distribution was used to simulate

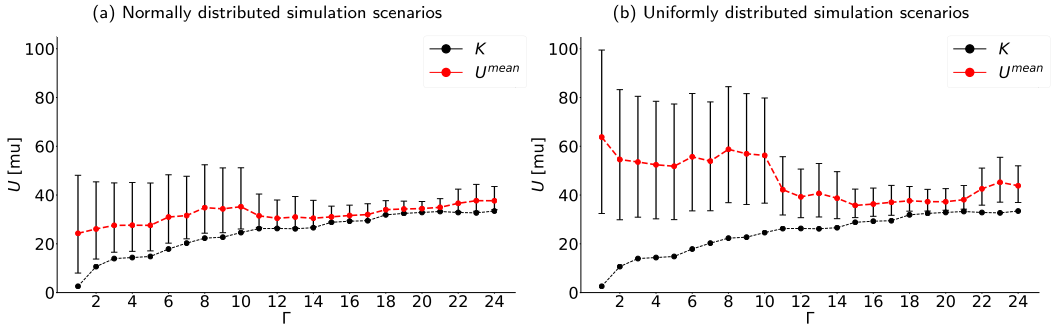

Fig. 4. Cost simulation for the robust model solution for different values of Γ. The simulation in (a) used balancing scenarios drawn from a normal distribution, while (b) used uniformly distributed scenarios. The procurement cost and the average total cost are shown as black and red points, respectively. The 5th and 95th percentiles of the total cost are shown as error bars for each value of Γ. (For interpretation of the references to colour in this figure legend, the reader is referred to the web version of this article.)

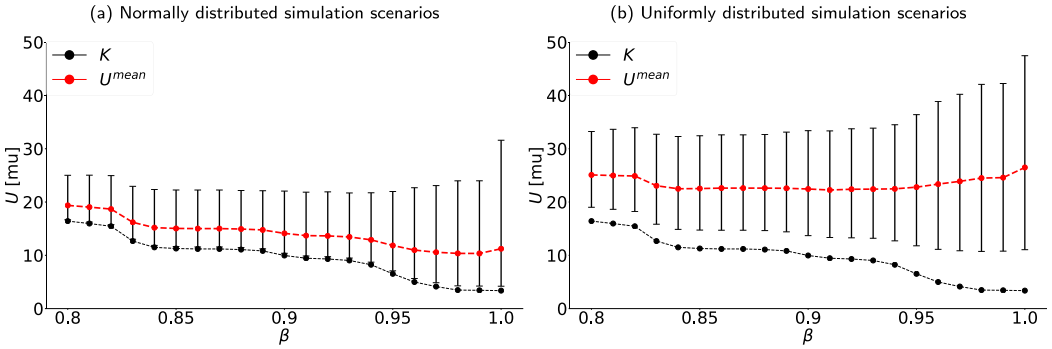

Fig. 5. Cost simulation for the robust model solution for different values of β. The simulation in (a) used balancing scenarios drawn from a normal distribution, while (b) used uniformly distributed scenarios. The procurement cost and the average total cost are shown as black and red points, respectively. The 5th and 95th percentiles of the total cost are shown as error bars for each value of β. (For interpretation of the references to colour in this figure legend, the reader is referred to the web version of this article.)

the costs. The deterministic model was solved with a static reserve requirement of $R_t = \Delta^{max} = 42$ MW. The stochastic model was solved with 50, 200 and 1000 scenarios drawn from the truncated normal distribution, where the 50 first scenarios are identical to the ones used in the mixed model. The results of the simulation are shown in Fig. 6 with accompanying numerical details given in Table 1. There are no instances of load shedding or power dumping penalties being used in any of the simulation runs for any of the models.

The first observation to note is the advantage of considering the activation of reserves in a cascaded hydropower system. The deterministic model procures the 42 MW of reserve capacity and does not shift the production schedule of any module from the schedule obtained when not procuring reserve capacity. This gives a low procurement cost of $K = 0$, but it is evident that the cost of actually balancing the system after the net load has been realized is high compared to all of the two-stage models. The average cost is 7–8 times higher for the deterministic model solution compared to the stochastic and mixed model solutions. The robust model with $\Gamma = 15$ is considered overly conservative in this comparison due to a high procurement cost. Note that the least conservative robust model with $\Gamma = 1$, see Fig. 4, also performs significantly worse than the other two-stage models. The stochastic model with 50 scenarios performs well in the simulation using the normal scenario batch but has high variability in the balancing cost and low robustness when the simulation is based on the uniform scenario batch. By increasing the number of scenarios in the stochastic model to 200 and 1000, the average total cost, variability, and robustness improve.

Table 1
Numeric values of the procurement cost, average total cost, 95th percentile of the total cost and the standard deviation of the total cost for the different model formulations. The simulation in (a) used balancing scenarios drawn from a normal distribution, while (b) used uniformly distributed scenarios.

(a) Normally distributed simulation scenarios

Model	K	U^{mean}	$U^{95\%}$	$\sigma(U_i)$
Deterministic	0.00	84.69	144.65	32.99
Robust, $\Gamma = 15$	28.82	31.06	35.45	2.11
Stochastic, 50 scen.	3.37	11.24	31.60	8.24
Stochastic, 200 scen.	3.12	10.06	23.11	6.58
Stochastic, 1000 scen.	3.11	9.72	21.99	5.91
Mixed, $\beta = 0.84$	11.50	15.19	22.36	3.37
Mixed, $\beta = 0.99$	3.43	10.35	23.99	6.23

(b) Uniformly distributed simulation scenarios

Model	K	U^{mean}	$U^{95\%}$	$\sigma(U_i)$
Deterministic	0.00	208.92	300.38	51.52
Robust, $\Gamma = 15$	28.82	35.74	42.44	3.59
Stochastic, 50 scen.	3.37	26.50	47.46	11.38
Stochastic, 200 scen.	3.12	24.38	42.31	9.82
Stochastic, 1000 scen.	3.11	23.68	40.48	9.28
Mixed, $\beta = 0.84$	11.50	22.49	32.29	5.42
Mixed, $\beta = 0.99$	3.43	24.58	42.25	9.58

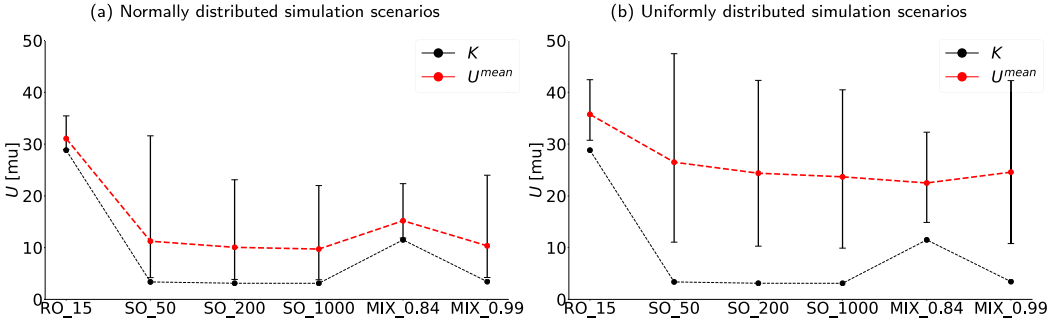

Fig. 6. Cost simulation comparing the robust, stochastic and mixed model solutions. The simulation in (a) used balancing scenarios drawn from a normal distribution, while (b) used uniformly distributed scenarios. The procurement cost and the average total cost are shown as black and red points, respectively. The 5th and 95th percentiles of the total cost are shown as error bars for each model. (For interpretation of the references to colour in this figure legend, the reader is referred to the web version of this article.)

However, this comes at the expense of model size and complexity, and the marginal improvement per scenario is low when going from 200 to 1000 scenarios. The mixed model only adds 12 new scenarios, but still manages to provide robust solutions without being overly conservative. The mixed model with $\beta = 0.84$ yields the most resilient solution when simulating with the uniform scenario batch, with a 95th percentile cost that is considerably lower than the other models. The increased procurement cost results in a higher average total cost in the normal scenario batch simulation, but the 95th percentile cost is still only slightly higher than the stochastic model with 1000 scenarios. When the mixed model is solved with $\beta = 0.99$, the result is a model which behaves similarly to the stochastic model with 200 scenarios. This model comparison shows that using robust scenarios in a stochastic model can drastically reduce the number of scenarios needed to improve robustness and average total cost.

To better understand the effect and importance of considering reserve capacity activation in the scheduling phase, Fig. 7 shows how some of the different models allocate and distribute the reserve capacity among the 12 hydropower plants. The deterministic model relies heavily on plant 4 for reserve capacity throughout the day, and fills the remaining reserve capacity need with reserves arbitrarily allocated on other plants that operate between 0 and P^{max}. There is no spatial coordination between plants that are selected for reserving capacity in the deterministic model. In this case, module 4 has ample energy stored upstream and additional storage space to ramp up or down production without issue, but this is purely by chance. The module is also located at the bottom of the cascaded system, and so any change in water discharged does not cause problems downstream. As seen in Table 1, the deterministic reserve procurement still turns out to be costly when it comes to balancing the system. Using plant 4 to balance most of the net load deviations results in poor water management according to the water values. All of the two-stage models also rely on plant 4 for their reserve capacity, but to a lesser extent. The shape of the forecasted net load curve, with a valley in hours 2–6 and a peak in hours 14–20, can be seen in the allocation of the reserve capacity, which reflects the fact that it is better to use different hydropower modules for balancing at different times of the day. Modules 1, 2 and 3 are located in a string with very limited storage capacity and are used for reserve capacity during the peak hours. Reserve capacity is allocated on these plants at the same time so that they can ramp up or down together to avoid issues caused by the low storage capacity in between them. The robust model allocates significantly more reserve capacity on plants 1, 2 and 3 compared to the stochastic and mixed models. This forces an increased use of the bypass gate from module 4 to module 3 to feed the three modules with additional water so that they can increase their production and deliver more spinning reserve capacity. Using the bypass gate incurs a small penalty, which increases the procurement cost of the robust model. It is clear that the robust model values protection in the peak hours. The worst-case system costs occur when positive deviations manifest in the peak hours since this forces the hydropower system to produce closer to its maximal capacity. The mixed model with $\beta = 0.84$ inherits the protection of the peak hours. It procures between 50 and 55 MW of reserve capacity in several hours in the peak period, which is over the necessary 42 MW to avoid load shedding and power dumping. The additional reserve capacity gives increased flexibility in the balancing stage, as different combinations of modules can be used to produce or retain the required balancing energy, even in the case where a maximal net load deviation is realized. Except for the peak hours, the stochastic and mixed models produce a similar reserve capacity procurement. This is to be expected since most of the weight is still allocated to the scenarios used in the stochastic model.

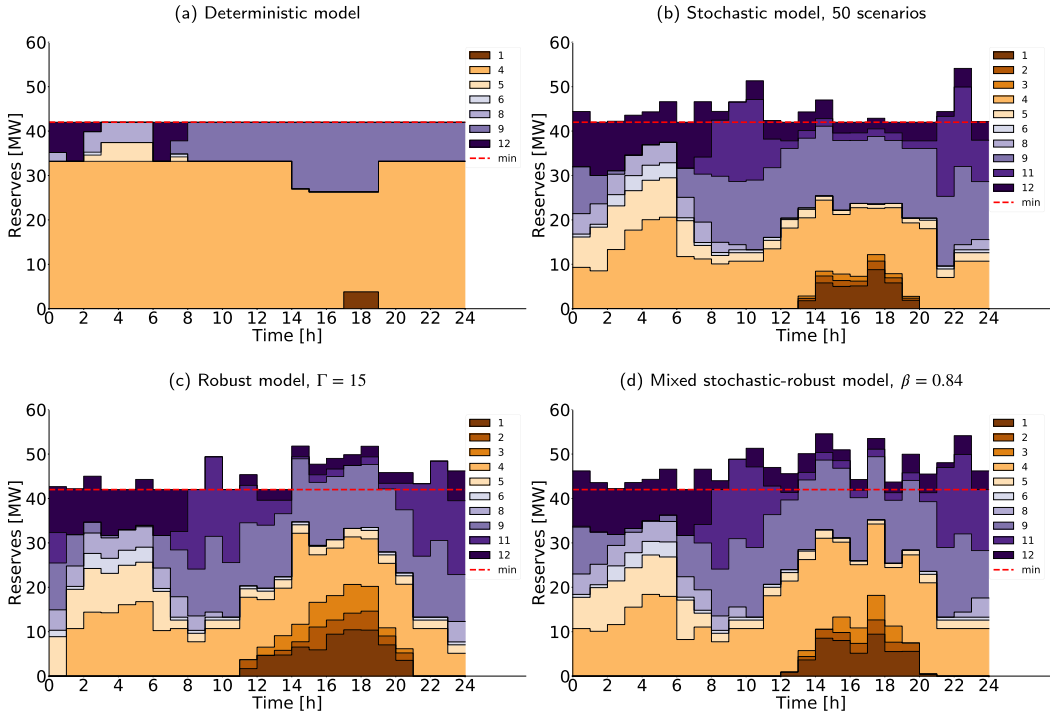

Fig. 7. Reserve allocation on the 12 hydropower modules for the different models. The minimal reserve required to avoid load shedding is shown as a red dashed line. (For interpretation of the references to colour in this figure legend, the reader is referred to the web version of this article.)

4. Conclusion

In this paper, the importance of considering the activation of reserved capacity in the scheduling phase for hydropower has been highlighted. If activation is not considered, having sufficient amounts of both stored energy and energy storage capacity can become issues in real-time operations. Cascaded hydropower systems have the added problem of being physically connected, and therefore, many plants will be affected by a single plant ramping up and down its production. In the presented case study, inefficient water management was the source of the high balancing cost of the deterministic model. Several two-stage formulations, which considers activation of reserves in combination with energy and topology constraints in the balancing stage, were proposed to solve this issue. One of these models is a new mixed stochastic-robust optimization model, which was shown to yield high-quality solutions compared to its pure stochastic and pure robust model ancestors. The mixed model can be viewed as a stochastic model augmented with extreme scenarios identified by solving a robust model with the CCG algorithm. The fact that a non-zero robust weight minimizes the total costs in the mixed model signifies a benefit of strengthening the stochastic model with robust scenarios. This is especially valid when the probability distribution used to generate the scenarios for the stochastic model is different from the actual distribution of the uncertainty, which can be the case when the underlying data is of poor quality.

The case study presented in this paper is based on a moderate case regarding the initial state and energy available in the system. Solving the daily scheduling problem over a longer period that captures the seasonal variations in the hydropower system, for instance by using a rolling horizon simulator, will give a complete picture of the effects of spatially coordinating the reserve capacity allocation based on accounting for activation.

CRediT authorship contribution statement

Christian Øyn Naversen: Writing - original draft, Methodology, Conceptualization, Software, Formal analysis, Data curation, Visualization. **Hossein Farahmand:** Conceptualization, Writing - review & editing, Supervision. **Arild Helseth:** Conceptualization, Writing - review & editing, Project administration, Funding acquisition, Supervision.

Declaration of Competing Interest

The authors declare that they have no known competing financial interests or personal relationships that could have appeared to influence the work reported in this paper.

Acknowledgements

This work was funded by The Research Council of Norway, Project No. 268014/E20.

References

[1] Abgottspon Hubert, Njálsson Karl, Bucher Matthias A, Andersson Göran. Risk-averse medium-term hydro optimization considering provision of spinning reserves. 2014 int. conf. probabilistic methods appl. to power syst. IEEE; 2014. p. 1–6. https://doi.org/10.1109/PMAPS.2014.6960657. ISBN 978-1-4799-3561-1.

[2] An Yu, Zeng Bo. Exploring the modeling capacity of two-stage robust optimization: variants of robust unit commitment model. IEEE Trans Power Syst 2015;30(1):109–22. https://doi.org/10.1109/TPWRS.2014.2320880.

[3] Apostolopoulou Dimitra, De Greve Zacharie, McCulloch Malcolm. Robust optimization for hydroelectric system operation under uncertainty. IEEE Trans Power Syst 2018;33(3):3337–48. https://doi.org/10.1109/TPWRS.2018.2807794.

[4] Bertsimas Dimitris, Sim Melvyn. The price of robustness. Oper Res 2004;52(1):35–53. https://doi.org/10.1287/opre.1030.0065.

[5] Bertsimas Dimitris, Litvinov Eugene, Sun Xu Andy, Zhao Jinye, Zheng Tongxin. Adaptive robust optimization for the security constrained unit commitment problem. IEEE Trans Power Syst 2013;28(1):52–63. https://doi.org/10.1109/TPWRS.2012.2205021.

[6] Birge John R, Louveaux François. Introduction to stochastic programming. ISBN 978-1-4614-0236-7 Springer series in operations research and financial engineeringNew York, NY: Springer New York; 2011. https://doi.org/10.1007/978-1-4614-0237-4.

[7] Blanco Ignacio, Morales Juan M. An efficient robust solution to the two-stage stochastic unit commitment problem. IEEE Trans Power Syst 2017;32(6):4477–88. https://doi.org/10.1109/TPWRS.2017.2683263.

[8] Bruninx Kenneth, Dvorkin Yury, Delarue Erik, Pandzic Hrvoje, Dhaeseleer William, Kirschen Daniel S. Coupling pumped hydro energy storage with unit commitment. IEEE Trans Sustain Energy 2016;7(2):786–96. https://doi.org/10.1109/TSTE.2015.2498555.

[9] Chazarra Manuel, García-González Javier, Pérez-Díaz Juan I, Arteseros Montserrat. Stochastic optimization model for the weekly scheduling of a hydropower system in day-ahead and secondary regulation reserve markets. Electr Power Syst Res 2016;130:67–77. https://doi.org/10.1016/j.epsr.2015.08.014.

[10] CPLEX Optimizer. Available online, accessed 16/7-2019. www.cplex.com.

[11] Dehghan Shahab, Amjady Nima, Vatani Behdad, Zareipour Hamidreza. A new hybrid stochastic-robust optimization approach for self-scheduling of generation companies: optimal self-scheduling of generating companies. Int Trans Electr Energ Syst 2016;26(6):1244–59. https://doi.org/10.1002/etep.v26.610.1002/etep.2132.

[12] Diniz Andre Luiz, Da Serra Fernanda, Costa Maria Elvira, Maceira Tiago Norbiato, Santos Dos, Lilian Chaves B, Santos Dos, Cabral Renato Neves. Short/Mid-term hydrothermal dispatch and spot pricing for large-scale systems-The case of Brazil. ISBN 9781910963104 20th Power Syst. Comput. Conf. PSCC 2018Institute of Electrical and Electronics Engineers Inc.; 2018. https://doi.org/10.23919/PSCC.2018.8442897.

[13] Farahmand H, Doorman GL. Balancing market integration in the Northern European continent. Appl Energy 2012;96:316–26. https://doi.org/10.1016/j.apenergy.2011.11.041.

[14] Gebrekiros Yonas, Doorman Gerard, Jaehnert Stefan. and Hossein Farahmand. Reserve procurement and transmission capacity reservation in the Northern European power market. Int J Electr Power Energy Syst 2015. https://doi.org/10.1016/j.ijepes.2014.12.042. ISSN 01420615.

[15] Gu Yang, Bakke Jordan, Zhou Zheng, Osborn Dale, Guo Tao, Bo Rui. A novel market simulation methodology on hydro storage. IEEE Trans Smart Grid 2014;5(2):1119–28. https://doi.org/10.1109/TSG.2013.2289915.

[16] Hart William E, Watson Jean-Paul, Woodruff David L. Pyomo: modeling and solving mathematical programs in Python. Math Prog Comp 2011;3(3):219–60. https://doi.org/10.1007/s12532-011-0026-8.

[17] Hart William E, Laird Carl D, Watson Jean-Paul, Woodruff David L, Hackebeil Gabriel A, Nicholson Bethany L, et al. Pyomo–optimization modeling in python vol. 67, 2nd ed.. Springer Science & Business Media; 2017.

[18] Helseth Arild, Fodstad Marte, Mo Birger. Optimal medium-term hydropower scheduling considering energy and reserve capacity markets. IEEE Trans Sustain Energy 2016;7(3):934–42. https://doi.org/10.1109/TSTE.2015.2509447.

[19] Helseth Arild, Mo Birger, Henden Arild Lote, Warland Geir. Detailed long-term hydro-thermal scheduling for expansion planning in the Nordic power system. IET Gener Transm Distrib 2018;120(2):441–7. https://doi.org/10.1049/iet-gtd.2017.0903.

[20] Hjelmeland Martin N, Larsen Camilla T, Korpås Magnus, Helseth Arild. Provision of rotating reserves from wind power in a hydro-dominated power system. 2016 Int conf probabilistic methods appl. to power syst IEEE; 2016. p. 1–7. https://doi.org/10.1109/PMAPS.2016.7764206. ISBN 978-1-5090-1970-0.

[21] Jaehnert Stefan, Doorman Gerard L. Assessing the benefits of regulating power market integration in Northern Europe. Int J Electr Power Energy Syst 2012;430(1):70–9. https://doi.org/10.1016/J.IJEPES.2012.05.01. ISSN 0142-0615.

[22] Jiang Ruiwei, Wang Jianhui, Guan Yongpei. Robust unit commitment with wind power and pumped storage hydro. IEEE Trans Power Syst 2012;270(2):800–10. https://doi.org/10.1109/TPWRS.2011.2169817. ISSN 0885-8950.

[23] Kazempour SJ, Moghaddam MP, Yousefi GR. Self-scheduling of a price-taker hydro producer in day-ahead energy and ancillary service markets. 2008 IEEE Canada electr power conf IEEE; 2008. p. 1–6. https://doi.org/10.1109/EPC.2008.4763320. ISBN 978-1-4244-2894-6.

[24] Kong Jiehong, Skjelbred Hans Ivar. Operational hydropower scheduling with post-spot distribution of reserve obligations. 2017 14th int conf Eur energy mark IEEE; 2017. p. 1–6. https://doi.org/10.1109/EEM.2017.7981874. ISBN 978-1-5090-5499-2.

[25] Kong Jiehong, Skjelbred Hans Ivar, Fosso Olav Bjarte. An overview on formulations and optimization methods for the unit-based short-term hydro scheduling problem. Electr Power Syst Res 2020;178. https://doi.org/10.1016/j.epsr.2019.106027. ISSN 03787796.

[26] Liu Dundun, Cheng Haozhong, Fang Sidun. Coupled stochastic and robust transmission expansion planning. 2017 IEEE power energy soc gen meet IEEE; 2017. p. 1–5. https://doi.org/10.1109/PESGM.2017.8274170. ISBN 978-1-5386-2212-4.

[27] Liu Guodong, Xu Yan, Tomsovic Kevin. Bidding strategy for microgrid in day-ahead market based on hybrid stochastic/robust optimization. IEEE Trans Smart Grid 2016;70(1):227–37. https://doi.org/10.1109/TSG.2015.2476669. ISSN 1949-3053.

[28] Löhndorf Nils, Wozabal David, Minner Stefan. Optimizing trading decisions for hydro storage systems using approximate dual dynamic programming. Oper Res 2013;610(4):810–23. https://doi.org/10.1287/opre.2013.1182. ISSN 0030-364X.

[29] Lorca Álvaro, Sun Xu Andy. Adaptive robust optimization with dynamic uncertainty sets for multi-period economic dispatch under significant wind. IEEE Trans Power

Syst 2015;300(4):1702–13. https://doi.org/10.1109/TPWRS.2014.2357714. ISSN 0885-8950.
[30] Lorca Álvaro, Sun Xu Andy. Multistage robust unit commitment with dynamic uncertainty sets and energy storage. IEEE Trans Power Syst 2017;320(3):1678–88. https://doi.org/10.1109/TPWRS.2016.2593422. ISSN 0885-8950.
[31] Lorca Á, Sun XA, Litvinov E, Zheng T. Multistage adaptive robust optimization for the unit commitment problem. Oper Res 2016;640(1):32–51. https://doi.org/10.1287/opre.2015.1456. ISSN 0030-364X.
[32] Morales Juan M, Conejo Antonio J, Madsen Henrik, Pinson Pierre, Zugno Marco. Integrating renewables in electricity markets. Volume 205 of International series in operations research & management science Boston (MA): Springer US; 2014. https://doi.org/10.1007/978-1-4614-9411-9. ISBN 978-1-4614-9410-2.
[33] Nasrolahpour Ehsan, Kazempour Jalal, Zareipour Hamidreza, Rosehart William D. A bilevel model for participation of a storage system in energy and reserve markets. IEEE Trans Sustain Energy 2018;90(2):582–98. https://doi.org/10.1109/TSTE.2017.2749434.
[34] Nord Pool. Available online [accessed 16/7-2019]. www.nordpoolgroup.com/Market-data1/Dayahead/Volumes/NO.
[35] Pandžic H, Dvorkin Y, Carrión M. Investments in merchant energy storage: Trading-off between energy and reserve markets. Appl Energy 2018;230:277–86. https://doi.org/10.1016/j.apenergy.2018.08.088. ISSN 03062619.
[36] Pozo David, Contreras Javier, Sauma Enzo E. Unit commitment with ideal and generic energy storage units. IEEE Trans Power Syst 2014;290(6):2974–84. https://doi.org/10.1109/TPWRS.2014.2313513. ISSN 08858950.
[37] Street Alexandre, Oliveira Fabrício, Arroyo José M. Contingency-constrained unit commitment with n-K security criterion: a robust optimization approach. IEEE Trans Power Syst 2011;260(3):1581–90. https://doi.org/10.1109/TPWRS.2010.2087367. ISSN 0885-8950.
[38] Street Alexandre, Brigatto Arthur, Valladão Davi M. Co-optimization of energy and ancillary services for hydrothermal operation planning under a general security criterion. IEEE Trans Power Syst 2017;320(6):4914–23. https://doi.org/10.1109/TPWRS.2017.2672555. ISSN 0885-8950.
[39] van Ackooij W, Danti Lopez I, Frangioni A, Lacalandra F, Tahanan M. Large-scale unit commitment under uncertainty: an updated literature survey. Ann Oper Res 2018;2710(1):11–85. https://doi.org/10.1007/s10479-018-3003-z. ISSN 0254-5330.
[40] Zeng Bo, Zhao Long. Solving two-stage robust optimization problems using a column-and- constraint generation method. Oper Res Lett 2013;410(5):457–61. https://doi.org/10.1016/j.orl.2013.05.003. ISSN 01676377.
[41] Zhao Chaoyue, Guan Yongpei. Unified stochastic and robust unit commitment. IEEE Trans Power Syst 2013;280(3):3353–61. https://doi.org/10.1109/TPWRS.2013.2251916. ISSN 0885-8950.
[42] Zhao Long, Zeng Bo. Robust unit commitment problem with demand response and wind energy. ISBN 9781467327275 IEEE power energy soc gen meetIEEE; 2012. p. 1–8. https://doi.org/10.1109/PESGM.2012.6344860.

Paper II

The paper **"Hydrothermal Scheduling in the Continuous-Time Framework"** is published by **Elsevier** in a special issue of **Electric Power Systems Research (EPSR)** as the proceedings of the **21st Power Systems Computation Conference**. The final published paper is reprinted here without changes in compliance with the CC-BY 4.0 license[3] it is published under.

Cite as:
C. Ø. Naversen, A. Helseth, B. Li, M. Parvania, H. Farahmand, and J. P. S. Catalão
"Hydrothermal scheduling in the continuous-time framework"
Electr. Power Syst. Res., vol. 189, p. 106787, Dec 2020
DOI: 10.1016/j.epsr.2020.106787
URL: `https://doi.org/10.1016/j.epsr.2020.106787`

[3]For licence details, see: `https://creativecommons.org/licenses/by/4.0/`.

Electric Power Systems Research 189 (2020) 106787

Contents lists available at ScienceDirect

Electric Power Systems Research

journal homepage: www.elsevier.com/locate/epsr

Hydrothermal scheduling in the continuous-time framework

Christian Øyn Naversen[*,a], Arild Helseth[b], Bosong Li[c], Masood Parvania[c], Hossein Farahmand[a], João P.S. Catalão[d]

[a] Department of Electric Power Engineering, Norwegian University of Science and Technology, Trondheim, Norway
[b] Department of Energy Systems, SINTEF Energy Research, Trondheim, Norway
[c] Department of Electrical and Computer Engineering, University of Utah, Salt Lake City, Utah, USA
[d] Faculty of Engineering of the University of Porto and INESC TEC, Porto, Portugal

ARTICLE INFO

Keywords:
Continuous-time optimization
Hydrothermal scheduling
Structural imbalances

ABSTRACT

Continuous-time optimization models have successfully been used to capture the impact of ramping limitations in power systems. In this paper, the continuous-time framework is adapted to model flexible hydropower resources interacting with slow-ramping thermal generators to minimize the hydrothermal system cost of operation. To accurately represent the non-linear hydropower production function with forbidden production zones, binary variables must be used when linearizing the discharge variables and the continuity constraints on individual hydropower units must be relaxed. To demonstrate the performance of the proposed continuous-time hydrothermal model, a small-scale case study of a hydropower area connected to a thermal area through a controllable high-voltage direct current (HVDC) cable is presented. Results show how the flexibility of the hydropower can reduce the need for ramping by thermal units triggered by intermittent renewable power generation. A reduction of 34% of the structural imbalances in the system is achieved by using the continuous-time model.

1. Introduction

The Norwegian power system is in an interesting state of transition towards tighter integration to the rest of Europe. New high-voltage direct current (HVDC) cable interconnections to Germany and Great Britain are under construction, which increases the potential of cross-zonal trading of both energy and balancing services. Hydropower dominates the Norwegian generation mix and is well suited to provide system balancing services due to its flexibility. A larger share of intermittent renewable generation means that hydropower will play an increasingly important role in providing flexibility to the interconnected North European system in the future. However, propagating the flexibility across HVDC cables is challenging with current practices related to the hourly day-ahead market structure. According to the Norwegian transmission system operator Statnett, changing the HVDC cable flow between areas on an hourly basis has the potential of increasing the structural (or deterministic) imbalances caused by the mismatch in the scheduled hourly production and real-time load [1]. In this paper, a modified version of the continuous-time optimization framework is proposed to impose a smooth and continuous flow of power between a hydropower area and a thermal area connected by an HVDC cable.

Continuous-time optimization was originally used to accurately describe the cost of ramping scarcity in thermal systems with large amounts of renewable power generation, such as the power system in California [2]. Ramping restrictions can be directly applied to the derivatives of the decision variables when they are allowed to be continuous and smooth functions of time instead of the usual piece-wise constant formulation. The continuous-time formulation relies on limiting the decision variables to be polynomials of degree r, which allows the variables to be expressed by the Bernstein polynomials of the same degree. The optimization problem can then be defined in terms of the coefficients of the Bernstein polynomials, which is a mixed-integer linear program (MILP) in the case of the unit commitment problem. The continuous-time framework has lately been expanded in several directions. The existence of a continuous-time marginal price for the economic dispatch problem was proven and calculated in [3] for a thermal system. This work was later extended to include energy storage devices in [4], which has applications in optimal control of charging electric vehicles according to queue theory [5,6] and the scheduling of batteries in balancing markets [7]. A stochastic continuous-time model was formulated for unit commitment and reserve scheduling problem in [8], with the inclusion of energy storage in [9] and a method for load

* Corresponding author.
E-mail address: christian.naversen@ntnu.no (C.Ø. Naversen).

https://doi.org/10.1016/j.epsr.2020.106787
Received 1 October 2019; Received in revised form 17 April 2020; Accepted 2 August 2020
Available online 13 August 2020

Nomenclature

Sets and indices

$\mathcal{J}$	Thermal generators, index j
$\mathcal{K}$	Water value cuts, index k
$\mathcal{L}$	HVDC cables, index l
$\mathcal{M}$	Hydropower plants and reservoirs, index m
$\mathcal{A}$	Areas in the system, index a
$\mathcal{I}_m^{d/b/o}$	Reservoirs that discharge/bypass/spill into m, index i
$\mathcal{N}_m$	Discharge segments in plant m, index n
$\mathcal{T}$	Time intervals, index h

Variables

α	Future expected system cost [mu]
$\bar{s}_m^{\uparrow/\downarrow}(t)$	Startup/shutdown of hydropower plant [MW]
$f_l(t)$, $\boldsymbol{f}_{lh}$	Flow on HVDC cable [MW]
$g_j(t)$, $\boldsymbol{g}_{jh}$	Generated thermal power [MW]
$p_m(t)$, $\boldsymbol{p}_{mh}$	Generated hydropower [MW]
$q_m^b(t)$, $\boldsymbol{q}_{mh}^b$	Flow through bypass gate [m^3/s]
$q_m^d(t)$, $\boldsymbol{q}_{mh}^d$	Flow through turbine [m^3/s]
$q_m^{net}(t)$, $\boldsymbol{q}_{mh}^{net}$	Net flow into reservoir [m^3/s]
$q_m^{out}(t)$, $\boldsymbol{q}_{mh}^{out}$	Total controlled flow out of reservoir [m^3/s]
$q_m^{in}(t)$, $\boldsymbol{q}_{mh}^{in}$	Total controlled flow into reservoir [m^3/s]
$q_m^o(t)$, $\boldsymbol{q}_{mh}^o$	Flow through spill gate [m^3/s]
$q_m^{rel}(t)$, $\boldsymbol{q}_{mh}^{rel}$	Total flow released out of reservoir [m^3/s]
$q_{mn}^s(t)$, $\boldsymbol{q}_{mnh}^s$	Flow through discharge segment [m^3/s]
$s_j^{\uparrow/\downarrow}(t)$	Startup/shutdown of thermal generator [MW]
$u_j(t)$	State of thermal unit, on/off
$v_m(t)$	Reservoir volume [m^3]
$w_{mn}(t)$	Discharge segment commitment decision
$z_m(t)$	State of hydropower unit, on/off

Parameters

δ_h	Length of time interval [s]
η_{mn}	Energy conversion factor [MWs/m^3]
C^b	Penalty for bypassing water [mu/m^3]
C^o	Penalty for spilling water [mu/m^3]
C_j	Marginal cost of thermal generator [mu/MW]
$C_j^{\uparrow/\downarrow}$	Thermal unit startup/shutdown cost [mu]
D_k	Water value cut constant [mu]
$F_l^{\max}$	Maximal flow limit on HVDC cable [MW]
$G_j^{max/min}$	Maximal/minimal thermal capacity [MW]
G_{la}	Line flow direction coefficient
$I_m^u(t)$	Natural inflow from creek intakes [m^3/s]
$I_m(t)$	Natural inflow into reservoir [m^3/s]
$L_a(t)$	Net area load [MW]
N	Number of time intervals in $\mathcal{T}$
$P_m^{max/min}$	Maximal/minimal hydropower capacity [MW]
Q_m^b	Maximal flow through bypass gate [m^3/s]
Q_m^d	Maximal flow through turbine [m^3/s]
Q_{mn}^s	Maximal flow through turbine segment [m^3/s]
$R_j^{\uparrow/\downarrow}$	Thermal ramping gain for starts/stops [MW/s]
$R_j^{u/d}$	Ramping limits of running thermal unit [MW/s]
$R_l^{u/d}$	Ramping limits of HVDC cable flow [MW/s]
V_m^0	Initial reservoir volume [m^3]
V_m	Maximal reservoir capacity [m^3]
WV_{mk}	Water value cut coefficient [mu/m^3]

estimation and scenario generation in [10]. Applications to other areas within the power system operations field are also emerging, such as the active distribution network model in [11].

Hydrothermal scheduling has been an active field of research for decades, which in turn has contributed to the advanced mathematical models used for system and operational planning in hydropower-dominated systems. Good examples of this are the models used in Norway [12–14] and Brazil [15,16]. Previous hydrothermal scheduling models have been based on the standard discrete-time formulation, which assumes piece-wise constant values for time-dependent variables and model input parameters. This paper concerns the novel integration of hydrothermal scheduling and the continuous-time framework. In particular, the integrated modeling of continuous-time operation of complex hydropower cascades poses several new challenges to both hydropower scheduling and continuity constraints. The novel contributions of this paper are outlined as follows:

- A continuous-time model including hydropower, thermal generation, and HVDC cables is formulated and studied. To the best of the authors' knowledge, this has not been published previously.
- A method for modelling the forbidden production zone of the hydropower production curve in the continuous-time framework is presented. This involves enforcing the continuity constraints on the sum of generated hydropower instead of on the individual plants.
- The issue of correct uploading of piece-wise linearized variables in the continuous-time framework is highlighted in relation to the hydropower production function, and a binary variable solution is presented.

Section 2 presents the novel continuous-time model in detail, which is then solved for a two-area system and compared to a discrete-time (hourly) model in Section 3. Concluding remarks are given in Section 4.

2. Model

2.1. Fundamentals of a continuous-time model

The core idea of the continuous-time framework is to represent time-dependent input and decision variables as polynomials of time instead of piece-wise constant functions. This increases the complexity of the model formulation, but sub-hourly effects and constraints related to derivatives with respect to time are easily captured. The motivation behind the original continuous-time unit commitment model in [2] was precisely to incorporate the impact of ramping scarcity into the market clearing. The time-dependent decision variables in the typical continuous-time optimization framework are defined through the Bernstein polynomials of degree r, $\boldsymbol{B}_r(t)$, which form a basis for any polynomials of at most degree r on the time interval [0,1]. By splitting the time horizon of the model into N intervals $h \in \mathcal{T}$ of length δ_h, the time-dependent decision variables can be expressed as polynomials of the form

$$x(t) = \sum_{h \in \mathcal{T}} \boldsymbol{x}_h^T \cdot \boldsymbol{B}_r(\tau_h)\Pi(\tau_h), \tag{1}$$

where τ_h and $\Pi(\tau_h)$ are defined as follows:

$$\tau_h = \frac{1}{\delta_h}\left(t - \sum_{i<h} \delta_i\right) \qquad \forall\, h \in \mathcal{T}, \tag{2}$$

$$\Pi(\tau_h) = \begin{cases} 1, & 0 \le \tau_h \le 1 \\ 0, & \text{otherwise} \end{cases} \qquad \forall\, h \in \mathcal{T}. \tag{3}$$

The vectors $\boldsymbol{x}_h$ contain the $r+1$ coefficients of the Bernstein polynomials in each time interval, which become the decision variables of the continuous-time model. It is necessary to use the scaled time τ_h and the operator Π to project the Bernstein polynomials into the correct

time interval while maintaining their property as basis functions. One of the main reason for using Bernstein polynomials is the convex hull property, which makes it possible to impose inequality constraints on $x(t)$ for all times t by directly bounding the coefficients $\boldsymbol{x}_h$ [2]. This paper uses Bernstein polynomials of degree 3 as the basis:

$$\boldsymbol{B}_3(t) = [(1-t)^3,\ \ 3t(1-t)^2,\ \ 3t^2(1-t),\ \ t^3]^T. \tag{4}$$

This is a popular choice in the literature, as it keeps the size of the model reasonable without sacrificing the ability to model complex time dependencies. Another advantage is the linear relationship to the cubic Hermite splines $\boldsymbol{H}(t)$, which can be used as an equivalent basis:

$$\boldsymbol{H}(t) = \begin{bmatrix} 1 & 1 & 0 & 0 \\ 0 & \frac{1}{3} & 0 & 0 \\ 0 & 0 & 1 & 1 \\ 0 & 0 & -\frac{1}{3} & 0 \end{bmatrix} \cdot \boldsymbol{B}_3(t) \equiv \boldsymbol{W} \cdot \boldsymbol{B}_3(t). \tag{5}$$

The coefficients of the Hermite splines have a physical interpretation as the value of $x(t)$ and its derivative $\dot{x}(t)$ at the start and end of the time interval h:

$$\boldsymbol{x}_h^{\boldsymbol{H}} = (\boldsymbol{W}^{-1})^T \cdot \boldsymbol{x}_h = [x_h^{start},\ \dot{x}_h^{start},\ x_h^{end},\ \dot{x}_h^{end}]^T. \tag{6}$$

This interpretation is useful for expressing the continuity of $x(t)$ across the time intervals h. The reader is referred to [2] for a more detailed introduction to the continuous-time formulation with further references to the properties of the Bernstein polynomials mentioned in this section.

2.2. Objective function

The objective of the proposed hydrothermal model is to minimize the future expected cost of the system, the penalties for bypassing and spilling water, and the operational, startup and shutdown costs of the thermal generators:

$$\begin{aligned} Z \ = \ & \alpha + \sum_{m \in \mathcal{M}} \int_0^{t^{end}} (C^b q_m^b(t) + C^o q_m^o(t))dt \\ & + \sum_{j \in \mathcal{J}} \int_0^{t^{end}} C_j g_j(t) dt + \sum_{j \in \mathcal{J}} \sum_{h \in \mathcal{T}} (C_j^{\uparrow} s_{jh}^{\uparrow} + C_j^{\downarrow} s_{jh}^{\downarrow}). \end{aligned} \tag{7}$$

Note that startup and shutdown cost are assumed to be negligible for the hydropower plants. The definite integral of the Bernstein polynomials of the third degree is $\int_0^1 \boldsymbol{B}_3(t)dt = \frac{1}{4}\boldsymbol{1}$, which simplifies the integrals in (7) to the sums

$$\begin{aligned} Z \ = & \alpha + \frac{1}{4} \sum_{m \in \mathcal{M}} \sum_{h \in \mathcal{T}} \delta_h \boldsymbol{1}^T \cdot (C^b \boldsymbol{q}_{mh}^b + C^o \boldsymbol{q}_{mh}^o) \\ & + \sum_{j \in \mathcal{J}} \sum_{h \in \mathcal{T}} \left(\frac{1}{4} \delta_h C_j \boldsymbol{1}^T \cdot \boldsymbol{g}_{jh} + C_j^{\uparrow} s_{jh}^{\uparrow} + C_j^{\downarrow} s_{jh}^{\downarrow} \right). \end{aligned} \tag{8}$$

As this paper focuses on modelling hydropower generation in the continuous-time framework, a simplified linear formulation of the thermal generation cost function is used in (8). More advanced modeling of quadratic and piece-wise linear cost functions in continuous-time unit commitment are available in the literature [2,9], and their integration in the model proposed in this paper is straightforward.

2.3. Hydropower topology constraints

The cascaded topology constraints dictate how water moves between the reservoirs. These constraints are equality constraints, see for instance [14], which means that equating the polynomial coefficients are sufficient to satisfy them in the continuous-time framework. The convex hull property of the Bernstein polynomials and the fact that $\boldsymbol{1}^T \cdot \boldsymbol{B}_3(t) = 1$ is used to enforce the physical bounds on the variables:

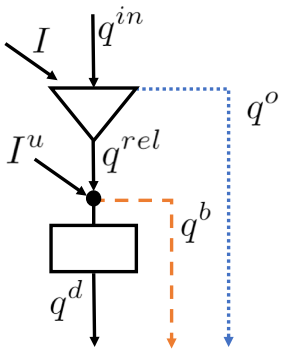

Fig. 1. Depiction of the different waterways for discharging, bypassing and spilling water between reservoirs. All waterways may lead to different downstream reservoirs or out of the system. Natural inflow enters the system in two different ways, either into the reservoir (triangle shape) or directly into the main tunnel of the plant (rectangle shape).

$$\boldsymbol{q}_{mh}^{net} = \boldsymbol{I}_{mh} + \boldsymbol{q}_{mh}^{in} - \boldsymbol{q}_{mh}^{out} \qquad \forall\ m, h \in \mathcal{M}, \mathcal{T} \tag{9}$$

$$\mathbf{q}_{mh}^{out} = \mathbf{q}_{mh}^{rel} + \mathbf{q}_{mh}^{o} \ \forall\ m, h \in \mathcal{M}, \mathcal{T} \tag{10}$$

$$\mathbf{q}_{mh}^{in} = \sum_{i \in I_m^d} \mathbf{q}_{ih}^{d} + \sum_{i \in I_m^b} \mathbf{q}_{ih}^{b} + \sum_{i \in I_m^o} \mathbf{q}_{ih}^{o} \ \forall\ m, h \in \mathcal{M}, \mathcal{T} \tag{11}$$

$$\mathbf{q}_{mh}^{rel} = \mathbf{q}_{mh}^{d} + \mathbf{q}_{mh}^{b} - \mathbf{I}_{mh}^{u} \ \forall\ m, h \in \mathcal{M}, \mathcal{T} \tag{12}$$

$$\mathbf{0} \le \mathbf{q}_{mh}^{d} \le Q_m^d \mathbf{1} \ \forall\ m, h \in \mathcal{M}, \mathcal{T} \tag{13}$$

$$\mathbf{0} \le \mathbf{q}_{mh}^{b} \le Q_m^b \mathbf{1} \ \forall\ m, h \in \mathcal{M}, \mathcal{T} \tag{14}$$

$$\mathbf{0} \le \mathbf{q}_{mh}^{o} \ \forall\ m, h \in \mathcal{M}, \mathcal{T} \tag{15}$$

$$\mathbf{0} \le \mathbf{q}_{mh}^{rel} \ \forall\ m, h \in \mathcal{M}, \mathcal{T}. \tag{16}$$

There are three waterways that connect reservoirs; discharge through the turbine, the bypass gate and the spill gate. Fig. 1 shows the relationship between the different waterways in addition to where natural inflow enters the system.

2.4. Volume constraints

The rate of change in the reservoir content is described by the differential equation:

$$\frac{dv_m(t)}{dt} = q_m^{net}(t) \qquad \forall\ m \in \mathcal{M}. \tag{17}$$

The integral of Bernstein polynomials of degree 3 can be expressed using Bernstein polynomials of degree 4 using a linear mapping matrix [4,9]:

$$\int \boldsymbol{B}_3(t)dt = \frac{1}{4} \begin{bmatrix} 0 & 1 & 1 & 1 & 1 \\ 0 & 0 & 1 & 1 & 1 \\ 0 & 0 & 0 & 1 & 1 \\ 0 & 0 & 0 & 0 & 1 \end{bmatrix} \boldsymbol{B}_4(t) \equiv \boldsymbol{N} \cdot \boldsymbol{B}_4(t) \tag{18}$$

which is further utilized to show the volume increase within a time interval h as follows:

$$\begin{aligned} v_m(t) - v_{mh} &= \int_{t(h)}^{t} \frac{dv(t')}{dt'} dt' = (\mathbf{q}_{mh}^{net})^T \cdot \int_{t(h)}^{t} \mathbf{B}_3(\tau_h') dt \\ &= \delta_h (\mathbf{q}_{mh}^{net})^T \cdot \mathbf{N} \cdot \mathbf{B}_4(\tau_h). \end{aligned} \tag{19}$$

Here, $t(h) = \sum_{i<h} \delta_i$ and the fact that $\boldsymbol{N} \cdot \boldsymbol{B}_4(0) = \boldsymbol{0}$ was used. Note that the volume variables v_{mh} denotes the volume at the start of interval h. Based on equation (19), the following volume balance constraints can

be added to the optimization problem:

$$v_{m0} = V_m^0 \ \forall\ m \in \mathcal{M} \tag{20}$$

$$v_{m,h+1} - v_{mh} = \frac{1}{4}\delta_h \boldsymbol{1}^T \cdot \mathbf{q}_{mh}^{net} \qquad \forall\ m, h \in \mathcal{M}, \mathcal{T} \tag{21}$$

$$\mathbf{0} \le v_{mh}\mathbf{1} + \delta_h \mathbf{N}^T \cdot \mathbf{q}_{mh}^{net} \le V_m \mathbf{1} \ \forall\ m, h \in \mathcal{M}, \mathcal{T}. \tag{22}$$

Constraint (20) sets the initial volume of each reservoir and (21) calculates the volume change from one time interval to the next by inserting $\boldsymbol{N}\cdot\boldsymbol{B}_4(1) = \frac{1}{4}\boldsymbol{1}$. Constraint (22) uses the convex hull property to bound the volume within the limits of the reservoir for all times t.

2.5. Future cost bounds

The future expected cost of the system is represented by a set of Benders cuts created by a hydrothermal long-term model such as [14]. The expected future cost depends on the state of all hydropower reservoirs in the system at the end of the last time interval N:

$$\alpha \ge \sum_{m\in\mathcal{M}} WV_{mk} v_{m,N+1} + D_k \qquad \forall\ k \in \mathcal{K}. \tag{23}$$

2.6. Hydropower production

The conversion from discharge through the turbine to generated power is a non-linear function which depends on the effective plant head and the efficiency curves of the turbine and generator [17]. By assuming a constant head for the planning horizon, the hydropower production function can be approximated as a single piece-wise linear curve, where the discharge variable is split into $n \in \mathcal{N}_m$ segments with constant gradient η_n. In an discrete-time model, the discharge segments will usually be uploaded in the correct order as long as the gradient is decreasing for increasing segment number. The exception is extreme situations where it is beneficial to dump as much water as possible while limiting the power produced, which can be the case in high inflow and low load scenarios. A similar effect of incorrect uploading of discharge segments has been observed in this work when the continuous-time framework was implemented. Segments with high efficiency are still favoured but there is no guarantee that segment n is at its maximal capacity for all times that segment $n+1$ is being used. The model will often start using the next segment too early to be able to fulfill the continuous-time power balance described in Section 2.7. To remedy this problem, binary variables $w_{mn}(t) = \sum_{h\in\mathcal{T}} w_{mnh}\boldsymbol{1}^T\cdot\boldsymbol{B}_3(\tau_h)\Pi(\tau_h)$ are used in this work to force the segments to be fully utilized before the next segment can be used:

$$\mathbf{q}_{mh}^d = \sum_{n\in\mathcal{N}_m} \mathbf{q}_{mnh}^s \qquad \forall\ m, h \in \mathcal{M}, \mathcal{T} \tag{24}$$

$$\mathbf{p}_{mh} = \sum_{n\in\mathcal{N}_m} \eta_{mn}\mathbf{q}_{mnh}^s \qquad \forall\ m, h \in \mathcal{M}, \mathcal{T} \tag{25}$$

$$Q_{mn}^s w_{mnh}\mathbf{1} \le \mathbf{q}_{mnh}^s \le Q_{mn}^s \mathbf{1} \ \forall\ m, h, n \in \mathcal{M}, \mathcal{T}, \mathcal{N}_m \tag{26}$$

$$\mathbf{q}_{mnh}^s \le Q_{mn}^s w_{m,n-1,h}\mathbf{1} \ \forall\ m, h, n \in \mathcal{M}, \mathcal{T}, \mathcal{N}_m\setminus\{0\}. \tag{27}$$

This modelling choice of the hydropower production function has the unfortunate effect of introducing additional binary variables into the model but also enables the use of non-concave linearizations of the hydropower production function. It is also possible to incorporate forbidden production regions within the operating range of the turbine by modifying (26) to $\mathbf{q}_{mnh}^s = Q_{mn}^s w_{mnh}\boldsymbol{1}$ for the segment representing the forbidden region.

2.7. Power balance and HVDC power flow

The power balance constraints must be satisfied in each node of the system. In this work, each node represents a larger market area assuming no internal power flow limits. The areas are connected with HVDC cables where the flow can be controlled by the system operator. The power balance constraints are formulated as

$$\sum_{m\in\mathcal{M}_a} \mathbf{p}_{mh} + \sum_{j\in\mathcal{J}_a} \mathbf{g}_{jh} - \sum_{l\in\mathcal{L}} G_{la}\mathbf{f}_{lh} = \mathbf{L}_{ah} \ \forall\ a, h \in \mathcal{A}, \mathcal{T}. \tag{28}$$

The coefficient G_{la} dictates the positive and negative direction of flow on each cable $l \in \mathcal{L}$ by taking the values ± 1, or zero if cable l is not connected to area a. $\mathcal{M}_a$ and $\mathcal{J}_a$ are the sets of hydropower and thermal units located in area a, respectively. The flow on the HVDC cables is constrained by maximal flow limits

$$-F_l^{max}\boldsymbol{1} \le \boldsymbol{f}_{lh} \le F_l^{max}\boldsymbol{1} \qquad \forall\ l, h \in \mathcal{L}, \mathcal{T}, \tag{29}$$

and additional limitations on the change of flow is imposed on the derivative $\dot{f}_l(t)$ to stay within the specified HVDC cable ramping limits used in the Nordic system [18]. By using the following property of the Bernstein polynomials,

$$\frac{d\boldsymbol{B}_3(t)}{dt} = 3\begin{bmatrix} -1 & 0 & 0 \\ 1 & -1 & 0 \\ 0 & 1 & -1 \\ 0 & 0 & 1 \end{bmatrix}\cdot\boldsymbol{B}_2(t) \equiv \boldsymbol{K}\cdot\boldsymbol{B}_2(t), \tag{30}$$

the minimum and maximum ramping limits can be expressed as:

$$-R_l^d\boldsymbol{1}^T \le \frac{1}{\delta_h}\boldsymbol{f}_{lh}^T\cdot\boldsymbol{K} \le R_l^u\boldsymbol{1}^T \qquad \forall\ l, h \in \mathcal{L}, \mathcal{T}. \tag{31}$$

2.8. Thermal generation constraints

The thermal generators are subject to unit commitment decisions which signify if a generator is offline or producing between the minimal and maximal production limits. The thermal unit commitment constraints are modelled by the use of the binary decision variables $u_j(t)$:

$$G_j^{\min}\mathbf{u}_{jh} \le \mathbf{g}_{jh} \le G_j^{\max}\mathbf{u}_{jh} \ \forall\ j, h \in \mathcal{J}, \mathcal{T} \tag{32}$$

$$\mathbf{u}_{jh} = [u_{jh}, u_{jh}, u_{j,h+1}, u_{j,h+1}]^T \ \forall\ j, h \in \mathcal{J}, \mathcal{T}\setminus\{N\} \tag{33}$$

$$\mathbf{u}_{jN} = u_{jN}\mathbf{1} \ \forall\ j \in \mathcal{J} \tag{34}$$

$$s_{jh}^{\uparrow} - s_{jh}^{\downarrow} = u_{j,h+1} - u_{jh} \ \forall\ j, h \in \mathcal{J}, \mathcal{T}\setminus\{N\} \tag{35}$$

$$s_{jh}^{\uparrow} + s_{jh}^{\downarrow} \le 1 \ \forall\ j, h \in \mathcal{J}, \mathcal{T} \tag{36}$$

$$u_{jh}, s_{jh}^{\uparrow/\downarrow} \in \{0, 1\} \ \forall\ j, h \in \mathcal{J}, \mathcal{T}. \tag{37}$$

The constraints closely follow the implementation used in [2] and [8], which are in turn adapted from the standard discrete-time unit commitment formulation found in for instance [19]. The choice of the commitment decision vector in (33) and (34) allows the thermal generator to use time interval h to ramp up from zero to above $G^{\min}$, or conversely ramp down production to zero. The smooth transition is necessary for the continuity constraints that will be applied to the thermal production variables in Section 2.10. Constraint (35) captures the startups and shutdowns of the generators, which are accounted for in the objective function (8). The up and down ramping constraints of thermal generators, taking into account the startup and shutdown ramp limitations, are modeled as follows:

$$\frac{1}{\delta_h}\mathbf{g}_{jh}^T\cdot\boldsymbol{K} \le (R_j^u + R_j^{\uparrow}s_{jh}^{\uparrow})\boldsymbol{1}^T \qquad \forall\ j, h \in \mathcal{J}, \mathcal{T} \tag{38}$$

$$\frac{1}{\delta_h}\mathbf{g}_{jh}^T\cdot\boldsymbol{K} \ge -(R_j^d + R_j^{\downarrow}s_{jh}^{\downarrow})\boldsymbol{1}^T \qquad \forall\ j, h \in \mathcal{J}, \mathcal{T}. \tag{39}$$

The minimum up and down time constraints of thermal generation is not considered in this paper, and the readers are referred to our previous works for details on modeling these constraints in the continuous-time unit commitment model [2].

2.9. Hydropower unit commitment

Due to operating characteristics such as mechanical vibration or loss of efficiency, hydropower turbines usually have one or several forbidden production regions depending on the turbine type. It is important to model these regions when looking at short-term scheduling of a hydropower system to have an accurate representation of the operating range of the hydropower plants. The unit commitment constraints of the hydropower plants in the continuous-time optimization model must account for the forbidden production region so that the flexibility of the plant is not overestimated. The hydropower unit commitment decisions $z_m(t)$ are used to model this in the following way:

$$P_m^{\min} \mathbf{z}_{mh} \leq \mathbf{p}_{mh} \leq P_m^{\max} \mathbf{z}_{mh} \;\forall\, m,\, h \in \mathcal{M},\, \mathcal{T} \tag{40}$$

$$\mathbf{z}_{mh} = z_{mh}\mathbf{1} \;\forall\, m,\, h \in \mathcal{M},\, \mathcal{T} \tag{41}$$

$$\bar{s}_{mh}^{\uparrow} - \bar{s}_{mh}^{\downarrow} = z_{m,h+1} - z_{mh} \;\forall\, m,\, h \in \mathcal{M},\, \mathcal{T}\backslash\{N\} \tag{42}$$

$$\bar{s}_{mh}^{\uparrow} + \bar{s}_{mh}^{\downarrow} \leq 1 \;\forall\, m,\, h \in \mathcal{M},\, \mathcal{T} \tag{43}$$

$$z_{mh},\, \bar{s}_{mh}^{\uparrow/\downarrow} \in \{0,\, 1\} \;\forall\, m,\, h \in \mathcal{M},\, \mathcal{T}. \tag{44}$$

In contrast to the choice of the thermal unit commitment vector in (33), the formulation in (41) forces the hydropower unit commitment decisions to be constant for the whole time interval so that the production is never between 0 and $P^{\min}$. However, this formulation is in opposition to the normal continuous-time formulation, as discontinuous jumps in power production must be allowed. If not, the hydropower plants will be unable to start and stop at all. These issues are addressed in Section 2.10.

2.10. Continuity constraints

The standard continuous-time optimization framework builds on the C^1 continuity of all decision variables $x(t)$. This requires both the value $x(t)$ and the value of the derivative $\dot{x}(t)$ to be continuous over the change of time intervals $h \in \mathcal{T}$. Such constraints are enforced by using the relationship between the Bernstein polynomials and the cubic spline functions, shown in (5). The interpretation of the coefficients of $\boldsymbol{H}(t)$ described in (6) simplifies the implementation of the C^1 continuity constraints. By labelling the components of the vector $\boldsymbol{x}$ as $\boldsymbol{x}[i]$ for $i \in \{0,\, 1,\, 2,\, 3\}$, the continuity constraints become:

$$\boldsymbol{x}_h^{\boldsymbol{H}}[2] = \boldsymbol{x}_{h+1}^{\boldsymbol{H}}[0] \qquad \forall\, h \in \mathcal{T}\backslash\{N\} \tag{45}$$

$$\boldsymbol{x}_h^{\boldsymbol{H}}[3] = \boldsymbol{x}_{h+1}^{\boldsymbol{H}}[1] \qquad \forall\, h \in \mathcal{T}\backslash\{N\}. \tag{46}$$

These constraints are applied to the thermal generation and HVDC flow variables:

$$\boldsymbol{g}_{jh}^{\boldsymbol{H}}[2] = \boldsymbol{g}_{j,h+1}^{\boldsymbol{H}}[0] \qquad \forall\, j,\, h \in \mathcal{J},\, \mathcal{T}\backslash\{N\} \tag{47}$$

$$\boldsymbol{g}_{jh}^{\boldsymbol{H}}[3] = \boldsymbol{g}_{j,h+1}^{\boldsymbol{H}}[1] \qquad \forall\, j,\, h \in \mathcal{J},\, \mathcal{T}\backslash\{N\} \tag{48}$$

$$\boldsymbol{f}_{lh}^{\boldsymbol{H}}[2] = \boldsymbol{f}_{l,h+1}^{\boldsymbol{H}}[0] \qquad \forall\, l,\, h \in \mathcal{L},\, \mathcal{T}\backslash\{N\} \tag{49}$$

$$\boldsymbol{f}_{lh}^{\boldsymbol{H}}[3] = \boldsymbol{f}_{l,h+1}^{\boldsymbol{H}}[1] \qquad \forall\, l,\, h \in \mathcal{L},\, \mathcal{T}\backslash\{N\}. \tag{50}$$

As mentioned in Section 2.9, discontinuous jumps in power production are required to model the forbidden production region of hydropower plants. Therefore, enforcing the C^1 continuity constraints on the variables related to the hydropower production is not possible. In addition, requiring continuous derivatives for water flow and hydropower production is strict when δ_h is longer than a few minutes. To avoid conservative solutions underestimating the ramping capabilities of hydropower, (46) is not implemented for any variable related to hydropower. The bypass and overflow variables are C^0 continuous:

$$\boldsymbol{q}_{mh}^{b,\boldsymbol{H}}[2] = \boldsymbol{q}_{m,h+1}^{b,\boldsymbol{H}}[0] \qquad \forall\, m,\, h \in \mathcal{M},\, \mathcal{T}\backslash\{N\} \tag{51}$$

$$\boldsymbol{q}_{mh}^{o,\boldsymbol{H}}[2] = \boldsymbol{q}_{m,h+1}^{o,\boldsymbol{H}}[0] \qquad \forall\, m,\, h \in \mathcal{M},\, \mathcal{T}\backslash\{N\}, \tag{52}$$

and the reservoir volume continuity is already secured by (21). The hydropower production is forced to be C^0 continuous unless a startup or shutdown happens in the time interval. This is modelled by replacing (45) by the following two inequalities:

$$\mathbf{p}_{mh}^{\mathbf{H}}[2] - \mathbf{p}_{m,h+1}^{\mathbf{H}}[0] \leq P_m^{\max} \bar{s}_{mh}^{\downarrow} \;\forall\, m,\, h \in \mathcal{M},\, \mathcal{T}\backslash\{N\} \tag{53}$$

$$\mathbf{p}_{m,h+1}^{\mathbf{H}}[0] - \mathbf{p}_{mh}^{\mathbf{H}}[2] \leq P_m^{\max} \bar{s}_{mh}^{\uparrow} \;\forall\, m,\, h \in \mathcal{M},\, \mathcal{T}\backslash\{N\} \tag{54}$$

which is consistent with the unit commitment constraints imposed in (40) to (44). Note that this relaxation produces a more constrained problem, as production in the forbidden region is impossible. Due to the connection between production and discharge in (25), the discharge variables $\boldsymbol{q}^s$ must also be allowed to have discontinuous jumps. However, the binary definitions of the discharge bounds in (26) and (27) take care of continuity when the hydropower plant is producing, so there is no need to apply any further constraints to the discharge variables. The continuity properties of the derived flow variables $\boldsymbol{q}^{net}$, $\boldsymbol{q}^{out}$, $\boldsymbol{q}^{in}$, and $\boldsymbol{q}^{rel}$ are also implicitly accounted for through (9) to (12).

It is important to note that even though the individual hydropower plants may have discontinuous jumps and discontinuous derivatives in the power production curve between time intervals, their sum is still forced to be C^1 continuous through the power balance constraint (28) since all other quantities in the equation are C^1 continuous. The C^1 continuity constraints of the flexible hydropower have effectively been lifted from the individual plant to the sum on an area level. The hydropower model formulation presented in this paper can be seen as an approximation of a fully C^1 continuous model where short time intervals have been inserted around every major time interval shift. By forcing the hydropower plants to only start or stop in these short intervals, an accurate production profile spending minimal time in the forbidden production zone would be achieved. By letting the length of short intervals go to zero, the partially C^0 continuous hydropower formulation used in this paper is recovered. Therefore, the alterations made to the continuity constraints for the hydropower-related variables will not drastically impact the operation of the hydropower, as long as δ_h is long compared to the time it takes to ramp up and down a hydropower plant, which is usually only a few minutes.

3. Case study

A small scale case study with two areas connected by a single HVDC cable is presented in this section. The continuous-time model proposed in Section 2 and an analogous discrete-time hourly model are both solved to show and compare the interaction between fast and slow ramping components in the system. Both models have been implemented in Pyomo and solved with CPLEX 12.8. One area contains only hydropower, while the other only contains thermal generation. The hydropower topology is based on a real Norwegian water course consisting of 12 reservoirs and plants which is described in more detail in [20], and the future expected cost of the hydropower system is calculated based on the long-term model described in [14]. The inflow is considered piece-wise constant within each hour in the entire hydropower area, which has a total hydropower production capacity of 537 MW. The thermal area contains four thermal generators with a total of 256 MW of production capacity and varying ramping capabilities and marginal, startup and shutdown costs. The areas are connected by an HVDC cable with a flow limit of 50 MW in either direction. The ramping limitations of the cable are based on the current practice of how fast the flow on an HVDC cable can be changed in the Nordic market, which is 600 MW/h [18]. The flow change is performed in a 20 min window around hourly shifts, which gives an effective ramping rate of 30 MW/min or 1800 MW/h [1]. The time horizon is set to 24 hours with hourly time intervals for both the hourly and the continuous-time model.

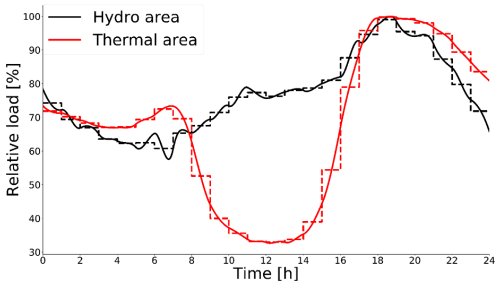

Fig. 2. The continuous-time load profiles of the thermal and hydropower areas are shown together with the hourly constant load approximations (solid and dashed lines, respectively). The profiles have been scaled by the value of the peak load.

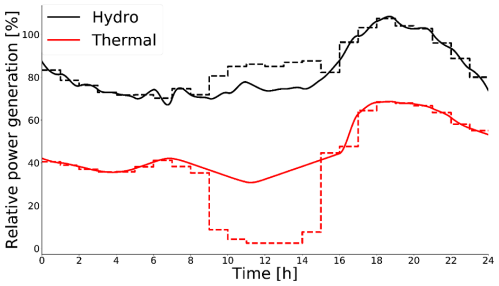

Fig. 3. The sum production in the thermal and hydropower areas relative to their respective load peaks in the hourly and continuous-time solution. The hourly and continuous-time solutions are shown as dashed and solid lines, respectively.

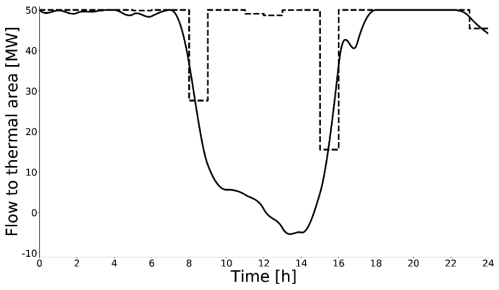

Fig. 4. The HVDC cable power flow from the hydropower area to the thermal area in the hourly (dashed line) and continuous-time (solid line) models. Negative values indicate flow in the opposite direction.

The scaled net load profiles for the two areas are shown in Fig. 2. The peak net load value in each area is used as a scale in the figure, which is 450 MW and 160 MW in the hydropower and thermal areas, respectively. The net load profiles are based on measured data from NYISO and CAISO from 1/1-2019, available at [21,22] with a 5-minute resolution. The CAISO net load has been used for the thermal area, which experiences significant ramping events in the morning and afternoon as solar plants start and stop producing power. The continuous-time load was calculated from the raw data by a standard least-squares error fit to the Bernstein polynomials, while the hourly load is the average load for each hour. The structural imbalances in both areas go down in the continuous-time model compared to the hourly model, with a reduction of 34% on system level. This represents 97 MWh of saved balancing energy, which is 0.9% of the total daily net system load. The reduction of imbalances is higher in the thermal area (87%) than the hydropower area (20%) because $\boldsymbol{B}_3(t)$ provides a better fit to the CAISO load data.

The size and solution times of the models are listed in Table 1, which shows the initial model size and the reduced size after CPLEX performs an automatic presolve routine. The number of continuous and binary variables and constraints are considerably higher in the continuous-time model compared to the hourly model, also after the presolve. The larger model size of the continuous-time model results in a longer solution time on a standard office laptop, i7-7600 CPU at 2.8 GHz with 4 cores, though solution time in MIP models can vary greatly based on the parameter settings given to the solver. A small relative MIP gap of 0.28% was reached in 60 seconds for the continuous-time model, but solving it to zero gap like the hourly model takes about 10 hours on a server with 36 cores. Upon investigation, it is clear that the hydropower production continuity constraints, (53) and (54), are the complicating constraints. If these constraints are removed, which means the hydropower production variables are discontinuous over the interval changes, the continuous-time model can be solved to zero MIP gap in 22 seconds. This is a trade-off between realistic physical modelling and tractability that should be considered when solving larger systems.

Table 1
Model size comparison of the continuous-time and hourly models. The problem size after the CPLEX presolve routine is listed under reduced model.

Parameter	Initial model		Reduced model	
	Hourly	Cont.-time	Hourly	Cont.-time
Binary variables	1152	2040	1106	1706
Continuous variables	2474	8954	2179	7371
Constraints	2706	16,962	2316	13,107
Solution time [s]			2.2	60.0
MIP gap [%]			0.0	0.28

The resulting sum production of hydropower and thermal generators are shown in Fig. 3. The figure shows that the hourly model overestimates the ramping capabilities of the thermal system during the extreme ramping events. Thermal production is shut down in the morning and turned back on in the afternoon, while the hydropower producers increase their production to cover the load in both areas in the meantime. This is not the case in the continuous-time model, as shutting down all thermal generators is either infeasible or very costly when following the net load during the ramping events. The cheapest and slowest thermal generator stays on for the whole 24 hours in the continuous-time model, contributing to the ramping in a modest way.

Most of the ramping is carried out by the hydropower system through the HVDC cable, which can be seen in Fig. 4. The figure shows how the hydropower system is able to mitigate the ramping in net load in both directions while keeping the thermal generator online. The power flow is kept close to 50 MW throughout the day in the hourly model since the hydropower is generally cheaper than the thermal generators. However, two major changes in flow occur when the thermal generators are shut down and then started back up in the thermal system. This behaviour is undesirable, as it can increase the structural imbalances in the system [1].

4. Conclusion

Hydropower is considered an important balancing resource due to its flexibility. A continuous-time hydrothermal unit commitment model with HVDC cables was formulated in this paper to show how excessive ramping in the thermal system can be avoided by hydropower and

active use of the HVDC cables. The structural imbalances in the system are reduced by 34% in the continuous-time model compared to the hourly discrete-time model since sub-hourly effects are captured by the polynomial expansion. Several modelling issues related to incorporating hydropower into the continuous-time framework have been uncovered in the process. The linearization of the hydropower production curve requires binary variables to avoid unphysical uploading, and modelling the forbidden production zone requires the relaxation of the continuity constraints of the individual hydropower plants. The overall continuity of the model is still preserved on a system level, as the power balance forces the sum of hydropower production to be C^1 continuous. Investigating other potential modelling choices of the hydropower production curve, calculating system prices, and expanding the model to cover cross-zonal reserve capacity procurement are interesting avenues of further research.

Declaration of Competing Interest

The authors declare that they have no known competing financial interests or personal relationships that could have appeared to influence the work reported in this paper.

Acknowledgments

This work was funded by The Research Council of Norway, Project No. 268014/E20.

References

[1] Statnett, Statnetts forslag til praktisk gjennomføring av EUs forordning for tilknytning av forbruk (DCC), Technical Report, Statnett, 2017.
[2] M. Parvania, A. Scaglione, Unit commitment with continuous-time generation and ramping trajectory models, IEEE Trans. Power Syst. 31 (4) (2016) 3169–3178, https://doi.org/10.1109/TPWRS.2015.2479644.
[3] M. Parvania, R. Khatami, Continuous-time marginal pricing of electricity, IEEE Trans. Power Syst. 32 (3) (2017) 1960–1969, https://doi.org/10.1109/TPWRS.2016.2597288.
[4] R. Khatami, M. Parvania, P.P. Khargonekar, Scheduling and pricing of energy generation and storage in power systems, IEEE Trans. Power Syst. 33 (4) (2018) 4308–4322, https://doi.org/10.1109/TPWRS.2017.2782676.
[5] R. Khatami, M. Parvania, K. Oikonomou, Continuous-time optimal charging control of plug-in Electric Vehicles, 2018 IEEE PES Innovative Smart Grid Technology (ISGT) Conference, (2018), pp. 1–5.
[6] R. Khatami, M. Parvania, A. Bagherinezhad, Continuous-time model predictive control for real-time flexibility scheduling of plugin electric vehicles, IFAC-PapersOnLine 51 (28) (2018) 498–503, https://doi.org/10.1016/J.IFACOL.2018.11.752.
[7] R. Khatami, M. Parvania, P. Khargonekar, Continuous-time look-ahead scheduling of energy storage in regulation markets, Proc. 52nd Hawaii Int. Conf. Syst. Sci. (2019), https://doi.org/10.24251/hicss.2019.435.
[8] K. Hreinsson, B. Analui, A. Scaglione, Continuous time multi-stage stochastic reserve and unit commitment, 2018 Power Syst. Comput. Conf. IEEE, 2018, pp. 1–7, https://doi.org/10.23919/PSCC.2018.8442490.
[9] K. Hreinsson, A. Scaglione, B. Analui, Continuous time multi-stage stochastic unit commitment with storage, IEEE Trans. Power Syst. (2019), https://doi.org/10.1109/tpwrs.2019.2923207.
[10] R. Khatami, M. Parvania, P. Khargonekar, A. Narayan, Continuous-time stochastic modeling and estimation of electricity load, 2018 IEEE Conf. Decis. Control, IEEE, 2018, pp. 3988–3993, https://doi.org/10.1109/CDC.2018.8619042.
[11] Z. Deng, M. Liu, H. Chen, W. Lu, P. Dong, Optimal scheduling of active distribution networks with limited switching operations using mixed-integer dynamic optimization, IEEE Trans. Smart Grid 10 (4) (2019) 4221–4234, https://doi.org/10.1109/TSG.2018.2853731.
[12] O.B. Fosso, A. Gjelsvik, A. Haugstad, B. Mo, I. Wangensteen, Generation scheduling in a deregulated system. the norwegian case, IEEE Trans. Power Syst. 14 (1) (1999) 75–80, https://doi.org/10.1109/59.744487.
[13] O. Wolfgang, A. Haugstad, B. Mo, A. Gjelsvik, I. Wangensteen, G. Doorman, Hydro reservoir handling in Norway before and after deregulation, Energy 34 (10) (2009) 1642–1651, https://doi.org/10.1016/J.ENERGY.2009.07.025.
[14] A. Helseth, B. Mo, A. Lote Henden, G. Warland, Detailed long-term hydro-thermal scheduling for expansion planning in the Nordic power system, IET Gener. Transm. Distrib. 12 (2) (2018) 441–447, https://doi.org/10.1049/iet-gtd.2017.0903.
[15] A.L. Diniz, F.D.S. Costa, M.E. Maceira, T.N. Dos Santos, L.C.B. Dos Santos, R.N. Cabral, Short/Mid-term hydrothermal dispatch and spot pricing for large-scale systems-The case of Brazil, 20th Power Syst. Comput. Conf. PSCC 2018, Institute of Electrical and Electronics Engineers Inc., 2018, https://doi.org/10.23919/PSCC.2018.8442897.
[16] M.E. Maceiral, D.D. Penna, A.L. Diniz, R.J. Pinto, A.C. Melo, C.V. Vasconcellos, C.B. Cruz, Twenty years of application of stochastic dual dynamic programming in official and agent studies in Brazil-main features and improvements on the NEWAVE model, 20th Power Syst. Comput. Conf. PSCC 2018, Institute of Electrical and Electronics Engineers Inc., 2018, https://doi.org/10.23919/PSCC.2018.8442754.
[17] J. Kong, H.I. Skjelbred, O.B. Fosso, An overview on formulations and optimization methods for the unit-based short-term hydro scheduling problem, Electr. Power Syst. Res. 178 (2020) 106027, https://doi.org/10.1016/j.epsr.2019.106027.
[18] Available online, accessed 3/9-2019: https://www.nordpoolgroup.com/trading/Day-ahead-trading/Ramping.
[19] M. Carrión, J.M. Arroyo, A computationally efficient mixed-integer linear formulation for the thermal unit commitment problem, IEEE Trans. Power Syst. 21 (3) (2006) 1371–1378, https://doi.org/10.1109/TPWRS.2006.876672.
[20] C.Ø. Naversen, H. Farahmand, A. Helseth, Accounting for reserve capacity activation when scheduling a hydropower dominated system, Int. J. Electr. Power Energy Syst. 119 (2020) 105864, https://doi.org/10.1016/j.ijepes.2020.105864.
[21] Available online, accessed 3/9-2019: http://www.nyiso.com.
[22] Available online, accessed 3/9-2019: http://www.caiso.com.

Paper III

Cite as:
M. L. Øvstebø, C. Ø. Naversen, A. Helseth, and H. Farahmand
"Continuous-time scheduling of a hydrothermal system with integration of offshore wind power"
17th Int. Conf. Eur. Energy Mark. (EEM), Oct 2020
DOI: 10.1109/EEM49802.2020.9221980
URL: `https://doi.org/10.1109/EEM49802.2020.9221980`

Continuous-time scheduling of a hydrothermal system with integration of offshore wind power

Mari Lund Øvstebø*†, Christian Øyn Naversen*, Arild Helseth‡ and Hossein Farahmand*
*Department of Electric Power Engineering, NTNU – Trondheim, Norway
‡Department of Energy Systems, SINTEF Energy Research – Trondheim, Norway
†Corresponding author: mariovs@stud.ntnu.no

***Abstract*—In this work, a continuous-time unit commitment formulation of a hydrothermal system with integration of offshore wind power is used to model the North European system operation. The cost of covering the structural imbalances in the system is quantified by a cost comparison to an analogous discrete-time model. If the discrete-time unit commitment is implemented for real-time operation, 55 MWh (0.22%) load shedding should be introduced since the demand in periods with high net-load ramping cannot be met. The simulation results demonstrate that the proposed framework reduces system balancing cost and the events of ramping scarcity in the real-time balancing.**

***Index Terms*—Continuous-time optimization, Hydrothermal scheduling, Offshore wind power, Unit commitment**

I. Introduction

A significant amount of offshore wind power is expected to be integrated into the European power system in the coming years [1]. The variable nature of wind power generation challenges the security of the power system as the flexibility of conventional generators are pushed to their limits. Cascaded hydropower is an existing flexible energy storage technology which can provide energy and flexibility on a system scale, and the Nordic countries have considerable amounts of hydropower installed in their current power systems. Several high voltage direct current (HVDC) cables between Norway and continental Europe (Netherlands and Denmark) have been constructed in recent years, and new interconnectors to Germany and Great Britain are under construction. The increased transmission capacity makes it possible to use Norwegian hydropower resources to help balance the wind power in the North European power system. Hydrothermal coordination in the presence of uncertain wind power generation has been studied in the literature, which includes both models with long time horizons [2]–[5] and short-term studies [6].

The discrete structure of the European day-ahead electricity markets cannot prevent the occurrence of a mismatch between the market cleared volumes and the actual production and consumption. These structural imbalances must be balanced in real-time by activating procured reserve capacity. As wind power can vary quickly and unpredictably within the span of a few minutes, the structural imbalances and need for balancing can be worsened by a high wind power penetration. Continuous-time optimization is a way of formulating the standard unit commitment and economic dispatch problems with continuously varying time-dependent variables and input data, originally formulated for a purely thermal system in [7]. The continuous-time framework has lately been extended to incorporate energy storage technology in [8], and multi-stage stochastic unit commitment and reserve scheduling models are developed in [9] and [10]. In previous work, we have derived the formulation of the cascaded hydropower constraints in the continuous-time framework [11]. This paper extends the model presented in [11] to include wind power generation. The main contributions of the paper are:

- Quantifying the cost of structural imbalances in a test system resembling the Northern European power system by comparing the costs obtained by a continuous-time unit commitment model and an analogous discrete-time model.
- Identifying specific periods where the discrete-time model overestimates the flexibility of the system. This is done by simulating operation with a continuous-time model, setting the binary commitment decisions equal to the discrete-time solution.

Section II defines the continuous-time model in detail, while the case study and results are presented in Section III. A concluding summary is found in Section IV.

II. Model

The mathematical formulation of the continuous-time model is based on [11]. In this paper, the model is extended to include offshore wind power, hence constraints for wind power production and wind curtailment are added to the model.

A. Continuous-time optimization framework

The continuous-time optimizations framework directly models sub-hourly variations by representing all time-varying data and variables as polynomials of time, which allows ramping and other inter-temporal constraints to be enforced continuously. Several spline models can be used to approximate the continuous-time trajectory curve of a data set, where the accuracy of the spline model is dependent on the order of the basis. A convenient spline model is the Bernstein polynomials, where the time dependent decision variables will be defined by using the Bernstein polynomials of degree n, which form a basis for any polynomials of degree equal or less than n on the interval $t \in [0, 1]$. For a given time interval $h \in \mathcal{T}$ with length δ_h, a time-varying decision variable $x(t)$ can be expressed as:

$$x(t) = \mathbf{x}_h^T \cdot \mathbf{B}_n\left(\frac{t - T_h}{\delta_h}\right), \quad T_h \le t \le T_{h+1}, \tag{1}$$

where $T_h = \sum_{i<h} \delta_i$ is the start time of interval h, $\mathbf{x}_h$ is a vector of $n+1$ Bernstein polynomial coefficients and $\mathbf{B}_n(t)$ is the vector of Bernstein polynomials of degree n. This definition gives a piece-wise polynomial description of time-dependent variables where the polynomial coefficients $\mathbf{x}_h$ become the decision variables in the optimization problem. Choosing Bernstein polynomials of degree zero recovers the usual discrete-time formulation of piece-wise constant variables.

In this paper, the Bernstein polynomials of degree three will be used as a basis for each time interval h:

$$\mathbf{B}_3(t) = \left[(1-t)^3,\ 3t(1-t)^2,\ 3t^2(1-t),\ t^3\right]. \tag{2}$$

This degree of freedom allows the application of C^1 continuity constraints between time intervals without drastically increasing the number of decision variables in the model. The C^1 continuity constraints can be expressed with the use of the Bernstein coefficients of the decision vector $\mathbf{x}$, where the coefficients can be labeled as $\mathbf{x}^i$ for $i \in \{0,1,2,3\}$. With this in mind, the continuity constraints can be expressed as:

$$\mathbf{x}_h^3 = \mathbf{x}_{h+1}^0 \qquad \forall h \in \mathcal{T}\backslash\{N\} \tag{3}$$
$$\mathbf{x}_h^3 - \mathbf{x}_h^2 = \mathbf{x}_{h+1}^1 - \mathbf{x}_{h+1}^0 \qquad \forall h \in \mathcal{T}\backslash\{N\}. \tag{4}$$

The result of integrating and differentiating $\mathbf{B}_n(t)$ can be represented by Bernstein polynomials of degree $\mathbf{B}_{n+1}(t)$ and $\mathbf{B}_{n-1}(t)$, respectively. These relationships are described by the linear matrices $\mathbf{K}$ and $\mathbf{N}$ for $\mathbf{B}_3(t)$ in eqs. (5) and (6). Another useful relation is the definite integral of the polynomials over the whole interval, shown in eq. (7).

$$\dot{\mathbf{B}}_3(t) = \mathbf{K} \cdot \mathbf{B}_2(t) \tag{5}$$
$$\int \mathbf{B}_3(t)dt = \mathbf{N} \cdot \mathbf{B}_4(t) \tag{6}$$
$$\int_0^1 \mathbf{B}_3(t)dt = \frac{1}{4} \cdot \mathbf{1} \tag{7}$$

These properties, together with the convex hull property, are some of the main reasons for using Bernstein polynomials in the continuous-time optimization framework. The convex hull property makes it possible to impose inequality constraints on the decision variable $x(t)$ by directly bounding the coefficient $\mathbf{x}_h$. For a more detailed introduction to continuous-time optimization in power systems, the reader is referred to for instance [7].

B. Mathematical formulation of continuous-time UC

1) Thermal constraints: The following constraints are defined for all thermal units $i \in \mathcal{I}$ over time intervals $h \in \mathcal{T}$. $u_i(t)$, $SU_i(t)$ and $SD_i(t)$ are binary variables describing the commitment status, startup and shutdown of thermal generator i, respectively. Constraints (8) and (9) ensure that the thermal generator can ramp up the production,$g_i(t)$, from zero to above G_i^{min}, or ramp down production to zero, during time interval h. This smooth ramping of the production is necessary when the continuity constraints for the thermal production variable will be applied in II-B4. Limitations on the derivative $\dot{g}_i(t)$ are imposed in (10) and (11) such that the ramping of the thermal production stays within specified limits R_i^u and R_i^d by utilizing property (5). When there is a startup or a shutdown, the ramping limit is increased to G_i^{max}. Constraints (12) and (13) counts the number of startup and shutdown events.

$$G_i^{min}\mathbf{u}_{i,h} \le \mathbf{g}_{i,h} \le G_i^{max}\mathbf{u}_{i,h} \tag{8}$$
$$\mathbf{u}_{i,h} = [u_{i,h},\ u_{i,h},\ u_{i,h+1},\ u_{i,h+1}]^T \tag{9}$$
$$\frac{1}{\delta_h}\mathbf{g}_{i,h}^T \cdot \mathbf{K} \le (R_i^u + (G_i^{max} - R_i^u)SU_{i,h})\mathbf{1}^T \tag{10}$$
$$\frac{1}{\delta_h}\mathbf{g}_{i,h}^T \cdot \mathbf{K} \ge -(R_i^d + (G_i^{max} - R_i^d)SD_{i,h})\mathbf{1}^T \tag{11}$$
$$SU_{i,h} - SD_{i,h} = u_{i,h+1} - u_{i,h} \tag{12}$$
$$SU_{i,h} + SD_{i,h} \le 1 \tag{13}$$
$$u_{i,h}, SU_{i,h}, SD_{i,h} \in \{0,1\} \tag{14}$$

2) Hydropower constraints: The constraints from (15) to (30) are added to the optimization problem for the hydro area and are defined for all hydropower plants $m \in \mathcal{M}$ over time intervals $h \in \mathcal{T}$.

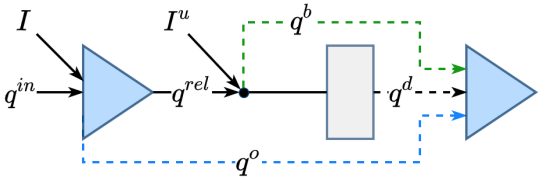

Fig. 1. A rotated illustration of the waterways between reservoirs together with regulated and unregulated natural inflow.

$$v_{m0} = V_m^0 \tag{15}$$
$$v_{m,h+1} - v_{m,h} = \frac{1}{4}\delta_h \mathbf{1}^T \cdot \mathbf{q}_{m,h}^{net} \tag{16}$$
$$\mathbf{0} \le v_{m,h}\mathbf{1} + \delta_h \mathbf{N}^T \cdot \mathbf{q}_{m,h}^{net} \le V_m \mathbf{1} \tag{17}$$
$$\mathbf{q}_{m,h}^{in} = \sum_{j \in \mathcal{J}_m^d} \sum_{n \in N_j} \mathbf{q}_{j,n,h}^d + \sum_{j \in \mathcal{J}_m^b} \mathbf{q}_{j,h}^b + \sum_{j \in \mathcal{J}_m^o} \mathbf{q}_{j,h}^o \tag{18}$$
$$\mathbf{q}_{m,h}^{net} = \mathbf{I}_{m,h} + \mathbf{q}_{m,h}^{in} - \mathbf{q}_{m,h}^{rel} - \mathbf{q}_{m,h}^o \tag{19}$$
$$\mathbf{q}_{m,h}^{rel} = \sum_{n \in N_m} \mathbf{q}_{m,n,h}^d + \mathbf{q}_{m,h}^b - \mathbf{I}_{m,h}^u \tag{20}$$
$$\mathbf{0} \le \mathbf{q}_{m,h}^b \le Q_m^b \cdot \mathbf{1} \tag{21}$$
$$\mathbf{0} \le \mathbf{q}_{m,h}^o \tag{22}$$
$$\mathbf{0} \le \mathbf{q}_{m,h}^{rel} \tag{23}$$
$$\mathbf{p}_{m,h} = \sum_{n \in N_m} \eta_{m,n}\mathbf{q}_{m,n,h}^d \tag{24}$$

$$Q^d_{m,n} w_{m,n,h} \mathbf{1} \leq \mathbf{q}^d_{m,n,h} \leq Q^d_{m,n} \mathbf{1} \quad (25)$$

$$\mathbf{q}^d_{m,n,h} \leq Q^d_{m,n} w_{m,n-1,h} \mathbf{1} \quad (26)$$

$$P^{min}_m z_{m,h} \mathbf{1} \leq \mathbf{p}_{m,h} \leq P^{max}_m z_{m,h} \mathbf{1} \quad (27)$$

$$SU_{m,h} - SD_{m,h} = z_{m,h+1} - z_{m,h} \quad (28)$$

$$SU_{m,h} - SD_{m,h} \leq 1 \quad (29)$$

$$z_{m,h}, SU_{m,h}, SD_{m,h} \in \{0, 1\}. \quad (30)$$

v_{mh} is the instantaneous volume at the beginning of interval h for reservoir m, and constraint (15) sets the initial volume for each reservoir. Constraint (16) calculates the change in volume between two time intervals by integrating the net inflow, $q^{net}_m(t)$, over the entire time interval by the use of (7). Constraint (17) bounds the reservoir volume within the time interval, found by using property (6), between zero and the maximal reservoir volume V_m. Figure 1 shows that the waterways of the cascaded system is modelled by three separate routes: the spill gate, $q^o_m(t)$, the bypass gate, $q^b_m(t)$, and the discharge through each turbine segment $n \in \mathcal{N}_m$, $q^d_{m,n}(t)$. The hydropower topology constraints, expressed in (18) to (23), implement this system description. $I_m(t)$, $I^u_m(t)$ and $q^{net}_m(t)$ represents regulated and unregulated natural inflow, and net flow into the reservoir, respectively. $q^{in}_m(t)$ is the sum of the controlled flow into the reservoir from the upstream system, while $q^{rel}_m(t)$ is the total released flow out of the reservoir. Q^b_m denotes the maximal bypass flow. The constraints for hydropower production and commitment is expressed in (24) to (30), where $p_m(t)$ is the generated hydropower. The conversion from discharge through the turbine to generated power is a non-linear function depending on the plant head and the efficiency curves of the generator and the turbine. In (24), this non-linear function is approximated as a piece-wise linear curve, where each segment of the discharge variable has a constant efficiency η_n. As discussed in [11], binary variables $w_{m,n}(t)$ are necessary in the continuous-time formulation to ensure that the discharge segments are uploaded in physically correct order. Constraint (25) and (26) bound the flow through each discharge segment within an upper and lower limit with the use of the binary variable, and these two constraints are defined for all discharge segments $n \in \mathcal{N}_m$.

Constraint (27) to (30) expresses the hydropower unit commitment constraints, where $z_m(t)$, $SU_m(t)$ and $SD_m(t)$ are binary variables describing the commitment status, startup and shutdown of a hydropower unit m, respectively. From constraint (27), it can be seen that all the Bernstein coefficients in the decision variable $p_m(t)$ for a given hour are related to the commitment of the generator in that given hour. This forces the hydropower unit commitment decision to be constant during a time interval h, and will ensure that the production never is between zero and P^{min}_m. Unlike the smooth operation enforced on the thermal generators, discontinuous jumps in the hydropower production curve when there are startups and shutdowns are therefore permitted.

3) Wind Power and System constraints: Area and system wide constraints in the model are the following:

$$\mathbf{0} \leq \mathbf{s}_{a,h} \leq \mathbf{W}_{a,h} \quad (31)$$

$$\boldsymbol{\rho}^c_{a,h} = \mathbf{W}_{a,h} - \mathbf{s}_{a,h} \quad (32)$$

$$\alpha \geq \sum_{m \in \mathcal{M}} WV_{m,k} v_{m,N+1} + D_k \quad (33)$$

$$-F^{max}_l \mathbf{1} \leq \mathbf{f}_{l,h} \leq F^{max}_l \mathbf{1} \quad (34)$$

$$\sum_{m \in \mathcal{M}_a} \mathbf{p}_{m,h} + \sum_{i \in \mathcal{I}_a} \mathbf{g}_{i,h} + \mathbf{s}_{a,h} - \sum_{l \in \mathcal{L}} G_{l,a} \mathbf{f}_{l,h} = \mathbf{L}_{a,h} - \boldsymbol{\rho}^s_{a,h}. \quad (35)$$

Constraint (31) and (32) expresses the wind power generation $s_a(t)$ and the wind curtailment $\rho^c_a(t)$, respectively, where both constraints are defined over time intervals $h \in \mathcal{T}$ and areas $a \in \mathcal{A}$. Generated wind power is bound within zero and the maximal available wind power curve $W(t)$. The future expected operating cost for the system, α, which is directly added to the objective function in (37), is bounded by constraint (33), which are a set of linear Benders cuts $k \in \mathcal{K}$. The cut coefficients $WV_{m,k}$ and the cut constants D_k can be calculated by long-term hydrothermal models such as the one in [12], and the future expected system cost ultimately depends on the end volume of water in each reservoir. The power flow on the HVDC cables, $f_l(t)$, is bound by a maximal flow limit F^{max}_l in (34), defined for all lines $l \in \mathcal{L}$ over time intervals $h \in \mathcal{T}$. Constraint (35) shows the power balance, which needs to be satisfied for each area $a \in \mathcal{A}$ over time intervals $h \in \mathcal{T}$. $\mathcal{M}_a$ and $\mathcal{I}_a$ are the sets of hydropower and thermal units located in area a, and $G_{l,a}$ is the adjacency matrix of the HVDC grid. $L_a(t)$ is the area load and $\rho^s_a(t)$ is the amount of load shedding within each area.

4) Continuity constraints: One important aspect of the continuous-time optimization framework is that the value of the decision variable and its derivative can be continuous over time interval shifts. The continuity constraints in (3) and (4) are added to the optimization problem for the thermal production decision variable $\mathbf{g}_{i,h}$, the offshore wind production decision variable $\mathbf{s}_{a,h}$ and for the power flow decision variable $\mathbf{f}_{l,h}$ for all times $h \in \mathcal{T}$. This enforces C^1 continuity, meaning that the curves have continuous values and derivatives for all points in time. Less strict continuity constraints are added for the variables connected to the hydropower units $m \in \mathcal{M}$ over time intervals $h \in \mathcal{T}$, which is discussed in more detail in [11]. The C^0 continuity constraint in (3) is applied to the flow through the bypass gate and spill gate, $\mathbf{q}^b_{m,h}$ and $\mathbf{q}^o_{m,h}$. As there is need for discontinuous jumps in the hydropower production during startups and shutdowns, enforcing C^0 continuity on $\mathbf{p}_{m,h}$ will not be possible. Instead, constraint (3) is replaced with the inequality constraints in (36), which makes the hydropower production C^0 continuous over time interval changes except if a startup or shutdown occurs:

$$-P^{max}_m SU_{m,h} \leq \mathbf{p}^3_{m,h} - \mathbf{p}^0_{m,h+1} \leq P^{max}_m SD_{m,h}. \quad (36)$$

5) Objective function: The objective function for the proposed model, presented in (37), is to minimize the total cost of the system. The total cost includes the future expected cost of the hydro system, α, the cost of spilling and bypassing water, and the operational, startup and shutdown costs for the thermal generators. In addition, a negligible penalty for curtailment of wind power and a high penalty for load shedding are included in the last line. Both startup and shutdown costs for the hydropower plants and the wind farms are assumed to be negligible in this model.

$$
\begin{aligned}
Z = \alpha &+ \frac{1}{4} \sum_{m \in \mathcal{M}} \sum_{h \in \mathcal{T}} \delta_h \mathbf{1}^T \cdot \left(C^b \mathbf{q}^b_{m,h} + C^o \mathbf{q}^o_{m,h} \right) \\
&+ \sum_{i \in \mathcal{I}} \sum_{h \in \mathcal{T}} \left(\frac{1}{4} \delta_h C_i \mathbf{1}^T \cdot \mathbf{g}_{i,h} + C^{start}_i SU_{i,h} + C^{stop}_i SD_{i,h} \right) \\
&+ \frac{1}{4} \sum_{h \in \mathcal{T}} \delta_h \mathbf{1}^T \cdot \left(C^c \boldsymbol{\rho}^c_h + C^s \boldsymbol{\rho}^s_h \right) \qquad (37)
\end{aligned}
$$

III. Case Study

A case study of a stylized three-area system resembling Northern Europe is presented in this section. The continuous-time model presented in Section II and an analogous discrete-time model are both solved to compare how the different components in the system reacts when variable offshore wind power is integrated into the power system. Both models have been implemented in Pyomo and solved with CPLEX 12.10.

A. System topology and input data

The stylized three-area system contains a hydro dominated Norwegian area, a thermal dominated Central European area and an offshore wind area in the North Sea, connected through HVDC cables. The hydropower area is based on a real Norwegian cascaded system containing 12 reservoirs and plants with a total hydropower production capacity of 535 MW. A detailed description of the hydropower topology can be found in [13]. The ratio between the capacity of the cascaded system and the total installed capacity in Norway (32 257 MW at the beginning of 2019 [14]), here referred to as the system scaling rate, is used to scale the capacities for the rest of the generation units and cables in the three-area system. The installed capacity of the offshore wind area and the wind series used in the case study is based on wind data from Denmark, found in [15], and scaled to match the total offshore wind capacity provided by Denmark, Germany and the Netherlands in the North Sea. The wind farms in the offshore wind area are clustered together as one big wind farm, with a total installed capacity of 172 MW after it is scaled down with the system scaling rate. The thermal area contains 104 thermal generators, divided into five groups after the primary-fuel; fossil gas, fossil hard coal, lignite, nuclear and fossil oil generators. The ramping capabilities, installed capacity and marginal, startup, and shutdown costs are based on operating thermal generators in Germany and the Netherlands [16], [17]. The total capacity of the thermal area is 921 MW after scaling. The three-area system is connected through two HVDC cables, where the hydro and the thermal area are connected by a 63 MW cable and the offshore wind area and the thermal area are connected by a 172 MW cable. The capacity of the cable connecting the thermal and the hydro area is based on the total installed capacity of the interconnectors between Norway and mainland Europe today [18], [19], including the 1400 MW Nordlink cable, which will be installed during 2020 [20]. This results in 63 MW of transmission capacity after it is scaled down with the system scaling rate. The interconnector capacity between the thermal area and the offshore wind area is assumed to be equal to the installed capacity of the offshore wind area, to ensure no limitations on the utilization of the possible offshore wind power production. The time horizon is set to 24 hours, with hourly time intervals in the continuous-time model. The discrete-time model has quarterly time intervals but hourly commitment decisions. The case study is based on data from 22/4-2019 where the reservoir volume in Norway was at 31.6%, its lowest during 2019 [21]. Fig. 2 shows the wind series for the offshore wind area and the load profiles for the demand in the other areas. For the thermal area, it is assumed that the peak load is 85% of the installed capacity, which implies a peak load of 783 MW. The hydro area has a peak load of 400 MW which is 75% of the installed capacity. The load profiles are based on data from Nord Pool [22] and ENTSO-E [23]. The offshore wind area has a peak wind production of 163.54 MW, where the wind series is based on data from [15]. The continuous time load and wind series are calculated from the data by a least-squares error fit to the Bernstein polynomials. For the piece-wise constant load and wind series, the average quarterly values are used.

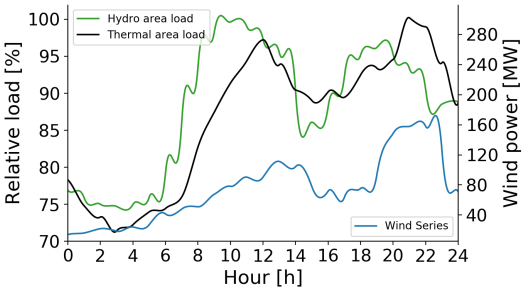

Fig. 2. The continuous-time load profiles of thermal and hydro areas scaled by the value of the peak load (left axis) together with the continuous-time wind power series for the offshore wind area (right axis).

B. Continuous-time and discrete-time model comparison

Both the discrete-time model and the continuous-time model are solved to optimality, meaning an absolute mip-gap of 0% was reached. The discrete-time model was solved within 80 sec., while the continuous-time model used 2 378 sec. to reach optimality on a single core 2.4 GHz machine. A breakdown of the objective function costs is listed in Table I.

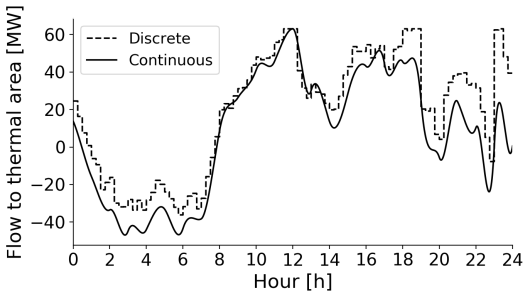

Fig. 3. Power flow on the HVDC cable from the hydro area to the thermal area.

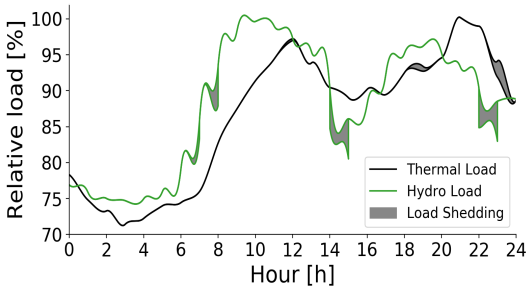

Fig. 4. Load shedding when the continuous-time model is solved with the fixed commitment solution from the discrete-time model.

For the thermal area, the discrete-time model schedules 51 generators to be committed during the whole optimization horizon. All fossil hard coal, lignite and nuclear generators are operating to cover the base load, while three fossil gas generators and zero oil-fired generators are committed. Six additional gas-fired generators are committed to meet the net-load variations in the continuous-time model. This result highlights that the continuous-time model sees the need to commit extra flexible units to cover sub-hourly net-load variations and peaks. This results in a 3.68% higher thermal cost and a 2.12% higher scheduled thermal production than in the discrete-time model. From Fig. 3 it can be seen that the power flow from the hydro area to the thermal area is higher for the discrete-time model during periods when the total load of the system is high, especially at the end of the scheduling period. This results in a 3.15% higher scheduled hydropower production and 2.15% higher hydropower related costs in the discrete-time model. Also note the rapid flow change in hour 23 in the discrete-time model caused by the drop in wind power production, which is not seen in the continuous-time solution. It is clear that such an abrupt change in flow is either infeasible or very costly when thermal generation and line flow continuity is enforced. The offshore wind power utilization is high entire scheduling period for both models, though a small amount of wind power is curtailed in the continuous-time model. Overall, the total cost of the system will be higher for the continuous-time model, with a 3 774.6 €/day (0.53%) increase compared to the discrete-time model.

TABLE I
COMPARISON OF THE TOTAL SYSTEM COSTS. ROW 3-5 REPRESENTS THE COST OF LINE 1-3 IN (37), RESPECTIVELY.

Cost	**Discrete-time**	**Continuous-time**
Objective value [€]	713 092.4	716 867.1
Hydro related costs [€]	388 795.7	380 623.0
Thermal related costs [€]	324 296.7	336 241.8
Curtailment and shedding costs [€]	0.0	2.3

C. Continuous-time simulator for real-time operation

To investigate where the discrete-time model overestimates the flexibility of the system, the continuous-time model is used as a simulator for real-time operation. The unit commitment decisions from the discrete-time model is used as input to the continuous-time model to identify in which periods the discrete-time model overestimates the system flexibility. From Fig. 4, it can be seen that the discrete-time model fails to commit enough units in periods when there are rapid changes in load and wind power. In these periods, an imbalance between the generated power and the actual load will occur, which will manifest as load shedding in the presented model. In total, 55 MWh load shedding will take place during the entire scheduling period, where the largest amount occurs in the hydropower area. This means that 0.22% of the total load will not be covered by the committed generators. In real system operations, the system operators need to activate reserves in these periods to balance the power system.

IV. Conclusion

We assess the structural imbalances in the interconnected North European power system by solving a continuous-time hydrothermal model with offshore wind power, and compare the results to an analogous discrete-time model. The increased cost of balancing the sub-hourly variations in the net-load was found to be 0.53% of the discrete-time model system costs per day. This cost increase is due to the overestimation of the system flexibility in the discrete-time model. The specific periods where the discrete-time model formulation overestimates the system flexibility were pinpointed by fixing the binary unit commitment decisions of the continuous-time model to be equal to the optimal discrete-time commitment solution. This resulted in a total of 55 MWh of load which could not be covered by the committed units and represents an additional requirement for fast system reserves that are not needed in the continuous-time solution.

V. Acknowledgments

This work was funded by the Research Council of Norway, Project No. 268014/E20.

REFERENCES

[1] "Offshore Wind Outlook 2019 – Analysis - IEA." [Online]. Available: https://www.iea.org/reports/offshore-wind-outlook-2019

[2] T. Aigner, S. Jaehnert, G. L. Doorman, and T. Gjengedal, "The effect of large-scale wind power on system balancing in Northern Europe," *IEEE Trans. Sustain. Energy*, vol. 3, no. 4, pp. 751–759, 2012.

[3] A. Helseth, A. Gjelsvik, B. Mo, and U. Linnet, "A model for optimal scheduling of hydro thermal systems including pumped-storage and wind power," *IET Gener. Transm. Distrib.*, vol. 7, no. 12, pp. 1426–1434, 2013.

[4] H. Farahmand, S. Jaehnert, T. Aigner, and D. Huertas-Hernando, "Nordic hydropower flexibility and transmission expansion to support integration of North European wind power," *Wind Energy*, vol. 18, no. 6, pp. 1075–1103, jun 2015.

[5] M. N. Hjelmeland, C. T. Larsen, M. Korpås, and A. Helseth, "Provision of rotating reserves from wind power in a hydro-dominated power system," in *2016 Int. Conf. Probabilistic Methods Appl. to Power Syst.* IEEE, oct 2016, pp. 1–7.

[6] B. P. Cotia, C. L. Borges, and A. L. Diniz, "Optimization of wind power generation to minimize operation costs in the daily scheduling of hydrothermal systems," *Int. J. Electr. Power Energy Syst.*, vol. 113, pp. 539–548, dec 2019.

[7] M. Parvania and A. Scaglione, "Unit Commitment With Continuous-Time Generation and Ramping Trajectory Models," *IEEE Trans. Power Syst.*, vol. 31, no. 4, pp. 3169–3178, jul 2016.

[8] R. Khatami, M. Parvania, and P. P. Khargonekar, "Scheduling and Pricing of Energy Generation and Storage in Power Systems," *IEEE Trans. Power Syst.*, vol. 33, no. 4, pp. 4308–4322, jul 2018.

[9] K. Hreinsson, B. Analui, and A. Scaglione, "Continuous Time Multi-Stage Stochastic Reserve and Unit Commitment," in *2018 Power Syst. Comput. Conf.* IEEE, jun 2018, pp. 1–7.

[10] R. Khatami, M. Parvania, and A. Narayan, "Flexibility Reserve in Power Systems: Definition and Stochastic Multi-Fidelity Optimization," *IEEE Trans. Smart Grid*, vol. 11, no. 1, pp. 644–654, jan 2020.

[11] C. Ø. Naversen, A. Helseth, B. Li, M. Parvania, H. Farahmand, and J. P. S. Catalão, "Hydrothermal scheduling in the continuous-time framework," *Electr. Power Syst. Res.*, vol. 189, p. 106787, dec 2020.

[12] A. Helseth, B. Mo, A. L. Henden, and G. Warland, "Detailed long-term hydro-thermal scheduling for expansion planning in the Nordic power system," *IET Gener. Transm. Distrib.*, vol. 12, no. 2, pp. 441–447, jan 2018.

[13] C. Ø. Naversen, H. Farahmand, and A. Helseth, "Accounting for reserve capacity activation when scheduling a hydropower dominated system," *Int. J. Electr. Power Energy Syst.*, vol. 119, p. 105864, jul 2020.

[14] Accessed 10/1-2019. [Online]. Available: https://www.nve.no/energiforsyning/kraftproduksjon/vannkraft/?ref=mainmenu

[15] Accessed 2/6-2019. [Online]. Available: https://www.energidataservice.dk/en/dataset/electricityprodex5minrealtime/resource_extract/06380963-b7c6-46b7-aec5-173d15e4648b

[16] Accessed 2/6-2019. [Online]. Available: https://www.eex-transparency.com/power/de/production/capacity/

[17] Accessed 2/6-2019. [Online]. Available: https://www.energy-charts.de/osm.htm

[18] Accessed 2/6-2019. [Online]. Available: https://www.nexans.no/eservice/Norway-en/navigatepub_142640_-34274/Royal_opening_of_Skagerrak_4.html

[19] J. Skog, K. Koreman, B. Pääjärvi, and T. Andersröd, "The NORNED HVDC cable link–a power transmission highway between norway and the netherlands," *ENERGEX 2006, Stavanger, Norway*, 01 2006.

[20] Accessed 2/6-2019. [Online]. Available: https://www.statnett.no/en/about-statnett/news-and-press-releases/News-archive-2018/norwegian-german-power-cable-being-installed/

[21] Accessed 3/3-2019. [Online]. Available: https://www.statnett.no/en/for-stakeholders-in-the-power-industry/data-from-the-power-system/#hydrological-data

[22] Accessed 2/6-2019. [Online]. Available: https://www.nordpoolgroup.com/Market-data1/Power-system-data/Consumption1/Consumption/NO/Hourly1/?view=table

[23] Accessed 2/6-2019. [Online]. Available: https://transparency.entsoe.eu/load-domain/r2/totalLoadR2/show

Paper IV

The paper **"Stochastic Flexibility Coordination in Hybrid Hydro-Thermal-Wind Power Systems"** was submitted for review to **IEEE** in the journal **IEEE Transactions on Power Systems** in September 2020.

Stochastic Flexibility Coordination in Hybrid Hydro-Thermal-Wind Power Systems

Christian Øyn Naversen, *Student Member, IEEE,* Bosong Li, *Member, IEEE,* Masood Parvania, *Senior Member, IEEE,* Arild Helseth, *Member, IEEE,* Hossein Farahmand, *Senior Member, IEEE*

***Abstract*—Using flexible resources to efficiently balance the fluctuations of variable renewable energy production is a crucial challenge for the operation of modern power systems. However, deterministic imbalances caused by the discrete day-ahead electricity market structures also takes away a substantial part of the balancing resources. This paper develops a stochastic continuous-time optimization model for coordinating the flexible operation of a hybrid power system with hydropower and thermal generation to compensate the uncertainty and variability of wind power in the system. The continuous-time model captures the sub-hourly variations of the wind power and load and accurately models the ramping capability of the system while enforcing a continuous power balance on the system. When compared to the prevailing hourly discrete-time model on a Northern European test system, the hydropower resources in the continuous-time model provides ramping flexibility to a greater extent. This helps the hybrid power system stay in balance during hours with quick ramping in the net-load but slightly less hydropower energy is produced.**

I. Introduction

A. Background and Literature Review

THE transition from traditional power systems dominated by conventional power generation to hybrid energy systems with significant amounts of variable renewable energy sources (VRES) is well underway in many power systems around the world. Such a fundamental shift is an important part of eventually reaching a zero net-emission and climate-neutral society, which is currently the stated long-term goal of the European Union [1]. There are several new challenges related to operating a hybrid system, mainly related to the variability of the renewable resources. The optimal coordination between different resources to mitigate the low flexibility of VRES is a central issue, which requires detailed modelling of the responsiveness of each generation type to fairly estimate the system flexibility. The stochastic nature of VRES must be considered in the scheduling of production and reserve capacity, as forecast errors will inevitably cause deviations between scheduled production and actual net load. Such imbalances can be modelled through stochastic optimization techniques, and are an essential driver behind the advancement of stochastic scheduling models in the last decades [2].

In addition to the issue of resource flexibility scarcity, hybrid systems are faced with the challenge of adapting to the current electricity market structure to handle ramping scarcity in real-time balancing. Structural imbalances are created by the granularity of the electricity markets [3], [4]. The day-ahead electricity markets in Europe typically have a time resolution of 15, 30, or 60 minutes, which results in piece-wise constant production schedules for each time interval after the market is cleared [5]. As the power output of VRES can change quickly within the span of a few minutes, reserved flexible resources must be used to balance high-ramping events even if they are anticipated in the forecasts. Another factor which could increase structural imbalances is increased HVDC transmission capacity between synchronous systems [6]. This effect reduces the number of flexible resources available to balance uncertain imbalances, causing additional strain on the system. Regulatory changes such as finer market trading granularity could alleviate some of the structural imbalances [7], though moving from trading energy to power profiles should be considered [8].

An example of a large hybrid system is the interconnected power system in Northern Europe, which contains flexible hydropower in Norway with large reservoirs, conventional thermal generation in Continental Europe, and considerable emerging offshore wind power resources in the North Sea [9]. The growth in HVDC transmission capacity from Norway to continental Europe and Great Britain increases the potential for utilizing the hydropower flexibility to help balance the larger system. The operational planning of hydrothermal systems has been investigated over several decades, resulting in various well-established models ranging from long-term scheduling [10], [11] to medium-term [12] and short-term operation [13].

B. Contribution and Paper Structure

Understanding the interaction between flexible resources, conventional thermal generation, and VRES on a system scale is of the utmost importance when it comes to efficient balancing of both structural and stochastic imbalances. There is need of a holistic approach to the complicated issue of dealing with these types of imbalances at the same time, and new modelling tools are required to evaluate the flexibility resources and limitations intrinsic to the system. In this context, this paper presents a novel stochastic continuous-time optimization model for optimal coordination of hydrothermal

This work was funded by The Research Council of Norway, Project No. 268014/E20. C. Ø. Naversen and H. Farahmand are with the Department of Electric Power Engineering, Norwegian University of Science and Technology, 7491 Trondheim, Norway (e-mails: christian.naversen@ntnu.no, hossein.farahmand@ntnu.no).

A. Helseth is with the Department of Energy Systems, SINTEF Energy Research, Sem Sælands vei 11, 7034 Trondheim, Norway (e-mail: Arild.Helseth@sintef.no).

B. Li and M. Parvania are with the Department of Electrical and Computer Engineering, University of Utah, Salt Lake City, UT 84112 USA (email: bosong.li@utah.edu, masood.parvania@utah.edu).

flexibility to compensate the uncertainty and variability of VRES. Continuous-time optimization for power system operation was initially developed in [14], which models time-dependent input parameters and decision variables as continuous and smooth functions of time. Since a continuous power balance is enforced instead of an average energy balance, the approach internalizes the structural imbalances of the system. Stochastic multi-stage [15], [16] and multi-fidelity [17], [18] continuous-time models have been formulated previously in the literature. The model presented in this work builds on our previous formulation of hydrothermal coordination in [19], [20] to formulate a two-stage stochastic reserve procurement and scheduling model for a hybrid power system with hydro, thermal and wind power generation, an example of which is based in the Northern European power system. The model addresses both the resource and market flexibility issues caused by high variability and quick ramping of the offshore wind power. The mathematical formulation of the proposed model represents the short-term operation of a hybrid system comprising cascaded hydropower, thermal generation and wind power. The model considers system dispatch under wind power uncertainty, followed by real-time balancing. The model enables the assessment of additional system operation costs associated with structural imbalances in the system. This assessment is based on comparing the continuous-time model with an analogous stochastic discrete-time model on a simplified equivalent data description of the Northern European power system.

The rest of this paper is organized as follows: the proposed stochastic continuous-time flexibility coordination model is formulated in Section II, the cases study based on the Northern European power system is presented in Section III, and the conclusions are drawn in Section IV.

II. The Proposed Flexibility Coordination Model

A two-stage continuous-time unit commitment and reserve procurement model for a hydrothermal system with offshore wind power joined by HVDC cables is formulated in Sections II-A to II-C. The fundamental properties of the continuous-time framework with an explanation of the notation is found in Appendix A. The goal of the model as a whole is to find the generation schedule and reserve capacity procurement for both the thermal and hydropower units which gives the lowest expected operational costs given the load and uncertainty in wind power. The most important first-stage decisions are thus to determine the unit commitment, production and reserve capacity schedules of all units, and the scheduled flow on the cables between the areas. The uncertainty in wind power generation is realized in the second stage, and so the procured reserve capacity from the first stage is activated to balance the deviation. Respecting the physical constraints of the system and individual units, such as ramping on thermal units and the water balance of the hydropower system, is essential in both the scheduling and balancing stages. The wind power is considered to be known for a short period at the beginning of the optimization horizon before branching into several possible scenarios, giving rise to the two-stage formulation. The variables of the model are written as lower case Latin letters, and variables and other symbols in bold signify a column vector representing the coefficients of the underlying Bernstein polynomials.

A. Objective Function

The objective function Ω for the stochastic model is to minimize the total expected cost of operating the interconnected hydrothermal system. It is defined for the time intervals $h \in \mathcal{T}$ of length δ_h, hydropower units $m \in \mathcal{M}$, thermal units $j \in \mathcal{J}$, and balancing scenarios $s \in \mathcal{S}$. The first-stage variables are expressed with Bernstein polynomials of degree three, while the second-stage variables are of fidelity five:

$$\begin{aligned}\min \Omega = \frac{1}{4}\mathbf{1}^\intercal \sum_{h\in\mathcal{T}} \delta_h \Bigg[& \sum_{m\in\mathcal{M}} \left(C^b \mathbf{q}^b_{mh} + C^o \mathbf{q}^o_{mh} \right) + \sum_{j\in\mathcal{J}} C_j \mathbf{g}_{jh} \\ & + \sum_{m\in\mathcal{M}} K^{\text{hyd}}_m \left(\mathbf{r}^{\text{hyd},\uparrow}_{mh} + \mathbf{r}^{\text{hyd},\downarrow}_{mh} \right) + \sum_{j\in\mathcal{J}} K^{\text{th}}_j \left(\mathbf{r}^{\text{th},\uparrow}_{jh} + \mathbf{r}^{\text{th},\downarrow}_{jh} \right) \Bigg] \\ & + \sum_{h\in\mathcal{T}} \sum_{m\in\mathcal{M}} \left(\overline{C}^{\text{hyd}}_m su^{\text{hyd}}_{mh} + \underline{C}^{\text{hyd}}_m sd^{\text{hyd}}_{mh} \right) \\ & + \sum_{h\in\mathcal{T}} \sum_{j\in\mathcal{J}} \left(\overline{C}^{\text{th}}_j su^{\text{th}}_{jh} + \underline{C}^{\text{th}}_j sd^{\text{th}}_{jh} \right) + \sum_{s\in\mathcal{S}} \pi_s \Delta\Omega_s. \end{aligned} \tag{1}$$

The first line of the objective is the total incurred spillage ($\mathbf{q}^o_{mh}$) and bypass ($\mathbf{q}^b_{mh}$) penalties, and the scheduled cost of the thermal generation ($\mathbf{g}_{jh}$). As in [17], an explicit cost for the reserved hydropower capacity ($\mathbf{r}^{\text{hyd},\uparrow/\downarrow}_{mh}$) and thermal capacity ($\mathbf{r}^{\text{th},\uparrow/\downarrow}_{jh}$) is added in the second line. The cost is assumed to be constant over the optimization horizon and equal for upward and downward reserve. The resulting objective function cost has been calculated by integrating the time-varying continuous curves of third degree over the whole optimization horizon by use of eq. (16) in Appendix A. The startup (su^{hyd}_{mh}, su^{th}_{jh}) and shutdown (sd^{hyd}_{mh}, sd^{th}_{jh}) costs of the thermal and hydropower plants are summed up in the third and fourth lines, while the last term in line four of eq. (1) is the expected cost of the balancing stage. The cost $\Delta\Omega_s$ is the sum of penalties and operational cost of the thermal and hydropower plants in scenario s with probability π_s:

$$\begin{aligned}\Delta\Omega_s = z_s + \frac{1}{6}\mathbf{1}^\intercal \sum_{h\in\mathcal{T}} \delta_h \Bigg[& \rho^{\text{hyd}} \sum_{m\in\mathcal{M}} \left(\Delta\mathbf{p}^+_{smh} + \Delta\mathbf{p}^-_{smh} \right) \\ & + \sum_{j\in\mathcal{J}} \left(C^+_j \Delta\mathbf{g}^+_{sjh} - C^-_j \Delta\mathbf{g}^-_{sjh} \right) \\ & + \sum_{m\in\mathcal{M}} \left(C^{o+} \Delta\mathbf{q}^{o+}_{smh} - C^{o-} \Delta\mathbf{q}^{o-}_{smh} \right) \\ & + \sum_{m\in\mathcal{M}} \left(C^{b+} \Delta\mathbf{q}^{b+}_{smh} - C^{b-} \Delta\mathbf{q}^{b-}_{smh} \right) \\ & + \sum_{a\in\mathcal{A}} \left(C^{\text{shd}} \mathbf{y}^{\text{shd}}_{sah} + C^{\text{crt}} \mathbf{y}^{\text{crt}}_{sah} \right) \Bigg] \end{aligned} \tag{2}$$

The expected future cost of the system (z_s) and the deployment cost of the activated hydropower reserves ($\Delta\mathbf{p}^{\pm}_{smh}$) make up the terms in the first line of eq. (2). The cost

of activating hydropower reserves ρ^{hyd} is the same in both directions and considered equal for all the hydropower units. The operational and deployment cost of the thermal reserves ($\Delta\mathbf{g}^{\pm}$) is found in the second line, where the cost coefficients $C_j^{\pm}$ are related to the marginal cost C_j of the thermal units so that $C_j^- < C_j < C_j^+$. This means that a deployment cost is paid when reserves are deployed in either direction in addition to the change in operational cost of the thermal units. Line three and four of the second-stage objective function apply the same cost structure to changing the bypass ($\Delta\mathbf{q}_{smh}^{b\pm}$) and spillage ($\Delta\mathbf{q}_{smh}^{o\pm}$) flows in the second stage. This is done to discourage the model from unnecessary changes in the bypass and spillage decisions in the balancing stage. Finally, the last line of eq. (2) is the cost of shedding load ($\mathbf{y}_{ah}^{\text{shd}}$) and curtailing wind ($\mathbf{y}_{ah}^{\text{crt}}$) in all areas $a \in \mathcal{A}$.

B. First-Stage Constraints

The first-stage constraints model the unit commitment decisions, reserve procurement, and scheduling decisions of the interconnected system using a continuous-time formulation of third degree.

1) Thermal production constraints: All thermal generators $j \in \mathcal{J}$ are scheduled for time intervals $h \in \mathcal{T}$ according to the following unit commitment and ramping constraints:

$$\mathbf{g}_{jh} + \mathbf{r}_{jh}^{\text{th},\uparrow} \leq G_j^{max}\mathbf{u}_{jh}^{\text{th}} \tag{3a}$$
$$\mathbf{g}_{jh} - \mathbf{r}_{jh}^{\text{th},\downarrow} \geq G_j^{min}\mathbf{u}_{jh}^{\text{th}} \tag{3b}$$
$$\mathbf{0} \leq \mathbf{r}_{jh}^{\text{th},\uparrow/\downarrow} \leq \left(G_j^{max} - G_j^{min}\right)\mathbf{1} \tag{3c}$$
$$\mathbf{u}_{jh}^{\text{th}} = \left[u_{jh}^{\text{th}}, u_{jh}^{\text{th}}, u_{j,h+1}^{\text{th}}, u_{j,h+1}^{\text{th}}\right]^{\intercal} \tag{3d}$$
$$\mathrm{F}^0(\mathbf{g}_{jh}) = 0, \;\; h \neq N \tag{3e}$$
$$\mathrm{F}^1(\mathbf{g}_{jh}) = 0, \;\; h \neq N \tag{3f}$$
$$su_{jh}^{\text{th}} - sd_{jh}^{\text{th}} = u_{j,h+1}^{\text{th}} - u_{jh}^{\text{th}} \tag{3g}$$
$$-\mathbf{R}_{jh}^{\downarrow} \leq \frac{1}{\delta_h}\mathbf{K}_3^{\intercal}\cdot\mathbf{g}_{jh} \leq \mathbf{R}_{jh}^{\uparrow} \tag{3h}$$
$$\mathbf{R}_{jh}^{\uparrow} = R_j^{\uparrow}\left[u_{jh}^{\text{th}}, u_{j,h+1}^{\text{th}} + \gamma_{jh}^{\uparrow} su_{jh}^{\text{th}}, u_{j,h+1}^{\text{th}}\right]^{\intercal} \tag{3i}$$
$$\mathbf{R}_{jh}^{\downarrow} = R_j^{\downarrow}\left[u_{jh}^{\text{th}}, u_{jh}^{\text{th}} + \gamma_{jh}^{\downarrow} sd_{jh}^{\text{th}}, u_{j,h+1}^{\text{th}}\right]^{\intercal} \tag{3j}$$
$$u_{jh}^{\text{th}} \in \{0,1\} \tag{3k}$$
$$0 \leq su_{jh}^{\text{th}} \leq 1 \tag{3l}$$
$$0 \leq sd_{jh}^{\text{th}} \leq 1 \tag{3m}$$
$$\{su_{jh}^{\text{th}}, sd_{jh}^{\text{th}}\} \text{ of SOS type 1} \tag{3n}$$

Theses constraints are primarily based on the formulation of [14]. The thermal generation $\mathbf{g}_{jh}$ and the procured reserve capacity $\mathbf{r}_{jh}^{\text{th},\uparrow/\downarrow}$ in the upward and downward direction must obey the minimum and maximum generation limits of the generator in eqs. (3a) to (3c). Note that the convex hull property in eq. (13) in Appendix A is used to ensure that the continuous curves represented by the coefficient vectors are within the generator bounds. The binary commitment variable u_{jh}^{th} can be interpreted as the commitment status of the generator at the beginning of interval h, and is incorporated into the generation limit constraints by the vector in eq. (3d). Note that this formulation requires $N+1$ commitment variables for each generator, as the commitment status at the end of the horizon is included. The formulation allows the thermal units to use the whole interval h to smoothly start up or shut down production, which is necessary since the generation trajectory is required to be C^1 continuous in eqs. (3e) and (3f). The startups (su_{jh}^{th}) and shutdowns (sd_{jh}^{th}) of the generators are counted in eq. (3g). The ramping constraints for the generators is formulated in eq. (3h), which is based on taking the derivative of the thermal production trajectory $g_j(t)$ and using the relation in eq. (14) in Appendix A. The upper and lower ramping trajectory bounds are formulated in eqs. (3i) and (3j). The commitment variables are used to make a tight formulation of the ramping constraint. Extra care must be taken for the middle vector component to ensure that the ramping constraints do not interfere with the upper and lower generation bounds when a unit is starting up or shutting down. Additional ramping capability $\gamma_{jh}^{\uparrow/\downarrow} R_j^{\uparrow/\downarrow}$ is used to relax the ramping constraint in this case, and must satisfy $\gamma_{jh}^{\uparrow/\downarrow} \geq \frac{3G_j^{min}}{\delta_h R_j^{\uparrow/\downarrow}} - 1$ for the unit to be able to start up or shut down. The startup and shutdown variables are formulated as continuous variables which are part of a special ordered set (SOS) of type 1 in eqs. (3l) to (3n), which means that at most one of the variables for each $j \in \mathcal{J}$ and $h \in \mathcal{T}$ can be nonzero.

2) Hydropower constraints: The constraints governing the management of the hydropower plants and reservoirs $m \in \mathcal{M}$ for time intervals $h \in \mathcal{T}$ are given in eqs. (4a) to (4v) and based on the formulation in [19]:

$$v_{m0} = V_m^0 \tag{4a}$$
$$v_{m,h+1} - v_{mh} = \frac{1}{4}\delta_h \mathbf{1}^{\intercal}\cdot\mathbf{q}_{mh}^{\text{net}} \tag{4b}$$
$$\mathbf{w}_{mh} = v_{mh}\mathbf{1} + \delta_h \mathbf{N}_3^{\intercal}\cdot\mathbf{q}_{mh}^{\text{net}} \tag{4c}$$
$$\mathbf{q}_{mh}^{\text{net}} = \mathbf{I}_{mh} + \mathbf{q}_{smh}^{\text{in}} - \mathbf{q}_{mh}^{\text{rel}} - \mathbf{q}_{mh}^{o} \tag{4d}$$
$$\mathbf{q}_{mh}^{\text{in}} = \sum_{i\in\mathcal{I}_m^d} \mathbf{q}_{ih}^{d} + \sum_{i\in\mathcal{I}_m^b} \mathbf{q}_{ih}^{b} + \sum_{i\in\mathcal{I}_m^o} \mathbf{q}_{ih}^{o} \tag{4e}$$
$$\mathbf{q}_{mh}^{\text{rel}} = \mathbf{q}_{mh}^{d} + \mathbf{q}_{mh}^{b} - \mathbf{I}_{mh}^{u} \tag{4f}$$
$$\mathbf{p}_{mh} = \eta_m \mathbf{q}_{mh}^{d} \tag{4g}$$
$$\mathbf{p}_{mh} + \mathbf{r}_{mh}^{\text{hyd},\uparrow} \leq P_m^{max} u_{mh}^{\text{hyd}}\mathbf{1} \tag{4h}$$
$$\mathbf{p}_{mh} - \mathbf{r}_{mh}^{\text{hyd},\downarrow} \geq P_m^{min} u_{mh}^{\text{hyd}}\mathbf{1} \tag{4i}$$
$$su_{mh}^{\text{hyd}} - sd_{mh}^{\text{hyd}} = u_{m,h+1}^{\text{hyd}} - u_{mh}^{\text{hyd}}, \;\; h \neq N \tag{4j}$$
$$\mathrm{F}^0(\mathbf{q}_{mh}^{o}) = 0, \;\; h \neq N \tag{4k}$$
$$\mathrm{F}^0(\mathbf{q}_{mh}^{b}) = 0, \;\; h \neq N \tag{4l}$$
$$\mathbf{0} \leq \mathbf{w}_{mh} \leq V_m\mathbf{1} \tag{4m}$$
$$\mathbf{0} \leq \mathbf{q}_{mh}^{d} \leq Q_m^{d}\mathbf{1} \tag{4n}$$
$$\mathbf{0} \leq \mathbf{q}_{mh}^{b} \leq Q_m^{b}\mathbf{1} \tag{4o}$$
$$\mathbf{0} \leq \mathbf{q}_{mh}^{o} \tag{4p}$$
$$\mathbf{0} \leq \mathbf{q}_{mh}^{\text{rel}} \tag{4q}$$
$$\mathbf{0} \leq \mathbf{r}_{mh}^{\text{hyd},\uparrow/\downarrow} \leq \left(P_m^{max} - P_m^{min}\right)\mathbf{1} \tag{4r}$$
$$u_{mh}^{\text{hyd}} \in \{0,1\} \tag{4s}$$
$$0 \leq su_{mh}^{\text{hyd}} \leq 1 \tag{4t}$$
$$0 \leq sd_{mh}^{\text{hyd}} \leq 1 \tag{4u}$$

$$\{su^{\text{hyd}}_{mh}, sd^{\text{hyd}}_{mh}\} \text{ of SOS type 1.} \tag{4v}$$

The volume balance of the reservoirs are kept by eqs. (4a) and (4b), where the volume variables v_{mh} is the volume at the start of interval h. The change in volume over a time interval is found by integrating the net flow into the reservoir, $q^{\text{net}}_m(t)$, by using the relation in eq. (16) in Appendix A . The time-varying volume within time interval h is found by using eq. (15) in Appendix A, and is described by $\mathbf{w}_{mh}$ in eq. (4c). Equations (4d) to (4f) describes how water can flow through the three different waterways between reservoirs. It is possible to discharge water through the turbine ($\mathbf{q}^d_{mh}$), bypass water around the power plant ($\mathbf{q}^b_{mh}$), or spill water out of the reservoir ($\mathbf{q}^o_{mh}$), see Figure 1 for an illustration. All waterways may lead to different downstream reservoirs or directly out of the system. The regulated flow into the reservoir ($\mathbf{q}^{\text{in}}_{mh}$) is found by summing up the discharge, bypass and spillage flows from the connected upstream reservoirs contained in the sets $\mathcal{I}^d_m$, $\mathcal{I}^b_m$, and $\mathcal{I}^o_m$, respectively. It is necessary to introduce the water released from the reservoir ($\mathbf{q}^{\text{rel}}_{mh}$) to properly model the unregulated inflow $\mathbf{I}^u_{mh}$ which enters the system between the reservoir and plant. Regulated inflow $\mathbf{I}_{mh}$ enters directly into the reservoirs and may therefore be stored. The power output of the generator $\mathbf{p}_{mh}$ is approximated as linearly related to the discharged water through the turbine in eq. (4g). Due to the large problems size we assume a concave hydropower production function, see [13] for more accurate treatment. The unit commitment and startup/shutdown constraints are found in eqs. (4h) to (4j), which includes the spinning reserve capacity procurement $\mathbf{r}^{\text{hyd},\uparrow/\downarrow}_{mh}$ and the binary commitment status u^{hyd}_{mh}. Note that the upper and lower generation limits of the hydropower units are not modelled in the same way as the thermal units in eqs. (3a) and (3b). Since starting a hydropower unit usually takes less than a minute, the hydropower production trajectories are not required to be continuous over the time intervals. Consequently, the hydropower units are allowed to instantaneously start up or shut down production from one interval to the next. The bypass and spillage variables are still forced to be C^0 continuous in eqs. (4k) and (4l). The remaining constraints from eqs. (4m) to (4v) are the imposed physical bounds for the variables.

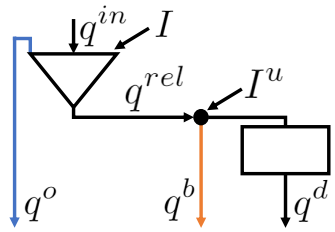

Fig. 1. Depiction of the different waterways for discharging, bypassing and spilling water between reservoirs. Natural inflow enters the system in two different ways, either into the reservoir (triangle) or directly into the main tunnel of the plant (rectangle).

3) System constraints: System wide constraints for the areas $a \in \mathcal{A}$ connected by HVDC transmission lines $l \in \mathcal{L}$ for all time intervals $h \in \mathcal{T}$ are the following:

$$\sum_{m\in\mathcal{M}_a} \mathbf{p}_{mh} + \sum_{j\in\mathcal{J}_a} \mathbf{g}_{jh} - \sum_{l\in\mathcal{L}} G_{la}\mathbf{f}_{lh} = \mathbf{L}_{ah} - \mathbf{W}_{ah} \tag{5a}$$

$$-F^{max}_l \mathbf{1} \le \mathbf{f}_{lh} \le F^{max}_l \mathbf{1} \tag{5b}$$

$$\mathrm{F}^0(\mathbf{f}_{lh}) = 0, \;\; h \neq N \tag{5c}$$

$$\mathrm{F}^1(\mathbf{f}_{lh}) = 0, \;\; h \neq N \tag{5d}$$

$$\sum_{j\in\mathcal{J}} \mathrm{F}^0(\mathbf{r}^{\text{th},\uparrow/\downarrow}_{jh}) = 0, \;\; h \neq N \tag{5e}$$

$$\sum_{m\in\mathcal{M}} \mathrm{F}^0(\mathbf{r}^{\text{hyd},\uparrow/\downarrow}_{mh}) = 0, \;\; h \neq N. \tag{5f}$$

The load $\mathbf{L}_{ah}$ and forecasted wind power $\mathbf{W}_{ah}$ are C^1 continuous input parameters, and must be balanced by the total thermal and hydropower generation in each area in addition to the imports and exports $\mathbf{f}_{lh}$ on the transmission lines in eq. (5a). The coefficient G_{la} is either ± 1 or 0, and dictates the positive flow direction on line l if it is connected to area a. Equation (5b) bounds the maximal and minimal flow on each transmission line, and eqs. (5c) and (5d) forces the line flow to be C^1 continuous. Even though the individual hydropower production variables are discontinuous over the time intervals, the C^1 continuity of all other components of the power balance constraint force the sum of the hydropower production to also be C^1 continuous. The total reserved thermal and hydropower capacity in both directions is also required to be C^0 continuous in eqs. (5e) and (5f).

C. Second-Stage Constraints

The uncertain wind power generation is realized in the second stage, and the reserved capacity of the generators of the system is deployed to keep the system in balance. The first h_0 time intervals of the optimization horizon is considered deterministic with known wind power output, and the second-stage variables are therefore only defined for the time periods $h \in \{h_0, \ldots, N\} \equiv \mathcal{T}_{scen}$. The second-stage variables are formulated as deviations from their first-stage values where applicable, signified by a preceding Δ symbol. The connection to the first-stage production schedule, reserve capacity procurement, and unit commitment decisions make up the tightest coupling between the stages. However, the first-stage water flow and reservoir volume plans also affect the second-stage hydropower operation, as shown in Section II-C2. The constraints listed in the following subsections are valid for all scenarios $s \in \mathcal{S}$, and scenario dependent data and decision variables are marked by a scenario subscript s. The time-dependent scenario variables are modelled using 5th degree Bernstein polynomials to capture the fast variations of the wind power production.

1) Thermal production constraints: The constraints dictating the change in thermal production as reserve capacity is deployed are valid for all thermal generators $j \in \mathcal{J}$ and time intervals $h \in \mathcal{T}_{scen}$:

$$-\mathbf{X}^{\intercal}_{3,5} \cdot \mathbf{r}^{\text{th},\downarrow}_{jh} \le \Delta\mathbf{g}_{sjh} \le \mathbf{X}^{\intercal}_{3,5} \cdot \mathbf{r}^{\text{th},\uparrow}_{jh} \tag{6a}$$

$$\frac{1}{\delta_h}\mathbf{K}^{\intercal}_5 \cdot \left(\mathbf{X}^{\intercal}_{3,5} \cdot \mathbf{g}_{jh} + \Delta\mathbf{g}_{sjh}\right) \le \mathbf{X}^{\intercal}_{2,4} \cdot \mathbf{R}^{\uparrow}_{jh} \tag{6b}$$

$$\frac{1}{\delta_h}\mathbf{K}_5^\intercal \cdot \left(\mathbf{X}_{3,5}^\intercal \cdot \mathbf{g}_{jh} + \Delta\mathbf{g}_{sjh}\right) \geq -\mathbf{X}_{2,4}^\intercal \cdot \mathbf{R}_{jh}^\downarrow \tag{6c}$$

$$\mathrm{F}^0(\Delta\mathbf{g}_{sjh}) = 0, \;\; h \neq N \tag{6d}$$

$$\mathrm{F}^1(\Delta\mathbf{g}_{sjh}) = 0, \;\; h \neq N \tag{6e}$$

$$\Delta\mathbf{g}_{sjh} = \Delta\mathbf{g}_{sjh}^+ - \Delta\mathbf{g}_{sjh}^- \tag{6f}$$

$$\mathbf{0} \leq \Delta\mathbf{g}_{sjh}^\pm \tag{6g}$$

The deployed thermal reserve power $\Delta\mathbf{g}_{sjh}$ is bound to be within the limits determined by the first-stage reserve procurement in Section II-B1. The elevation matrix $\mathbf{X}_{3,5}$ is used to lift the first-stage reserve variables to the higher fidelity of the second-stage variables. Ramping constraints are applied to the entire second-stage generation in eqs. (6b) and (6c) which enforce the same upper and lower ramping trajectories as in the first-stage eqs. (3i) and (3j). The second-stage change in production is required to be C^1 continuous in eqs. (6d) and (6e), and is explicitly split into positive and negative parts $\Delta\mathbf{g}_{sjh}^\pm$ in eqs. (6f) and (6g) to distinguish upward and downward reserve activation.

2) Hydropower constraints: The second-stage hydropower related decisions for all plants $m \in \mathcal{M}$ and time intervals $h \in \mathcal{T}_{scen}$ are also formulated as deviations from the first-stage solution governed by the constraints in Section II-B2:

$$\Delta v_{sm,h_0} = 0 \tag{7a}$$

$$\Delta v_{sm,h+1} - \Delta v_{smh} = \frac{1}{6}\delta_h \mathbf{1}^\intercal \cdot \Delta\mathbf{q}_{smh}^{\text{net}} \tag{7b}$$

$$\Delta\mathbf{w}_{smh} = \Delta v_{smh}\mathbf{1} + \delta_h \mathbf{N}_5^\intercal \cdot \Delta\mathbf{q}_{smh}^{\text{net}} \tag{7c}$$

$$\Delta\mathbf{q}_{smh}^{\text{net}} = \Delta\mathbf{q}_{smh}^{\text{in}} - \Delta\mathbf{q}_{smh}^{\text{rel}} - \Delta\mathbf{q}_{smh}^{o} \tag{7d}$$

$$\Delta\mathbf{q}_{smh}^{\text{in}} = \sum_{i\in\mathcal{I}_m^d} \Delta\mathbf{q}_{sih}^{d} + \sum_{i\in\mathcal{I}_m^b} \Delta\mathbf{q}_{sih}^{b} + \sum_{i\in\mathcal{I}_m^o} \Delta\mathbf{q}_{sih}^{o} \tag{7e}$$

$$\Delta\mathbf{q}_{smh}^{\text{rel}} = \Delta\mathbf{q}_{smh}^{d} + \Delta\mathbf{q}_{smh}^{b} \tag{7f}$$

$$\Delta\mathbf{p}_{smh} = \eta_m \Delta\mathbf{q}_{smh}^{d} \tag{7g}$$

$$-\mathbf{X}_{3,5}^\intercal \cdot \mathbf{r}_{mh}^{\text{hyd},\downarrow} \leq \Delta\mathbf{p}_{smh} \leq \mathbf{X}_{3,5}^\intercal \cdot \mathbf{r}_{mh}^{\text{hyd},\uparrow} \tag{7h}$$

$$\mathrm{F}^0(\Delta\mathbf{q}_{smh}^{o}) = 0, \;\; h \neq N \tag{7i}$$

$$\mathrm{F}^0(\Delta\mathbf{q}_{smh}^{b}) = 0, \;\; h \neq N \tag{7j}$$

$$\mathbf{0} \leq \mathbf{X}_{4,6}^\intercal \cdot \mathbf{w}_{mh} + \Delta\mathbf{w}_{smh} \leq V_m\mathbf{1} \tag{7k}$$

$$\mathbf{0} \leq \mathbf{X}_{3,5}^\intercal \cdot \mathbf{q}_{mh}^{d} + \Delta\mathbf{q}_{smh}^{d} \leq Q_m^d\mathbf{1} \tag{7l}$$

$$\mathbf{0} \leq \mathbf{X}_{3,5}^\intercal \cdot \mathbf{q}_{mh}^{b} + \Delta\mathbf{q}_{smh}^{b} \leq Q_m^b\mathbf{1} \tag{7m}$$

$$\mathbf{0} \leq \mathbf{X}_{3,5}^\intercal \cdot \mathbf{q}_{mh}^{o} + \Delta\mathbf{q}_{smh}^{o} \tag{7n}$$

$$\mathbf{0} \leq \mathbf{X}_{3,5}^\intercal \cdot \mathbf{q}_{mh}^{\text{rel}} + \Delta\mathbf{q}_{smh}^{\text{rel}} \tag{7o}$$

$$\Delta\mathbf{q}_{smh}^{o} = \Delta\mathbf{q}_{smh}^{o+} - \Delta\mathbf{q}_{smh}^{o-} \tag{7p}$$

$$\Delta\mathbf{q}_{smh}^{b} = \Delta\mathbf{q}_{smh}^{b+} - \Delta\mathbf{q}_{smh}^{b-} \tag{7q}$$

$$\Delta\mathbf{p}_{smh} = \Delta\mathbf{p}_{smh}^{+} - \Delta\mathbf{p}_{smh}^{-} \tag{7r}$$

$$\mathbf{0} \leq \Delta\mathbf{q}_{smh}^{o\pm} \tag{7s}$$

$$\mathbf{0} \leq \Delta\mathbf{q}_{smh}^{b\pm} \tag{7t}$$

$$\mathbf{0} \leq \Delta\mathbf{p}_{smh}^{\pm}. \tag{7u}$$

The change in volume and flow between the reservoirs, eqs. (7a) to (7g), are analogous to the first-stage constraints eqs. (4a) to (4g). Note that the inflow is deterministic and is therefore not a part of the second-stage volume and flow deviation constraints. The change in hydropower production is constrained to be within the bounds of the procured reserve capacity in eq. (7h), and the spillage and bypass is forced to remain C^0 continuous in the second stage by eqs. (7i) and (7j). The total volume, discharge and bypass in the second stage must still be within their respective physical bounds, which is ensured by constraining the sum of the first-stage and second-stage variables in eqs. (7k) to (7m). Similarly, the total spillage and reservoir release is kept non-negative by adding eqs. (7n) and (7o). The change in spillage, bypass and hydropower production are split into positive and negative parts in eqs. (7p) to (7u). As was the case for the change in thermal generation, the split of the second-stage hydropower production variables is done to correctly identify upward and downward reserve deployment.

3) System constraints: The deviation between realized wind power and forecasted wind power, $\Delta\mathbf{W}_{sah}$, must be balanced in the second stage for all areas $a \in \mathcal{A}$ and time intervals $h \in \mathcal{T}_{scen}$. In addition, the future expected cost of the system, z_s, is taken into account for all Benders cuts $k \in \mathcal{K}$:

$$z_s \geq \sum_{m\in\mathcal{M}} WV_{mk}(v_{m,N+1} + \Delta v_{sm,N+1}) + D_k \tag{8a}$$

$$\sum_{m\in\mathcal{M}_a} \Delta\mathbf{p}_{smh} + \sum_{j\in\mathcal{J}_a} \Delta\mathbf{g}_{sjh} - \sum_{l\in\mathcal{L}} G_{la}\Delta\mathbf{f}_{slh} = -\Delta\mathbf{W}_{sah} - \mathbf{y}_{sah}^{\text{shd}} + \mathbf{y}_{sah}^{\text{crt}} \tag{8b}$$

$$-F_l^{max}\mathbf{1} \leq \mathbf{X}_{3,5}^\intercal \cdot \mathbf{f}_{lh} + \Delta\mathbf{f}_{slh} \leq F_l^{max}\mathbf{1} \tag{8c}$$

$$\mathrm{F}^0(\Delta\mathbf{f}_{slh}) = 0, \;\; h \neq N \tag{8d}$$

$$\mathrm{F}^1(\Delta\mathbf{f}_{slh}) = 0, \;\; h \neq N \tag{8e}$$

$$\sum_{m\in\mathcal{M}_a} \mathrm{F}^0(\Delta\mathbf{p}_{smh}) = 0, \;\; h \neq N \tag{8f}$$

$$\sum_{m\in\mathcal{M}_a} \mathrm{F}^1(\Delta\mathbf{p}_{smh}) = 0, \;\; h \neq N \tag{8g}$$

$$\mathbf{0} \leq \mathbf{y}_{sah}^{\text{crt}} \leq \max\{\mathbf{0}, \Delta\mathbf{W}_{sah}\} \tag{8h}$$

$$\mathbf{0} \leq \mathbf{y}_{sah}^{\text{shd}} \tag{8i}$$

The future expected cost of the hydrothermal system z_s is defined by the linear Benders cuts $k \in \mathcal{K}$ in eq. (8a), which depends on the total final volume of all hydropower reservoirs in scenario s. The cut coefficients WV_{mk} and constant term D_k are calculated by the use of long-term hydrothermal scheduling models that consider the operation of the system on a time horizon of several seasons, such as [10]. Using more or less water in a given scenario results in higher or lower future expected costs according to the cuts. The power balance in eq. (8b) allows the change in wind to be balanced by deploying thermal and hydropower reserves and changing the flow on the HVDC lines. In addition, wind curtailment $\mathbf{y}_{sah}^{\text{crt}}$ and load shedding $\mathbf{y}_{sah}^{\text{shd}}$ are possible options for keeping the balance. Note that eq. (8h) only allow the curtailment of wind down to the forecasted wind power value. The total flow on the HVDC lines are bound by the transmission capacity in eq. (8c), and is still required to be C^1 continuous in eqs. (8d) and (8e). The C^1 continuity of the sum of the hydropower production is enforced directly by eqs. (8f) and (8g).

4) Initial continuity constraints: The continuity constraints applied to the second-stage variables in the previous subsec-

tions do not ensure a smooth transition from the schedule in the initial deterministic period to the real-time operation in each scenario. To remedy this, the following constraints based on eqs. (19) and (20) in Appendix A are added:

$$\Delta\mathbf{g}^{(0)}_{sj,h_0}, \quad \Delta\mathbf{g}^{(1)}_{sj,h_0} = 0 \qquad \forall j \in \mathcal{J} \quad (9a)$$

$$\Delta\mathbf{f}^{(0)}_{sl,h_0}, \quad \Delta\mathbf{f}^{(1)}_{sl,h_0} = 0 \qquad \forall l \in \mathcal{L} \quad (9b)$$

$$\Delta\mathbf{q}^{b,(0)}_{sm,h_0} = 0 \qquad \forall m \in \mathcal{M} \quad (9c)$$

$$\Delta\mathbf{q}^{o,(0)}_{sm,h_0} = 0 \qquad \forall m \in \mathcal{M} \quad (9d)$$

$$\sum_{m\in\mathcal{M}} \Delta\mathbf{p}^{(0)}_{sm,h_0}, \quad \sum_{m\in\mathcal{M}} \Delta\mathbf{p}^{(1)}_{sm,h_0} = 0. \quad (9e)$$

Constraint eq. (9a) force the thermal production and ramping in all scenarios to be continuous at time $t = h_0$ with respect to the scheduled first-stage production. The other constraints have a similar effect of enforcing C^0 and/or C^1 continuity at time $t = h_0$.

III. Case study

A. System Description

The hydrothermal system used in the following sections is based on a simplified version of the Northern European system. An area containing only hydropower production is connected to a thermal area with an HVDC line, while a third wind power area is connected to the thermal area. This represents the coupling of the hydropower-dominated Norwegian system to the continental European system (Netherlands, Germany and Denmark) with considerable offshore wind power resources. A cascaded hydropower topology is used in the hydropower area, which is based on a real Norwegian watercourse with a total of 535.3 MW installed capacity divided among 12 linked reservoir-plant pairs, see [21] for a more detailed description of the hydropower system. The hydropower area is considered to represent the total Norwegian hydropower capacity of roughly 32 GW. The thermal units, HVDC cables, and installed wind power in the rest of the system are scaled down by an equivalent amount to resemble a miniature Northern European system. The thermal area consists of 20 units (one nuclear, one oil, 9 gas and 9 coal) picked from the 2019 update of the IEEE reliability test system [22]. After scaling the thermal units, a total of 921.2 MW thermal capacity is located in the thermal area. The transmission capacity between the hydropower and thermal areas amounts to 63 MW, while the offshore wind power capacity is 172 MW.

B. Input Data and Wind Power Scenario Generation

The Benders cut description used in eq. (8a) was calculated by the long-term hydropower scheduling model in [10] by optimizing the use of the hydrothermal system over a period of 156 weeks, and the initial volumes of every reservoir is set to 60% of its maximal volume. Inflow to the hydropower system are based on historic inflow data during winter, and is considered to be deterministic and is kept as a discrete hourly time series in the continuous-time model. The thermal marginal costs C_j were calculated based on the data in [22], and the same is true for the thermal startup and shutdown costs. The other cost parameters of the objective function are listed in Table I. The hydropower reserve capacity and activation costs are 40% and 30%, respectively, of an estimated "marginal cost" for the hydropower system based on the coefficients of the binding cut when the end volume is assumed to be the same as the initial volume. Similarly, the thermal reserve costs parameters are based on the marginal costs, in accordance with [17].

TABLE I
Objective function cost parameters

Cost parameter	Symbol	Value
Bypass	C^b	100 €/Mm^3
Spillage	C^o	200 €/Mm^3
Bypass change	$C^{b\pm}$	$(1 \pm 0.1)C^b$
Spillage change	$C^{o\pm}$	$(1 \pm 0.1)C^o$
Hydropower startup, shutdown	$\overline{C}^{\text{hyd}}_m, \underline{C}^{\text{hyd}}_m$	100 €
Hydropower reserve capacity	K^{hyd}_m	9 €/MWh
Hydropower reserve activation	ρ^{hyd}	6.75 €/MWh
Thermal reserve capacity	K^{th}_j	$0.4C_j$
Thermal reserve activation	$C^{\pm}_j$	$(1 \pm 0.3)C_j$
Load shedding	C^{shd}	4500 €/MWh
Wind curtailment	C^{crt}	60 €/MWh

The generated wind power production scenarios, see Figure 2, are based on forecasted and realized wind power time series from western Denmark from October 2019 to April 2020 [23]. The stochastic model has a 6 hour period in the beginning which is deterministic, while the remaining 24 hours have uncertain wind power production. The piece-wise constant forecast error for each day was calculated in 15 min resolution, and this data was then fitted to a multivariate Gaussian kernel density function of 96 random variables. 200 equiprobable discrete-time scenarios of 15 minute resolution and 24 hour length was generated from the estimated distribution and added to the discrete-time wind power forecast. Values exceeding the wind power capacity or falling below zero were truncated to these limits. The scenarios were then reduced down to 20 by the standard backward scenario reduction algorithm [24]. The deterministic wind power data is based on realized wind power from 18:00 to 24:00 on October 13th, while the forecasted wind is based on the forecasted wind power for the following day. The continuous-time data is created by using the discrete-time data as input to a constrained least square error optimization program with the Bernstein coefficients as variables. Continuity constraints and bounds on the coefficients are included in this program, and all scenarios are forced to have the same value and derivative as the forecast at the beginning of the stochastic period.

The load for the hydropower area and thermal area is considered deterministic for the whole period, and is calculated based on load data from Norway and Germany from January 2nd 18:00 to January 3rd 24:00 in 2020 [25], [26]. The load series for the two areas are scaled down to have peaks of 85% of the installed thermal and hydropower capacity, respectively.

C. Model Results

The stochastic continuous-time hydrothermal model is implemented and solved using Pyomo and CPLEX 12.10. The

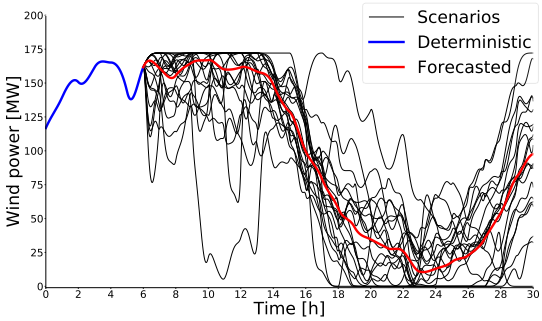

Fig. 2. Wind power input data used in the stochastic continuous-time model. The wind power production in the first 6 hours are deterministic (blue line), while the forecasted wind power (red line) and wind power scenarios (black lines) apply for the following 24 hours.

extensive form of the stochastic model contains about 680k constraints and 420k variables, including 980 binary and 948 SOS 1 variables. A MIP gap of 0.09% (768 €) was reached after 72 hours on a machine with 24 CPUs at 3.50 GHz and 128 GiB RAM, though a reasonable gap of 0.78% is found after 16 hours. The long calculation time can likely be reduced by employing decomposition techniques instead of solving the extensive form directly. Such performance enhancement issues are not the focus of this paper, though it is an important factor in broadening the appeal of stochastic models in general. For comparison, an hourly stochastic discrete-time model based on the same input data was also solved. This model is significantly smaller with 102k constraints and 74k variables (960 binary and 928 SOS 1), and can be solved to a MIP gap of 100 €, or 0.01%, in 10 hours. This discrete-time model is equivalent to the continuous-time model when using Bernstein polynomials of degree zero in both stages and omitting continuity constraints.

TABLE II
OBJECTIVE FUNCTION COST COMPARISON. THE LAST COLUMN IS THE COST DIFFERENCE BETWEEN THE MODELS WITH THE DISCRETE-TIME MODEL AS REFERENCE.

Cost	Disc.-time	Cont.-time	Change
Total objective [€]	839 172.4	842 592.4	3 420.0
Hydro reserve capacity cost [€]	9 988.2	11 199.7	1 211.5
Thermal reserve capacity cost [€]	6 801.0	7 732.3	931.3
Hydro operational costs [€]	525 803.5	524 251.1	-1 552.4
Thermal operational costs [€]	295 337.2	297 696.0	2 358.8
Load shedding [€]	0.0	407.7	407.7
Wind curtailment [€]	1 242.5	1 305.6	63.1

An objective function cost breakdown comparing the models is listed in Table II, which shows that the total system cost in the continuous-time model is 3 420 € higher than in the discrete-time model, corresponding to an increase of 0.4% of the total system costs. Note that the cost difference at optimum is somewhere in the range 2 652 € to 3 520 € given the absolute MIP gaps of both solutions. The cost increase is mainly due to more procured reserve capacity on both hydro and thermal units, slightly higher wind curtailment

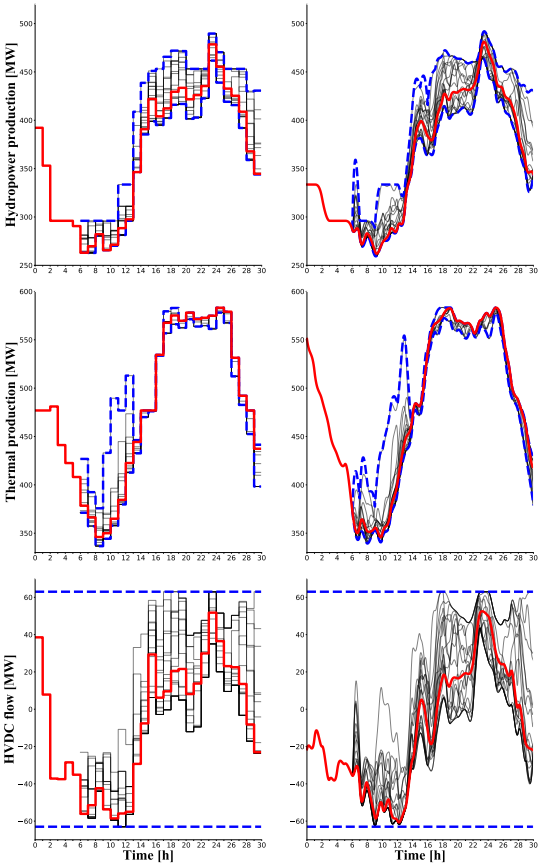

Fig. 3. The left and right columns show selected results of the discrete-time and continuous-time models, respectively. The red lines represent the first-stage schedule and black lines show the second-stage adjustments. The blue dashed lines are the boundaries of the second-stage solution, which is the procured reserve capacity for hydropower and thermal generation, and the transmission capacity for the flow on the HVDC line. Note that positive flow on the line is out of the hydropower area.

and load shedding, in addition to increased operational costs, which include both first-stage scheduling costs and expected second-stage deployment costs. If the continuous-time load and wind power series are assumed to be the actual real-time values of the data, the objective cost increase is the cost of implicitly balancing all structural imbalances in the system in all considered realizations of the uncertain wind power. The stochastic discrete-time model overestimates the flexibility of the system, as it is able to utilize more hydropower and less thermal generation compared to the continuous-time model. The amount of expected curtailed wind power is 5.1% higher in the continuous-time model, which again suggest an overestimation of the flexibility and wind power absorption potential. The hydropower is the major contributor of balancing in the system, providing about 62% of the upward reserve capacity and 51% of the downward reserve capacity in the continuous-

time model. 12.3% (21.8 MWh) of the expected downward regulation energy is also provided by wind curtailment in the continuous-time model. Compared to the discrete-time model, the continuous-time model procures 9.8% and 14.5% more total reserved capacity in the upward and downward directions, respectively. The increase in upward reserve capacity is split fairly equally between the hydropower (53%) and thermal units, while most (66%) of the additional downward reserve capacity is covered by the hydropower units.

The sum hydropower and thermal production in the system in the two models, as well as the flow on the HVDC line, are shown in Figure 3. The flow on the line between the hydropower and thermal areas shows that the hydropower area imports close to the maximal transmission capacity from hour 6 to 12 while providing upward balancing reserves in both models. The activation of hydropower reserves in hour 6 to balance the lowest wind power scenario in Figure 2 is handled very differently in the two models, which shows the importance of handling the sub-hourly variations. The discrete-time model rapidly increases hydropower production and export to the thermal area in the following hours 12 to 16 to keep thermal generation low. These high-ramping hours are handled differently in the continuous-time model, as both the thermal units and line flow are smoothly ramped up to meet the continuously increasing net load. The same situation arises towards the end of the horizon when load is decreasing while wind power production is picking up. This means that the hydropower provides ramping flexibility in addition to cheap energy to the system in the continuous-time model.

IV. Conclusion

A stochastic continuous-time hydrothermal model with uncertain wind power was presented in this paper to model both stochastic and structural imbalances in the power system. The case study of operating a simplified Northern European system shows that the total objective function cost is increased by 0.4% in the continuous-time model compared to an hourly discrete-time model. This represents the additional expected cost of maintaining a power balance compared to an hourly energy balance with a more accurate model of the system flexibility. The continuous-time model more accurately estimates the flexibility of the combined system, which results in using the hydropower resources for alleviating ramping scarcity in the thermal system to a greater extent. The presented model serves as a benchmark for optimal coordination of flexible hydropower units, conventional thermal generation, and intermittent wind power generation when it comes to scheduling and subsequently balancing an interconnected system.

References

[1] "Available online, accessed 27/8-2020," https://ec.europa.eu/clima/policies/strategies/2050.

[2] Q. P. Zheng, J. Wang, and A. L. Liu, "Stochastic Optimization for Unit Commitment - A Review," *IEEE Trans. Power Syst.*, vol. 30, no. 4, pp. 1913–1924, jul 2015.

[3] T. Weissbach and E. Welfonder, "High frequency deviations within the european power system: Origins and proposals for improvement," in *IEEE/PES Power Syst. Conf. Expo. PSCE*, 2009.

[4] M. Persson and P. Chen, "Frequency evaluation of the Nordic power system using PMU measurements," *IET Gener. Transm. Distrib.*, vol. 11, no. 11, pp. 2879–2887, aug 2017.

[5] I. Pavic, M. Beus, H. Pandzic, T. Capuder, and I. Stritof, "Electricity markets overview - Market participation possibilities for renewable and distributed energy resources," in *14th Int. Conf. Eur. Energy Mark. EEM*, jul 2017.

[6] T. Haugland, G. Doorman, and J. Hystad, "Structural imbalances in the Nordic power system - Causes, future expectations and remedies," in *11th Int. Conf. Eur. Energy Mark. EEM*, may 2014, pp. 1–5.

[7] C. Koch and L. Hirth, "Short-term electricity trading for system balancing: An empirical analysis of the role of intraday trading in balancing Germany's electricity system," *Renew. Sustain. Energy Rev.*, vol. 113, p. 109275, oct 2019.

[8] G. Fridgen, A. Michaelis, M. Rinck, M. Schöpf, and M. Weibelzahl, "The search for the perfect match: Aligning power-trading products to the energy transition," *Energy Policy*, vol. 144, p. 111523, sep 2020.

[9] IEA, "Offshore Wind Outlook 2019," IEA, Tech. Rep., 2019, https://www.iea.org/reports/offshore-wind-outlook-2019.

[10] A. Helseth, B. Mo, A. L. Henden, and G. Warland, "Detailed long-term hydro-thermal scheduling for expansion planning in the Nordic power system," *IET Gener. Transm. Distrib.*, vol. 12, no. 2, pp. 441–447, 2018.

[11] M. E. P. Maceira, D. D. Penna, A. L. Diniz, R. J. Pinto, A. C. Melo, C. V. Vasconcellos, and C. B. Cruz, "Twenty years of application of stochastic dual dynamic programming in official and agent studies in Brazil-main features and improvements on the NEWAVE model," in *20th Power Syst. Comput. Conf. PSCC*, aug 2018.

[12] A. L. Diniz, F. D. S. Costa, M. E. Maceira, T. N. Dos Santos, L. C. B. Dos Santos, and R. N. Cabral, "Short/Mid-term hydrothermal dispatch and spot pricing for large-scale systems-The case of Brazil," in *20th Power Syst. Comput. Conf. PSCC*, aug 2018.

[13] J. Kong, H. I. Skjelbred, and O. B. Fosso, "An overview on formulations and optimization methods for the unit-based short-term hydro scheduling problem," *Electr. Power Syst. Res.*, vol. 178, p. 106027, jan 2020.

[14] M. Parvania and A. Scaglione, "Unit Commitment With Continuous-Time Generation and Ramping Trajectory Models," *IEEE Trans. Power Syst.*, vol. 31, no. 4, pp. 3169–3178, jul 2016.

[15] K. Hreinsson, B. Analui, and A. Scaglione, "Continuous Time Multi-Stage Stochastic Reserve and Unit Commitment," in *20th Power Syst. Comput. Conf. PSCC*, jun 2018, pp. 1–7.

[16] K. Hreinsson, A. Scaglione, and B. Analui, "Continuous Time Multi-Stage Stochastic Unit Commitment with Storage," *IEEE Trans. Power Syst.*, pp. 1–1, 2019.

[17] R. Khatami and M. Parvania, "Stochastic Multi-Fidelity Scheduling of Flexibility Reserve for Energy Storage," *IEEE Trans. Sustain. Energy*, pp. 1–1, 2019.

[18] R. Khatami, M. Parvania, and A. Narayan, "Flexibility Reserve in Power Systems: Definition and Stochastic Multi-Fidelity Optimization," *IEEE Trans. Smart Grid*, vol. 11, no. 1, pp. 644–654, jan 2020.

[19] C. Ø. Naversen, A. Helseth, B. Li, M. Parvania, H. Farahmand, and J. P. S. Catalão, "Hydrothermal scheduling in the continuous-time framework," *Electr. Power Syst. Res.*, vol. 189, p. 106787, dec 2020.

[20] M. L. Øvstebø, C. Ø. Naversen, A. Helseth, and H. Farahmand, "Continuous-time scheduling of a hydrothermal system with integration of offshore wind power," *Accepted for publication in the proceedings of the 17th Int. Conf. Eur. Energy Mark. EEM*, 2020.

[21] C. Ø. Naversen, H. Farahmand, and A. Helseth, "Accounting for reserve capacity activation when scheduling a hydropower dominated system," *Int. J. Electr. Power Energy Syst.*, vol. 119, p. 105864, jul 2020.

[22] C. Barrows, E. Preston, A. Staid, G. Stephen, J. P. Watson, A. Bloom, A. Ehlen, J. Ikaheimo, J. Jorgenson, D. Krishnamurthy, J. Lau, B. McBennett, and M. O'Connell, "The IEEE Reliability Test System: A Proposed 2019 Update," *IEEE Trans. Power Syst.*, vol. 35, no. 1, pp. 119–127, jan 2020.

[23] "Available online, accessed 30/6-2020," https://www.energidataservice.dk.

[24] J. Dupačová, N. Gröwe-Kuska, and W. Römisch, "Scenario reduction in stochastic programming An approach using probability metrics," *Math. Program. Ser. B*, vol. 95, no. 3, pp. 493–511, mar 2003.

[25] "Available online, accessed 30/6-2020," https://www.nordpoolgroup.com.

[26] "Available online, accessed 30/6-2020," https://transparency.entsoe.eu.

APPENDIX
FUNDAMENTAL PROPERTIES AND NOTATION

For further reading and references concerning the properties mentioned here, the reader is directed to [14]. In the continuous-time framework, time-dependent input data and variables are described by Bernstein polynomials of a finite degree n. There are $n+1$ of these polynomials:

$$B_{in}(t) = \binom{n}{i} t^i (1-t)^{n-i}, \quad i \in \{0, 1, ..., n\}, \tag{10}$$

and they form a basis for polynomials of positive degree less than or equal to n on the time interval $t \in [0, 1]$. Vector notation simplifies further definitions, denoted using bold text:

$$\mathbf{B}_n(t) = \left[B_{0n}(t), B_{1n}(t), ..., B_{nn}(t)\right]^\mathsf{T}. \tag{11}$$

A continuous curve $x(t)$ on the interval $t \in [0, 1]$ can be constructed by finding the vector of appropriate polynomial coefficients $\mathbf{x}$ such that

$$x(t) = \mathbf{x}^\mathsf{T} \cdot \mathbf{B}_n(t). \tag{12}$$

The curve $x(t)$ is easily bounded by the use of the convex hull property, which guarantees that the curve is confined within the limits of the coefficients:

$$\mathbf{x} \leq x^{max}\mathbf{1} \quad \Rightarrow \quad x(t) \leq x^{max}. \tag{13}$$

Note that $\mathbf{1}$ denotes a constant vector of ones with appropriate length, which is used to describe the constant x^{max} in polynomial space since $\mathbf{1}^\mathsf{T} \cdot \mathbf{B}_n(t) = 1$. When using the representation in eq. (12), the derivatives and integrals of $x(t)$ can be described by the linear relationships

$$\frac{d\mathbf{B}_n(t)}{dt} = \mathbf{K}_n \cdot \mathbf{B}_{n-1}(t) \tag{14}$$

$$\int \mathbf{B}_n(t)dt = \mathbf{N}_n \cdot \mathbf{B}_{n+1}(t), \tag{15}$$

where $\mathbf{K}_n$ and $\mathbf{N}_n$ are matrices of size $(n+1) \times n$ and $(n+1) \times (n+2)$, respectively. Note that the definite integral over the whole interval reduces down to

$$\int_0^1 \mathbf{B}_n(t)dt = \frac{1}{n+1}\mathbf{1}. \tag{16}$$

As the Bernstein polynomials form a basis, Bernstein polynomials of degree n can be represented as Bernstein polynomials of any higher degree m by using the $(n+1) \times (m+1)$ elevation matrix $\mathbf{X}_{nm}$:

$$\mathbf{B}_n(t) = \mathbf{X}_{nm}\mathbf{B}_m(t), \quad n \leq m. \tag{17}$$

The definition in eq. (12) can be extended to form a piecewise polynomial representation of the curve $x(t)$ on a longer time horizon $t \in [0, N]$. The time horizon is first discretized into several time intervals $h \in \mathcal{T}$ of length δ_h, then the curve can be represented as

$$x(t) = \mathbf{x}_h^\mathsf{T} \cdot \mathbf{B}_n\left(\frac{t - t_h}{\delta_h}\right), \qquad t_h \leq t \leq t_{h+1}. \tag{18}$$

Here, t_h represents the start time of interval h. To enforce continuity on $x(t)$ in the change from interval h to $h+1$, two functions F^0 and F^1 are defined as follows:

$$\mathrm{F}^0(\mathbf{x}_h) = \mathbf{x}_h^{(n)} - \mathbf{x}_{h+1}^{(0)} \tag{19}$$

$$\mathrm{F}^1(\mathbf{x}_h) = \mathbf{x}_h^{(n)} - \mathbf{x}_h^{(n-1)} - \mathbf{x}_{h+1}^{(1)} + \mathbf{x}_{h+1}^{(0)}, \tag{20}$$

where the notation $\mathbf{x}_h^{(j)}$ represents the jth vector component. The constraints $\mathrm{F}^0(\mathbf{x}_h) = 0$ and $\mathrm{F}^1(\mathbf{x}_h) = 0$ impose continuous values and derivatives on $x(t)$ over the interval change, respectively.

The time-dependent input data and decisions of the continuous-time model formulated in Section II are based on the definition in eq. (18) and the properties in eqs. (13) to (17) as well as the continuity requirements of eqs. (19) and (20). The decision variables of the model become the vector coefficients of the Bernstein polynomials in addition to binary unit commitment variables, and a mixed integer linear problem formulation is recovered.

Appendices

Appendix A: Hydropower System Topology

The same cascaded hydropower system has been used in all of the papers included in this thesis. The system is based on the Nea-Nidelv watercourse, primarily located in Trøndelag in Norway and stretching over the Swedish border. This watercourse has been regulated for a long time, with the first power station being built at the start of the 20^{th} century. Figure A.1 shows a schematic representation of the cascaded system as implemented in the optimization models. The system was chosen since it is complex enough to exhibit interesting behavior, as it consists of both large and small interconnected reservoirs with different dynamics. On the other hand, the system is simple enough to be solved efficiently in most cases. Using the same system across all models also gives a better framework for comparing results.

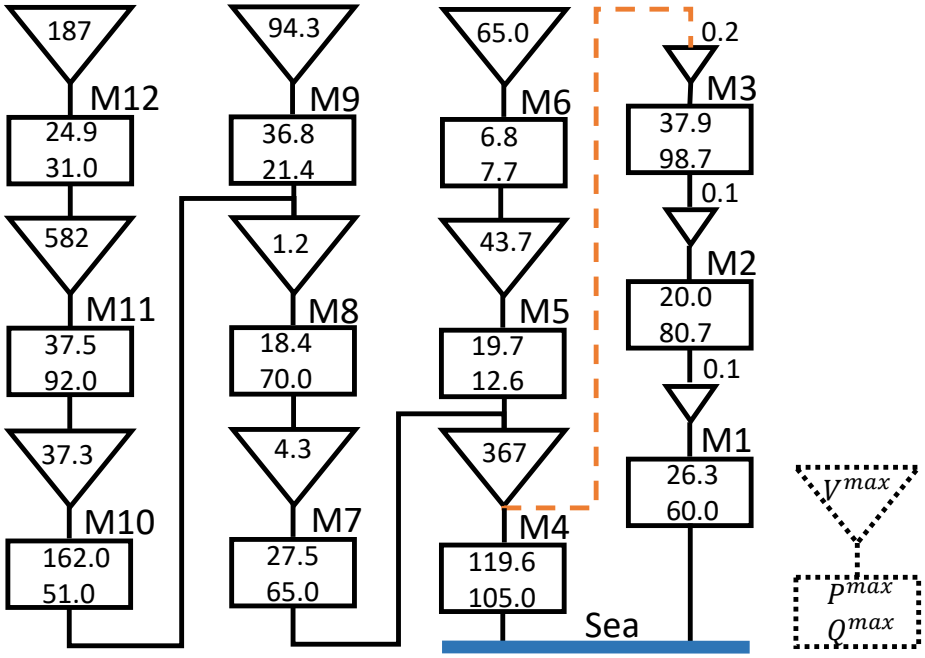

Figure A.1: The cascaded hydropower topology used as a test system, figure originally published in [108]. Reservoirs are shown as triangles and power stations as rectangles. A bypass gate from M4 to M3 is marked by a dashed line, while the main water routs are shown as black solid lines.

Appendix B: Robust Optimization

This appendix provides a short introduction to two-stage robust optimization and how it can be reformulated and solved efficiently.

B.1 The Two-Stage Robust Formulation

A two-stage stochastic optimization program generally aims at minimizing the expected value of the first-stage and second-stage cost functions f and g [57]:

$$\min_{x \in \mathcal{X}} \Big[f(x) + \min_{y \in \mathcal{Y}(x,z)} \mathbb{E}_{z \in \Omega} \Big(g(y) \Big) \Big]. \tag{B.1}$$

The first-stage decisions x are taken before the uncertain variables z are realized, while the second-stage recourse decisions y are made after the actual realization of the stochastic process. The decisions are bounded by the constraints in the sets $\mathcal{X}$ and $\mathcal{Y}(x, z)$, where the second-stage decisions are affected by both x and z. The random variables are in turn contained within the known probability space Ω. A standard way to solve the stochastic program in practical terms is to create a finite set of scenario realizations $\mathcal{S}$ of the uncertain variables by sampling from Ω. The solution of eq. (B.1) can then be approximated by solving the extensive form of the problem:

$$\min_{\substack{x \in \mathcal{X} \\ y_s \in \mathcal{Y}(x, z_s)}} \Big[f(x) + \sum_{s \in \mathcal{S}} \pi_s g(y_s) \Big]. \tag{B.2}$$

Here, π_s is the probability of the sampled scenario $s \in \mathcal{S}$ occurring. The discretization of Ω into a finite set of scenarios allows the expected value to be represented by a summation. Equation (B.2) may be solved directly as a single optimization program or by decomposition techniques. In contrast to stochastic optimization, two-stage robust optimization tries to minimize the cost of the worst-case realization of the uncertainty [65]:

$$\min_{x \in \mathcal{X}} \Big[f(x) + \max_{z \in \mathcal{Z}} \min_{y \in \mathcal{Y}(x,z)} g(y) \Big]. \tag{B.3}$$

Protecting against the edge cases of the uncertainty realization is likely to give an

overly conservative solution, as the model considers only extreme events with a very low probability. To temper the conservativeness of the robust model and help tractability, the complete probability space Ω is replaced by a simpler uncertainty set $\mathcal{Z}$ in eq. (B.3).

B.2 The Uncertainty Set

The concept of the uncertainty set in robust optimization is key to achieving a tractable formulation. For a thorough introduction to uncertainty sets, the reader is referred to [63]. This section will provide a simple example to help visualize the idea.

Consider a single-period optimization problem where the goal is to minimize the operational cost of a power system with two wind generators with uncertain power production, W_1 and W_2. The wind power output is guaranteed to be within the technical production boundaries of 0 and 1 for both W_1 and W_2, but assume that it also follows a two-dimensional normal distribution[1] with some mean and standard deviation. Solving the stochastic problem in eq. (B.2) can be done by generating scenarios based on sampling the normal distribution and possibly applying scenario reduction techniques to reduce the computational burden subsequently. It is possible, albeit very improbable, that the wind power output is close to the technical boundaries of zero or maximal production, which can be seen from the illustrations of the sample space in Figure B.1. Without a specified uncertainty set in the robust case, the worst-case realization of the uncertainty will lie in one of the vertices on the technical maximum/minimum production border. To reduce the conservativeness, the uncertainty set $\mathcal{Z}$ can be defined in several ways in order to more closely mimic the underlying uncertainty distribution. Figure B.1a shows an elliptical uncertainty set, illustrated as a blue elliptical curve in $W_1 - W_2-$space, which is described as

$$\mathcal{Z} := \left\{ W_1, W_2 \middle| \left(\frac{W_1}{r_1}\right)^2 + \left(\frac{W_2}{r_2}\right)^2 \leq 1 \right\}. \tag{B.4}$$

The minor and major axes of the ellipse are set to 3 times the standard deviation in each dimension in the figure. The uncertainty set forces the robust model to only consider realizations of the uncertainty within the elliptical curve. The quadratic constraints involving W_1 and W_2 are complicated constraints that increase computational effort. The linear uncertainty set in Figure B.1b represents a significantly simpler way of constructing the uncertainty set as a collection of

[1]The support of the normal distribution is infinite, so the folded normal distribution that projects all points outside the technical boundary to lie on the boundary can be used instead.

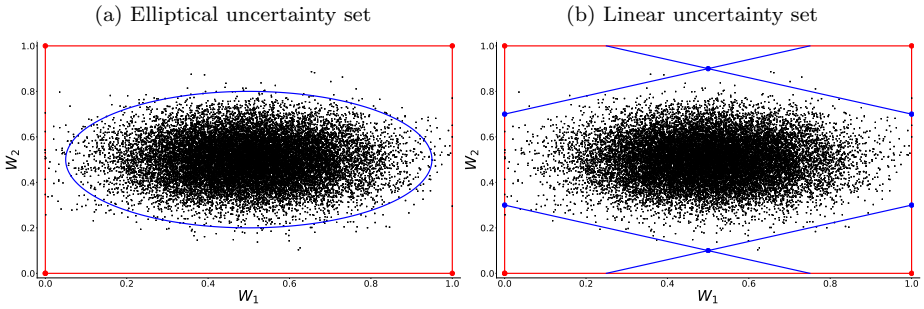

Figure B.1: Shows a simple 2D example of elliptical and linear uncertainty sets in robust optimization. The black dots are 20000 samples of a folded normal distribution that are contained within the sample space of the red lines, representing wind power production between 0 and max for two wind power plants. The blue lines constitute possible robust uncertainty sets.

linear inequality constraints i:

$$\mathcal{Z} := \left\{ W_1, W_2 \middle| \quad a_i W_1 + b_i W_2 \leq c_i \quad \forall i \right\}. \tag{B.5}$$

By introducing the uncertainty set $\mathcal{Z}$, the random variable z has become a decision variable of the robust optimization model in eq. (B.3). The two-stage robust model aims to minimize the total cost given that z is realized as the worst-case outcome contained in $\mathcal{Z}$. The construction of the uncertainty set is therefore essential for the conservativeness of the robust model.

B.3 Reformulation and Solution Strategies

The solution of the min-max-min formulation of eq. (B.3) cannot be computed directly by any standard optimization solver, and it is therefore necessary to reformulate and decompose the problem. There are two standard ways of reformulating such two-stage robust problems, either with a *Benders decomposition* technique or by *column-and-constraint generation (CCG)*. Both of the procedures follow the same initial steps, and the following explanation is based on the detailed guide in [65]. For clarity and without much loss of generality, let the inner minimization problem be written in matrix form as:

$$\begin{aligned} \min_{y} \quad & g(y) : \mathbf{c}^{\intercal} \cdot \mathbf{y} \\ & \mathbf{A} \cdot \mathbf{y} + \mathbf{B} \cdot \mathbf{x}^{*} + \mathbf{C} \cdot \mathbf{z}^{*} \leq \mathbf{d} \qquad (\boldsymbol{\lambda}) \\ & \mathbf{y} \geq 0. \end{aligned} \tag{B.6}$$

The objective is assumed to be linear in the recourse decisions with cost vector $\mathbf{c}$. The constraint matrices $\mathbf{A}$, $\mathbf{B}$, and $\mathbf{C}$ represent the coupling between the stages, and $\boldsymbol{\lambda}$ is the vector of dual variables related to the constraints. The vectors of the first-stage decisions $\mathbf{x}^{*}$ and the realization of the uncertainty $\mathbf{z}^{*}$ are fixed in the recourse problem and therefore marked by an asterisk. For simplicity, the recourse problem in eq. (B.6) is assumed to have complete recourse, which means that it is feasible for every value of $x^{*} \in \mathcal{X}$ and $z^{*} \in \mathcal{Z}$. Having complete recourse can be ensured by including penalty variables for all potentially problematic constraints. Since eq. (B.6) is assumed to be a simple linear and convex problem with respect to $\mathbf{y}$, its dual form can be constructed as [109]:

$$\begin{aligned} \max_{\lambda} \quad & w(x^{*}, z^{*}, \lambda) : \boldsymbol{\lambda}^{\intercal} \cdot (\mathbf{d} - \mathbf{B} \cdot \mathbf{x}^{*} - \mathbf{C} \cdot \mathbf{z}^{*}) \\ & \mathbf{A}^{\intercal} \cdot \boldsymbol{\lambda} \leq \mathbf{c} \\ & \boldsymbol{\lambda} \leq 0. \end{aligned} \tag{B.7}$$

As discussed in [65], the maximization step in eq. (B.7) can be merged with the outer maximization over z:

$$\max_{z \in \mathcal{Z}} \min_{y \in \mathcal{Y}(x^{*}, z)} g(y) \Longleftrightarrow \max_{\substack{z \in \mathcal{Z} \\ \lambda \in \Lambda}} \; w(x^{*}, z, \lambda). \tag{B.8}$$

The solution of the dualized second-stage problem is a function of x:

$$W(x) = \max_{\substack{z \in \mathcal{Z} \\ \lambda \in \Lambda}} w(x, z, \lambda). \tag{B.9}$$

The constraints of the dual problem in eq. (B.7) are represented as $\lambda \in \Lambda$ in the above formulations for compactness. Note that solving eq. (B.9) is complicated due to the fact that the objective $w(x^{*}, z, \lambda)$ contains bi-linear terms of $z \cdot \lambda$. A special case where z is expressed through binary variables allows the bi-linear terms to be reformulated into binary constraints so that eq. (B.9) becomes a mixed-integer linear program. In the general case of continuous z variables, other

approximation techniques or non-linear solvers must be employed. Either way, the min-max-min structure of the original problem in eq. (B.3) has been turned into a min-max problem:

$$\min_{x \in \mathcal{X}} \Big[f(x) + \max_{\substack{z \in \mathcal{Z} \\ \lambda \in \Lambda}} w(x, z, \lambda) \Big]. \tag{B.10}$$

Note that even though finding the solution of eq. (B.9) involves solving a non-convex problem, the function $W(x)$ is still convex in x since it is the result of a maximization of a set of affine functions in x [65]. This means that it is possible to approximate the second stage by an outer approximation algorithm such as Benders decomposition and CCG.

B.3.1 Benders decomposition

Benders decomposition, also referred to as the L-shaped method, has been used to efficiently solve many different types of optimization problems for many decades [57]. The Benders decomposition solution approach for eq. (B.10) involves decomposing the problem into a master problem:

$$\begin{aligned} &\min_{x, \theta} \quad f(x) + \theta \\ &x \in \mathcal{X} \\ &\theta \geq w(x, z_i, \lambda_i) \quad \forall i, \end{aligned} \tag{B.11}$$

and the sub problem in eq. (B.9). The auxiliary variable θ approximates the value of $W(x)$ in eq. (B.9) as it is bound from below by the second-stage objective w for a set of solutions (z_i, λ_i). The overall solution procedure is as follows:

1. Find an initial feasible first-stage solution $x \in \mathcal{X}$.
2. Solve eq. (B.9) for the fixed value of x to obtain a solution (z_i, λ_i).
3. Add a new constraint for θ to the master problem eq. (B.11) given (z_i, λ_i), and solve for updated values of x and θ.
4. If the value of θ is within the wanted numerical tolerance with respect to the most recent objective value of eq. (B.9), the problem has converged. If not, go back to step 2 with the new value of x.

A benefit of Benders decomposition is that only a single constraint for bounding θ is added to the master problem in each iteration. The modest size increase over the iterations ensures that the tractability of eq. (B.11) is not worsened drastically over the course of the solution procedure. A potential drawback is that all of the second-stage dynamics that impact the objective function are propagated by a single constraint, which can lead to slow convergence for some model formulations.

B.3.2 Column-and-constraint generation

The CCG solution procedure is similar to the Benders decomposition scheme but adds primal constraints to the master problem instead of the dual-based constraints seen in eq. (B.11). The method is relatively new, first published by B. Zeng and L. Zhao in 2012 and 2013 [75, 76]. The master problem for CCG is

$$\begin{aligned} &\min_{x,y_i,\theta} \quad f(x) + \theta \\ &x \in \mathcal{X} \\ &\theta \geq g(y_i) \\ &y_i \in \mathcal{Y}(x, z_i) \quad \forall i. \end{aligned} \tag{B.12}$$

The second-stage cost approximated θ is bounded by the primal objective $g(y)$ in eq. (B.12). In addition, several sets of the primal second-stage variables and constraints are added for different worst-case realizations z_i. The solution algorithm is similar to the Benders strategy:

1. Find an initial feasible first-stage solution $x \in \mathcal{X}$.
2. Solve eq. (B.9) for the fixed value of x to obtain a new worst-case realization z_i.
3. Add new variables y_i and all primal second-stage constraints from eq. (B.6) to the master problem eq. (B.12) based on z_i. Also add a new constraint for θ, and solve the master problem to get updated values for x and θ.
4. If the value of θ is within the wanted numerical tolerance with respect to the most recent objective value of eq. (B.9), the problem has converged. If not, go back to step 2 with the new value of x.

The size of the master problem grows much quicker in the CCG algorithm compared to Benders decomposition, as many new variables and constraints are added

in each iteration. This slows down the solution time of each iteration. However, the number of iterations needed for CCG to converge can in many cases be relatively low, as the feasible region of the master problem is tightened significantly by the addition of the second-stage constraints. The best choice of solution algorithm will vary based on the problem at hand, although the CCG algorithm was found to be significantly faster for the robust formulation used in Paper I.

Appendix C: The Continuous-time Optimization Framework

It is always challenging to find enough space in a paper to give the fundamental mathematical concepts of the continuous-time optimization framework the attention they deserve. Even simple optimization models quickly turn quite abstract and difficult to understand at first glance, and continuous-time models doubly so. This appendix aims to give a thorough and detailed description of how the continuous-time framework for optimization models is constructed from the bottom-up but is hopefully still accessible for anyone interested in formulating their own continuous-time model. Appendix C.1 derives all of the essential properties of the so-called Bernstein polynomials, which are then applied to convert a simple discrete-time optimization model to a continuous-time model in Appendix C.2. More complicated time-linking constraints and constraints dealing with binary variables are finally discussed in Appendix C.3, with examples from the field of power system planning and operation.

The formulations and derivations of the different features of a continuous-time model found in this appendix are based on the fundamental properties of the Bernstein polynomials, where [110] is a good reference. The application to power system optimization models discussed in Appendix C.3 is based on the original model formulations of the literature listed in Section 2.3.

C.1 Properties of the Bernstein Polynomials

At the heart of any continuous-time model formulation lies a spectral decomposition into polynomial space. This means that time-varying input data, e.g. load, is approximated as polynomials of some finite degree, and the time series is therefore fully defined by a set of basis functions with accompanying coefficients. The time-varying variables in the optimization model, such as generated power, must also be represented as polynomials. If not, there will be no hope of satisfying the equality constraints of the model. The Bernstein basis polynomials are vital for successfully transitioning the polynomial representation of all time series and decision variables into a tractable optimization model. The Bernstein polynomials are named after their creator, the Russian mathematician Sergei Natanovich Bernstein (1880 - 1968), who was central in the creation of the constructive theory of functions [111].

C.1.1 Definition

The simplest choice of basis functions for representing a polynomial $f(t)$ of degree $n \geq 0$ is the set of functions $\{1, t, t^2, ..., t^n\}$. It is obvious that these functions form a basis for polynomials of degree n, as they are linearly independent and any polynomial can be constructed by them through linear combination. By introducing the vector of these basis functions,

$$\boldsymbol{\tau}_n(t) = \left[1, t, t^2, ..., t^n\right]^\mathsf{T}, \tag{C.1}$$

the polynomial $f(t)$ can be expressed as

$$f(t) = \mathbf{a}^\mathsf{T} \cdot \boldsymbol{\tau}_n(t) = \sum_{i=0}^{n} a_i t^i. \tag{C.2}$$

The vector $\mathbf{a}$ of the $n+1$ coefficients a_i fully determines the shape of $f(t)$ when $\boldsymbol{\tau}_n(t)$ is used as a basis. Although eq. (C.1) might seem the simplest basis to use, it turns out to be difficult to work with in constrained optimization models. Finding simple ways of expressing inequality constraints for $f(t)$ when using eq. (C.1) is one of the biggest difficulties. The Bernstein polynomials of degree n have several advantages in this regard since they are easily bounded, which will be derived in Appendix C.1.2. They are defined as [110]

$$B_{in}(t) = \binom{n}{i} t^i (1-t)^{n-i}, \quad i \in \{0, 1, ..., n\}, \tag{C.3}$$

where $\binom{n}{i} = \frac{n!}{i!(n-i)!}$ is the binomial coefficient, and are represented in vector notation as

$$\mathbf{B}_n(t) = \left[B_{0n}(t), B_{1n}(t), ..., B_{nn}(t)\right]^\mathsf{T}. \tag{C.4}$$

The functions $\mathbf{B}_n(t)$ form an equivalent basis to that of $\boldsymbol{\tau}_n(t)$ for polynomials of positive degree n, which means it is possible to express $f(t)$ in terms of $\mathbf{B}_n(t)$. To be convinced of this, it is sufficient to show that they are linearly independent and that a linear combination of them can be used to express the polynomial $f(t)$. No rigorous mathematical proof will be attempted here, but rather a direct explanation based on basic linear algebra. Using the binomial expansion formula [112]

$$(x+y)^n = \sum_{i=0}^{n} \binom{n}{i} x^i y^{n-i} \tag{C.5}$$

on the definition in eq. (C.3), $B_{in}(t)$ can be written as

$$\begin{aligned} B_{in}(t) &= \binom{n}{i} t^i \sum_{j=0}^{n-i} \binom{n-i}{j} (-t)^j 1^{n-i-j} = \sum_{j=0}^{n-i} (-1)^j \binom{n}{i} \binom{n-i}{j} t^{i+j} \\ &\equiv \sum_{j=0}^{n-i} M_{ij} t^{i+j}. \end{aligned} \tag{C.6}$$

The expression in eq. (C.6) shows that the polynomial $B_{in}(t)$ only includes terms of degree from i and up to n. The matrix $\mathbf{M}_n$ in the relationship

$$\mathbf{B}_n(t) = \mathbf{M}_n \cdot \boldsymbol{\tau}_n(t), \tag{C.7}$$

is therefore an upper triangular matrix. Such matrices are always invertible if all of the diagonal elements are non-zero[1], which is the case for matrix $\mathbf{M}_n$ with diagonal elements $\binom{n}{i} \geq 1$. As the matrix is invertible, the Bernstein polynomials must be linearly independent. The polynomial $f(t)$ can be written as a linear combination of $\mathbf{B}_n(t)$ by using the basis property of $\boldsymbol{\tau}_n(t)$ defined in eq. (C.1) and the invertibility of $\mathbf{M}_n$:

$$f(t) = \mathbf{a}^\mathsf{T} \cdot \boldsymbol{\tau}_n(t) = \mathbf{a}^\mathsf{T} \cdot \mathbf{M}_n^{-1} \cdot \mathbf{B}_n(t) \equiv \mathbf{b}^\mathsf{T} \cdot \mathbf{B}_n(t). \tag{C.8}$$

The Bernstein polynomials of degree n are therefore an equivalent basis to $\boldsymbol{\tau}_n(t)$ by modifying the coefficient vector.

The basis property of $\mathbf{B}_n(t)$ means that the Bernstein polynomials of a certain degree can always be expressed as Bernstein polynomials of a higher degree:

$$\mathbf{B}_n(t) = \mathbf{X}_{nm} \cdot \mathbf{B}_m(t), \quad m \geq n. \tag{C.9}$$

The elevation matrix $\mathbf{X}_{nm}$ of size $(n+1) \times (m+1)$ can be calculated in several ways, for instance by direct calculation through eq. (C.7):

[1] The determinant of an upper triangular matrix can be shown to be the product of its diagonal elements by direct calculation, which means that the matrix is singular only if there is a zero along the diagonal.

$$\begin{aligned} & \mathbf{B}_n(t) = \mathbf{M}_n \cdot \boldsymbol{\tau}_n(t) = \mathbf{M}_n \cdot \mathbf{J}_{nm} \cdot \boldsymbol{\tau}_m(t) \\ \Rightarrow \quad & \mathbf{M}_n \cdot \mathbf{J}_{nm} \cdot \boldsymbol{\tau}_m(t) = \mathbf{X}_{nm} \cdot \mathbf{M}_m \cdot \boldsymbol{\tau}_m(t) \\ \Rightarrow \quad & \mathbf{X}_{nm} = \mathbf{M}_n \cdot \mathbf{J}_{nm} \cdot \mathbf{M}_m^{-1}. \end{aligned} \tag{C.10}$$

The elevation matrix $\mathbf{J}_{nm}$ for the basis functions $\boldsymbol{\tau}_n$ is straightforward to calculate, and is essentially the identity matrix $\mathbf{I}_{n+1}$ appended with columns of zeros to reach size $(n+1) \times (m+1)$.

C.1.2 Convex hull property

The Bernstein polynomials $\mathbf{B}_n(t)$ form a basis for the whole interval $t \in (-\infty, \infty)$, but are only useful in the context of optimization models when limited to the interval $t \in [0, 1]$. From the definition in eq. (C.3), it is clear that both factors t^i and $(1-t)^{n-i}$ are non-negative on the interval from 0 to 1, which means that

$$B_{in}(t) \geq 0, \quad t \in [0, 1]. \tag{C.11}$$

In addition to the non-negativity, $\mathbf{B}_n(t)$ are bounded from above on this interval. First note that the sum of $B_{in}(t)$ can be calculated by the binomial expansion formula in eq. (C.5), which turns out to be constant:

$$\sum_{i=0}^{n} B_{in}(t) = \sum_{i=0}^{n} \binom{n}{i} t^i (1-t)^{n-i} = \Big(t + (1-t)\Big)^n = 1. \tag{C.12}$$

Combined with the non-negativity shown in eq. (C.11), the property in eq. (C.12) means that

$$B_{in}(t) \leq 1, \quad t \in [0, 1]. \tag{C.13}$$

Figure C.1 shows a plot of $\mathbf{B}_3(t)$ which visualizes the bounded nature of the polynomials. Since the Bernstein polynomials are bounded between 0 and 1 on the interval $t \in [0, 1]$, any polynomial $f(t)$ expressed with $\mathbf{B}_n(t)$ is also bounded by its expansion coefficients:

$$f(t) = \mathbf{b}^\intercal \cdot \mathbf{B}_n(t) = \sum_{i=0}^{n} b_i B_{in}(t) = \sum_{i=0}^{n} (b^{\max} - \Delta_i) B_{in}(t)$$
$$= b^{\max} - \sum_{i=0}^{n} \Delta_i B_{in}(t) \leq b^{\max}. \tag{C.14}$$

The highest coefficient $b^{\max} = \max\{b_i\}$ is used to express all coefficients b_i with some deviation $\Delta_i \geq 0$ in eq. (C.14). Since all Δ_i and $B_{in}(t)$ are non-negative when $t \in [0, 1]$, the function $f(t)$ will always be bounded by its highest coefficient on this interval. It can be shown in a similar way that $f(t)$ is bounded from below by its smallest coefficient, so that:

$$f(t) = \mathbf{b}^\intercal \cdot \mathbf{B}_n(t) \quad \Longrightarrow \quad b^{\min} \leq f(t) \leq b^{\max}, \qquad t \in [0, 1]. \tag{C.15}$$

Equation (C.15) is known as the convex hull property [78], which is very useful for enforcing inequality constraints in continuous-time optimization models. This is further discussed in Appendix C.2.

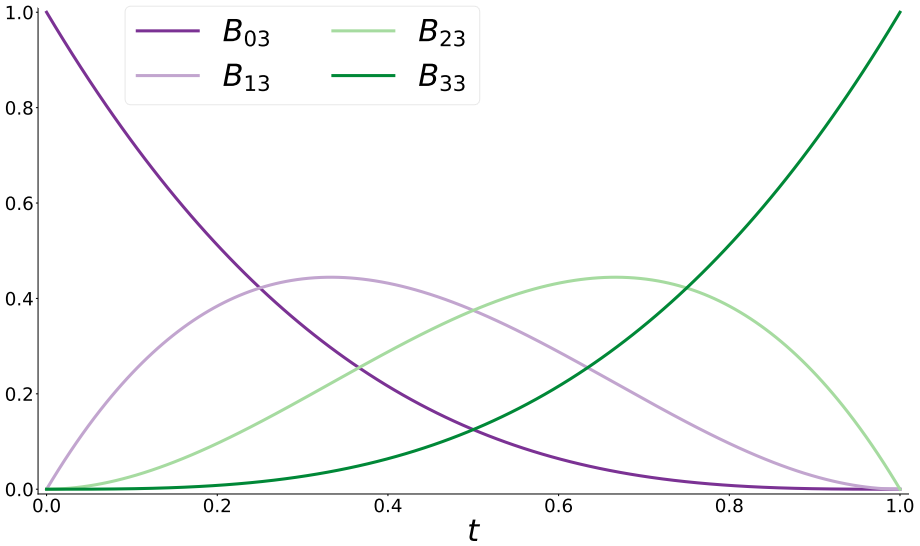

Figure C.1: The four Bernstein polynomials of third degree plotted on the interval $t \in [0, 1]$.

C.1.3 Differentiation and integration

Differentiating the Bernstein polynomials can be performed directly based on eq. (C.3):

$$\begin{aligned}\frac{dB_{in}(t)}{dt} &= \binom{n}{i}\Big(it^{i-1}(1-t)^{n-i} - (n-i)t^i(1-t)^{n-i-1}\Big) \\ &= n\Big(B_{i-1,n-1}(t) - B_{i,n-1}(t)\Big). \end{aligned} \tag{C.16}$$

Note the convention of defining $B_{in}(t) = 0$ for $i < 0$ and $i > n$. The derivatives of $\mathbf{B}_n(t)$ can thus be described by a linear combination of $\mathbf{B}_{n-1}(t)$. Equation (C.16) can be formulated in vector notation as

$$\frac{d\mathbf{B}_n(t)}{dt} = \mathbf{K}_n \cdot \mathbf{B}_{n-1}(t) \tag{C.17}$$

$$\mathbf{K}_n = n \begin{bmatrix} -1 & 0 & 0 & \dots & 0 & 0 \\ 1 & -1 & 0 & \dots & 0 & 0 \\ 0 & 1 & -1 & \dots & 0 & 0 \\ \vdots & \vdots & \vdots & \dots & \vdots & \vdots \\ 0 & 0 & 0 & \dots & 1 & -1 \\ 0 & 0 & 0 & \dots & 0 & 1 \end{bmatrix}, \tag{C.18}$$

where $\mathbf{K}_n$ is a matrix of dimensions $(n+1) \times n$.

The indefinite integrals $I_{in}(t)$ of $B_{in}(t)$ can also be directly calculated. It is simple to evaluate in the case of $I_{nn}(t)$:

$$\begin{aligned} I_{nn}(t) &= \int B_{nn}(t)dt = \int t^n dt = \frac{1}{n+1}t^{n+1} + c_n \\ &= \frac{1}{n+1}B_{n+1,n+1}(t) + c_n. \end{aligned} \tag{C.19}$$

It is possible to find a recursive relationship between the integrals for $i < n$ by performing an integration by parts and then substituting in the value found in eq. (C.19):

$$
\begin{aligned}
I_{in}(t) &= \int \binom{n}{i} t^i (1-t)^{n-i} dt \\
&= \binom{n}{i} \left(\frac{1}{i+1} t^{i+1} (1-t)^{n-i} + \frac{n-i}{i+1} \int t^{i+1} (1-t)^{n-i-1} \right) \\
&= \frac{\binom{n}{i}}{(i+1)\binom{n+1}{i+1}} B_{i+1,n+1}(t) + \frac{n-i}{i+1} \frac{\binom{n}{i}}{\binom{n}{i+1}} I_{i+1,n}(t) \\
&= \frac{1}{n+1} B_{i+1,n+1}(t) + I_{i+1,n}(t) = \frac{1}{n+1} \sum_{k=i+1}^{n} B_{k,n+1}(t) + I_{nn}(t) \\
&= \frac{1}{n+1} \sum_{k=i+1}^{n+1} B_{k,n+1}(t) + c_i. \qquad \text{(C.20)}
\end{aligned}
$$

The constant of integration was omitted from eq. (C.20) until the end for simplicity. Another equivalent integral representation can be found by reversing the order of the integration by parts in eq. (C.20) to obtain

$$
I_{in}(t) = -\frac{1}{n+1} \sum_{k=0}^{i} B_{k,n+1}(t) + \overline{c_i}. \qquad \text{(C.21)}
$$

The two formulations are only separated by a constant of integration, which can be seen by equating eqs. (C.20) and (C.21) and applying eq. (C.12). Using the convention in eq. (C.20), the integral relationship can be written in vector notation as

$$
\int \mathbf{B}_n(t) dt = \mathbf{N}_n \cdot \mathbf{B}_{n+1}(t) + \mathbf{c} \qquad \text{(C.22)}
$$

$$
\mathbf{N}_n = \frac{1}{n+1} \begin{bmatrix} 0 & 1 & 1 & \dots & 1 & 1 \\ 0 & 0 & 1 & \dots & 1 & 1 \\ 0 & 0 & 0 & \dots & 1 & 1 \\ \vdots & \vdots & \vdots & \dots & \vdots & \vdots \\ 0 & 0 & 0 & \dots & 1 & 1 \\ 0 & 0 & 0 & \dots & 0 & 1 \end{bmatrix}, \qquad \text{(C.23)}
$$

where $\mathbf{N}_n$ is of size $(n+1) \times (n+2)$. Note that the definite integral over the interval $t \in [0, 1]$ is:

$$\int_0^1 B_{in}(t)dt = \frac{1}{n+1}\sum_{k=i+1}^{n+1}\Big(B_{k,n+1}(1) - B_{k,n+1}(0)\Big) = \frac{1}{n+1}. \tag{C.24}$$

Only the term for $k = n+1$ participates in the summation in eq. (C.24), as all the other polynomials present have roots at both $t = 0$ and $t = 1$. In vector notation the definite integral becomes

$$\int_0^1 \mathbf{B}_n(t)dt = \frac{1}{n+1}\mathbf{1}, \tag{C.25}$$

where $\mathbf{1}$ is a vector of ones of length $n+1$.

The application of the derivative and integral relationships presented here is useful in the context of optimization models when describing time-linking constraints. This issue is discussed in Appendix C.3.

C.1.4 Discretization and continuity

The Bernstein polynomials can also be used to describe piece-wise polynomial functions with smooth transitions over the breakpoints. If the whole time horizon $t \in [0, T^{\text{end}}]$ is split into h time intervals of length δ_h, a piece-wise polynomial function $f(t)$ can be expressed as

$$f(t) = \mathbf{b}_h^{\intercal} \cdot \mathbf{B}_n\left(\frac{t - t_h}{\delta_h}\right), \quad \forall h, \quad t \in [t_h, t_{h+1}]. \tag{C.26}$$

Here, the times $t_h = \sum_{j<h}\delta_j$ are the points where the time intervals are separated. Note that a scaled time parameter is given to the Bernstein polynomials so that they are defined over the interval 0 to 1. The function $f(t)$ is described by a linear combination of Bernstein polynomials for each time interval h with separate coefficients $\mathbf{b}_h$. It is possible to avoid discontinuous jumps over the time interval changes by relating the coefficients $\mathbf{b}_h$ and $\mathbf{b}_{h+1}$. This can be derived by requiring the following continuity limit to hold:

$$
\begin{aligned}
& \lim_{\Delta \to 0} \Big(f\left(t_{h+1} - \Delta\right) - f\left(t_{h+1} + \Delta\right) \Big) = 0 \\
\Rightarrow \quad & \mathbf{b}_h^{\intercal} \cdot \mathbf{B}_n(1) - \mathbf{b}_{h+1}^{\intercal} \cdot \mathbf{B}_n(0) = 0 \\
\Rightarrow \quad & \mathbf{b}_h^{\intercal} \cdot \left[0, 0, \ldots, 1\right]^{\intercal} = \mathbf{b}_{h+1}^{\intercal} \cdot \left[1, 0, \ldots, 0\right]^{\intercal} \\
\Rightarrow \quad & b_{hn} = b_{h+1,0}
\end{aligned} \tag{C.27}
$$

The limit states that the value of $f(t)$ on both sides of the interval breakpoint t_{h+1} must be the same, and that this is achieved if the two coefficients b_{hn} and $b_{h+1,0}$ are equal. A similar limit can be applied to ensure continuous derivatives, which leads to the relationship

$$
b_{hn} - b_{h,n-1} = b_{h+1,1} - b_{h+1,0}. \tag{C.28}
$$

When both eq. (C.27) and eq. (C.28) are enforced, the curve $f(t)$ is continuous and smooth over interval change $h \to h+1$, and is said to be C^1 continuous over the interval shift [78]. If only the continuity constraint eq. (C.27) holds, $f(t)$ is C^0 continuous over the interval change with a potentially discontinuous derivative. Some of the different possible levels of smoothness over interval transitions is shown in Figure C.2.

C.2 Formulating a Simple Continuous-time Optimization Model

Roughly speaking, a continuous-time optimization model is an optimization model where the input time series data and time dependent decision variables are described by continuous functions of time. It is the natural extension of a "normal" discrete-time model with piece-wise constant time series and variables, but some additional steps are required to transform the model into a linear problem which can be solved by standard optimization tools. Converting the original continuous-time model formulation to a tractable optimization program is covered in this section. As a basis, assume that a discrete-time model is defined as below:

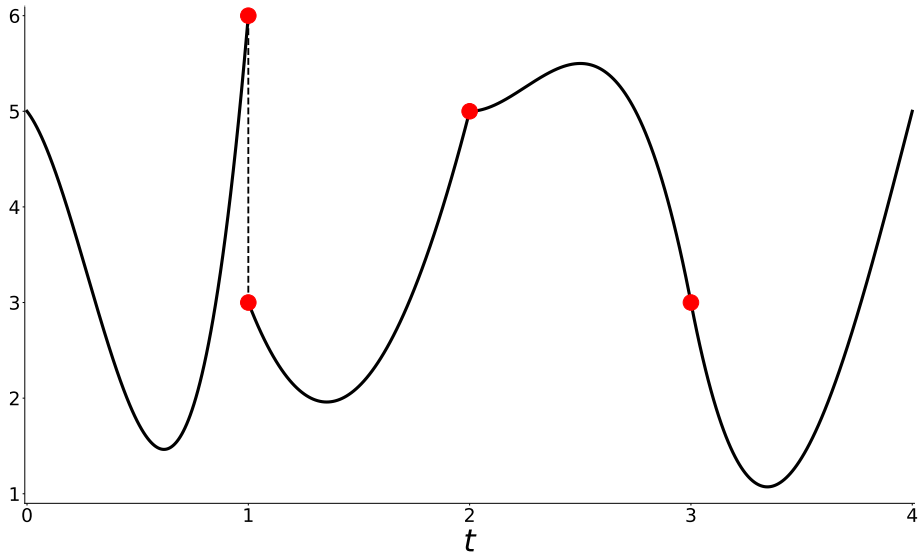

Figure C.2: A piece-wise polynomial function with one polynomial representation in each time interval. The first interval transition at $t = 1$ is discontinuous, while the transitions at $t = 2$ and $t = 3$ are C^0 and C^1 continuous, respectively.

$$\begin{aligned} \min_{x_{hi}} Z^{\text{disc}} &= \sum_{i,h} \delta_h c_{hi} x_{hi} \\ \text{s.t.} \quad & \sum_i a_{ji} x_{hi} = u_{hj} \quad \forall j, h \\ & \sum_i d_{ki} x_{hi} \leq v_{hk} \quad \forall k, h. \end{aligned} \tag{C.29}$$

The optimization horizon is split into intervals h with length δ_h, and the piece-wise constant decision variables are denoted as x_{hi}. The objective function Z^{disc} is the total cost associated with decisions x_{hi} based on the cost rate c_{hi}. Time-dependent input data u_{hj} and v_{hk} are part of equality constraints j and inequality constraints k, respectively. The coefficients a_{ji} and d_{ki} are constants. The model in eq. (C.29) can be converted into a continuous-time model in a few steps, which are covered in the following subsections.

C.2.1 Input data and variables

Some or all of the time dependent input data in the discrete-time model in eq. (C.29) are assumed to be continuous and smooth functions of time instead of piece-wise constant values in reality. The electrical load at each node in a power system is an example of a continuous function of time which is approximated to be a piece-wise constant value in discrete-time models. Using the Bernstein polynomials as a basis for a piece-wise polynomial representation as in eq. (C.26), the input data are transformed:

$$c_{hi} \Rightarrow \mathbf{c}_{hi}^{\mathsf{T}} \cdot \mathbf{B}_n \left(\frac{t - t_h}{\delta_h} \right) \qquad \forall i, h \tag{C.30}$$

$$u_{hj} \Rightarrow \mathbf{u}_{hj}^{\mathsf{T}} \cdot \mathbf{B}_n \left(\frac{t - t_h}{\delta_h} \right) \qquad \forall j, h \tag{C.31}$$

$$v_{hk} \Rightarrow \mathbf{v}_{hk}^{\mathsf{T}} \cdot \mathbf{B}_n \left(\frac{t - t_h}{\delta_h} \right) \qquad \forall k, h \tag{C.32}$$

To ensure smoothness, the equations eq. (C.27) and eq. (C.28) must hold for the input data and should be incorporated into the polynomial fitting tool used to calculate the Bernstein coefficients. Note that it is still possible to have piece-wise constant values without smooth interval transitions by choosing Bernstein polynomials of degree $n = 0$ as a basis for specific input parameters. It is common for the bounds of the inequality constraints $v_k(t)$ to be constant, such as the maximal power generation limit for a generating unit. These special cases are easily handled by using eq. (C.12), as any constant y can be expressed as

$$y = y \cdot 1 = y \sum_{i=0}^{n} B_{i,n}(t) = y \; \mathbf{1}^{\mathsf{T}} \cdot \mathbf{B}_n(t). \tag{C.33}$$

The time-dependent variables must be transformed in the same way:

$$x_{hi} \Rightarrow \mathbf{x}_{hi}^{\mathsf{T}} \cdot \mathbf{B}_n \left(\frac{t - t_h}{\delta_h} \right) \quad \forall i, h. \tag{C.34}$$

Note that the variables in the continuous-time model will be the Bernstein polynomial coefficients $\mathbf{x}_{hi}$, increasing the number of variables by a factor of $n+1$. It is now possible to add eq. (C.27) and eq. (C.28) as constraints to the optimization problem to force $x_i(t)$ to be C^1 continuous curves. Otherwise, there will be a discontinuous jump in $x_i(t)$ at the interval changes.

C.2.2 Equality constraints

After transforming the input data and variables to a piece-wise polynomial definition, the equality constraints of eq. (C.29) become:

$$\sum_i a_{ji}\mathbf{x}_{hi}^\intercal \cdot \mathbf{B}_n\left(\frac{t-t_h}{\delta_h}\right) = \mathbf{u}_{hj}^\intercal \cdot \mathbf{B}_n\left(\frac{t-t_h}{\delta_h}\right) \quad \forall j,h. \tag{C.35}$$

The only way for the equality to hold for all times $t \in [t_h, t_{h+1}]$ is to equate the coefficients of the same Bernstein polynomials on both sides. This results in the new equality constraints

$$\sum_i a_{ji}\mathbf{x}_{hi} = \mathbf{u}_{hj} \quad \forall j,h. \tag{C.36}$$

All the non-linearity of the Bernstein polynomials is removed from the constraints by simply matching coefficients, and the remaining constraints in eq. (C.36) are still entirely linear. However, the number of equality constraints has increased by a factor of $n+1$. It is possible to enforce the equality even if $u_j(t)$ and $x_i(t)$ use different degrees of Bernstein polynomials as a basis, but only if the variables are defined using a higher degree than the input data. The elevation relationship in eq. (C.9) is used in such cases, and the constraints remain linear.

C.2.3 Inequality constraints

To ensure that the inequality constraints in eq. (C.29) remain valid after the transformation to continuous-time, it is necessary to use the convex hull property of the Bernstein polynomials shown in eq. (C.15). Bounding the coefficients of $\mathbf{B}_n(t)$ is sufficient to bound the function as a whole for all times:

$$\begin{aligned}
&\sum_i d_{ki}\mathbf{x}_{hi}^\intercal \cdot \mathbf{B}_n\left(\frac{t-t_h}{\delta_h}\right) \leq \mathbf{v}_{hk}^\intercal \cdot \mathbf{B}_n\left(\frac{t-t_h}{\delta_h}\right) \quad \forall k,h \\
\implies &\left(\sum_i d_{ki}\mathbf{x}_{hi}^\intercal - \mathbf{v}_{hk}^\intercal\right) \cdot \mathbf{B}_n\left(\frac{t-t_h}{\delta_h}\right) \leq 0 \quad \forall k,h \\
\implies &\sum_i d_{ki}\mathbf{x}_{hi} \leq \mathbf{v}_{hk} \quad \forall k,h.
\end{aligned} \tag{C.37}$$

This step is the most important reason for using Bernstein polynomials as a basis,

as it results in linear inequality constraints.

C.2.4 Objective function

The objective function used in eq. (C.29) defines the cost of using each variable for the whole optimization horizon. This is equivalent to an integral in continuous-time:

$$Z^{\text{cont}} = \int_0^{T^{\text{end}}} \sum_i c_i(t) x_i(t) dt. \tag{C.38}$$

There is nothing stopping the polynomial expansions of $c_i(t)$ and $x_i(t)$ beeing of different degrees n_1 and n_2. In the general case, the objective in eq. (C.38) can be calculated to be

$$\begin{aligned}
Z^{\text{cont}} &= \sum_{i,h} \int_{t_h}^{t_{h+1}} \mathbf{c}_{hi}^{\intercal} \cdot \mathbf{B}_{n_1}\left(\frac{t-t_h}{\delta_h}\right) \cdot \mathbf{x}_{hi}^{\intercal} \cdot \mathbf{B}_{n_2}\left(\frac{t-t_h}{\delta_h}\right) dt \\
&= \sum_{i,h} \delta_h \int_0^1 \mathbf{c}_{hi}^{\intercal} \cdot \mathbf{B}_{n_1}(t) \cdot \mathbf{x}_{hi}^{\intercal} \cdot \mathbf{B}_{n_2}(t) dt \\
&= \sum_{i,h} \delta_h \int_0^1 \sum_{p,q} c_{hip} x_{hiq} B_{pn_1}(t) B_{qn_2}(t) dt \\
&= \sum_{i,h} \delta_h \int_0^1 \sum_{p,q} c_{hip} x_{hiq} \frac{\binom{n_1}{p}\binom{n_2}{q}}{\binom{n_1+n_2}{p+q}} B_{p+q,n_1+n_2}(t) dt \\
&= \frac{1}{n_1+n_2+1} \sum_{i,h,p,q} \delta_h c_{hip} x_{hiq} \frac{\binom{n_1}{p}\binom{n_2}{q}}{\binom{n_1+n_2}{p+q}}.
\end{aligned} \tag{C.39}$$

The definite integral property in eq. (C.24) was used in the above expression, in addition to the fact that the product of two Bernstein polynomials can be expressed as a Bernstein polynomial of a higher degree:

$$B_{in} \cdot B_{jm} = \binom{n}{i} t^i (1-t)^{n-i} \cdot \binom{m}{j} t^j (1-t)^{m-j}$$
$$= \binom{n}{i}\binom{m}{j} t^{i+j}(1-t)^{n+m-(i+j)} = \frac{\binom{n}{i}\binom{m}{j}}{\binom{n+m}{i+j}} B_{i+j,n+m} \tag{C.40}$$

Even when the cost function and variables are described by Bernstein polynomials of different degrees, the integral reduces down to a linear sum over the variables. The cost $c_i(t)$ is often constant over time, which means that $n_1 = 0$ and $c_{hip} = c_i$ in the above calculation. This greatly simplifies the objective function to

$$Z^{\text{cont}} = \frac{1}{n+1} \sum_{i,h,q} \delta_h c_i x_{hiq} = \frac{1}{n+1} \sum_{i,h} \delta_h c_i \mathbf{x}_{hi}^\intercal \cdot \mathbf{1}. \tag{C.41}$$

Note that the normal discrete-time objective function of eq. (C.29) is recovered if $n_1 = n_2 = 0$. The objective function was in this instance linear in $x_i(t)$, but quadratic cost functions are quite common in many types of optimization models. This poses a challenge when using Bernstein polynomials, as bi-linear cross terms appear in the objective function from integrals of the form:

$$\int_0^1 x(t)^2 dt = \int_0^1 \sum_{p,q} x_p x_q B_{pn}(t) B_{qn}(t) dt = \frac{1}{2n+1} \sum_{p,q} x_p x_q \frac{\binom{n}{p}\binom{n}{q}}{\binom{2n}{p+q}}. \tag{C.42}$$

To avoid the non-convex bi-linear terms, a transformation from the Bernstein polynomials to an orthogonal basis is necessary. This idea is described in [91] with the use of the shifted Legendre polynomials. The orthogonality of the Legendre polynomials means that the coefficient of the bi-linear terms of the transformed variables will be zero, and a purely quadratic objective function remains.

C.2.5 Analogous continuous-time model

The continuous-time model which is analogous to eq. (C.29) is found by combining the results of Appendices C.2.1 to C.2.4. In addition, C^1 continuity is enforced on the decision variables by adding constraints eqs. (C.27) and (C.28) to $\mathbf{x}_{hi}$. Assuming that $c_i(t)$ is constant over time:

$$\min_{\mathbf{x}_{hi}} Z^{\text{cont}} = \frac{1}{n+1} \sum_{i,h} \delta_h c_i \mathbf{x}_{hi}^{\intercal} \cdot \mathbf{1} \tag{C.43}$$

$$\text{s.t.} \quad \sum_i a_{ji} \mathbf{x}_{hi} = \mathbf{u}_{hj} \quad \forall j, h$$

$$\sum_i d_{ki} \mathbf{x}_{hi} \leq \mathbf{v}_{hk} \quad \forall k, h$$

$$x_{hin} = x_{h+1,i0} \quad \forall i, h \neq T$$

$$x_{hin} - x_{hi,n-1} = x_{h+1,i1} - x_{h+1,i0} \quad \forall i, h \neq T$$

The simple model in eq. (C.29) does not include any time-linking constraints and can be solved independently for each time interval. The continuity constraints added to eq. (C.43) do not only break the model's separability in time, they also couple variables related to different Bernstein polynomials. Without these constraints, the continuous-time model could be separated and solved for each time interval and Bernstein polynomial coefficient number, and would be equivalent in complexity to solving $n + 1$ separate versions of eq. (C.29). This shows that the continuity constraints fundamentally change the model structure compared to a discrete-time model, as the other constraints remain equal in shape and form. The imposed continuity on the variables $x_i(t)$ also require continuity of the functions $u_j(t)$ due to the equality constraints.

C.3 Complicated Constraints

It might seem straightforward to convert a discrete-time model to a continuous-time model by following the procedures in Appendix C.2. However, there are several complicated types of constraints that need special attention. Time-linking constraints must be carefully considered as they often stem from differential equations. Binary variables used to model non-convexities in discrete-time models can also require a different implementation in continuous-time to avoid breaking continuity. The following sections focus on the most common time-linking and binary constraints found in power system operation and planning models, and are based on the models cited in Section 2.3.1 and Paper II, III, and IV.

C.3.1 Time-linking constraints due to differential equations

Differential equations are abundant in nature, and are therefore also found as constraints in optimization models trying to describe physical processes in the real world. The differential equations of special interest in continuous-time opti-

mization models deal with derivatives with respect to time. Such derivatives must be approximated in discrete-time models but can easily be expressed analytically in the continuous-time framework. The simplest example of a constraint dealing with time derivatives from the realm of power system operation and planning is the ramping restriction often imposed on slow-ramping thermal units. The ramping is the rate of change of the power $p(t)$ generated by a unit. To keep the ramping within safe or realistic limits $R^{\uparrow/\downarrow}$ in the optimization model, inequality constraints of the following form should be added:

$$-R^{\downarrow} \leq \frac{dp(t)}{dt} \leq R^{\uparrow}. \tag{C.44}$$

In discrete-time models, the derivative is approximated as the change in production between two neighbouring time intervals h and $h+1$ of length δ_h:

$$-R^{\downarrow} \leq \frac{p_{h+1} - p_h}{\delta_h} \leq R^{\uparrow} \quad \forall h. \tag{C.45}$$

By applying the relationship between the Bernstein polynomials and their derivatives from eq. (C.17), the derivative of $p(t) = \mathbf{p}_h^{\intercal} \cdot \mathbf{B}_n \left(\frac{t-t_h}{\delta_h}\right)$ can be bounded directly:

$$-R^{\downarrow}\mathbf{1}^{\intercal} \leq \frac{1}{\delta_h}\mathbf{p}_h^{\intercal} \cdot \mathbf{K}_n \leq R^{\uparrow}\mathbf{1}^{\intercal} \quad \forall h. \tag{C.46}$$

Note the factor of $1/\delta_h$ appearing from the differentiation of $\mathbf{B}_n \left(\frac{t-t_h}{\delta_h}\right)$. This is a more accurate and restrictive formulation of the ramping constraints compared to eq. (C.45), as the derivative is bounded for all points in time. See Appendix C.3.3 for a more detailed and careful ramping constraint formulation.

The energy content of an energy storage device, such as a hydropower reservoir, is another example of a differential equation needed as a constraint in an optimization model. The rate of change of the volume $v(t)$ in a reservoir is the net inflow of water $q^{net}(t)$:

$$\frac{dv(t)}{dt} = q^{net}(t). \tag{C.47}$$

Similarly to the approximation in eq. (C.45), the discrete-time constraint reads:

$$v_{h+1} = v_h + \delta_h q_h^{net}, \quad \forall h, \tag{C.48}$$

where v_h is the volume at the start of time interval h. An initial condition is also required here, which is the start volume in the reservoir. In a continuous-time model, it is clear that $v(t)$ must be expressed by Bernstein polynomials of one degree higher than the decision variables $q^{net}(t)$. It is possible to use eq. (C.17) to formulate the continuous-time constraint as in eq. (C.46), but a more intuitive formulation is reached by integrating both sides of the equation from the start of an interval h. Using eq. (C.22) and eq. (C.25) results in the following formula:

$$
\begin{aligned}
& \int_{t_h}^{t} \frac{dv(u)}{du} du = \int_{t_h}^{t} q^{net}(u) du. \\
\implies \quad & v(t) - v(t_h) = \int_{t_h}^{t} (\mathbf{q}_h^{net})^{\intercal} \cdot \mathbf{B}_n\Big(\frac{u - t_h}{\delta_h}\Big) du \\
\implies \quad & v(t) - v(t_h) = \delta_h (\mathbf{q}_h^{net})^{\intercal} \cdot \int_0^{\frac{t-t_h}{\delta_h}} \mathbf{B}_n(x) dx \\
\implies \quad & v(t) - v(t_h) = \delta_h (\mathbf{q}_h^{net})^{\intercal} \cdot \mathbf{N}_n \cdot \left(\mathbf{B}_{n+1}\Big(\frac{t - t_h}{\delta_h}\Big) - \mathbf{B}_{n+1}(0) \right). \qquad \text{(C.49)}
\end{aligned}
$$

The volume $v(t_h)$ is the same as v_h used in eq. (C.48). Due to the definition of $\mathbf{N}_n$ in eq. (C.23) and the fact that $\mathbf{B}_{n+1}(0) = \big[1, 0, \ldots, 0\big]^{\intercal}$, the last term of eq. (C.49) vanishes: $\mathbf{N}_n \cdot \mathbf{B}_{n+1}(0) = \mathbf{0}$. The evolution of the volume within the time interval h is therefore:

$$
v(t) = \left(v_h \mathbf{1} + \delta_h \mathbf{N}_n^{\intercal} \cdot \mathbf{q}_h^{net} \right)^{\intercal} \cdot \mathbf{B}_{n+1}\Big(\frac{t - t_h}{\delta_h}\Big), \qquad t_h \le t \le t_{h+1}, \quad \forall h. \quad \text{(C.50)}
$$

The start volumes of each interval v_h are found by integrating over the whole time interval and using eq. (C.24):

$$
v_{h+1} = v_h + \frac{1}{n+1} \delta_h \mathbf{1}^{\intercal} \cdot \mathbf{q}_h^{net}, \quad \forall h. \qquad \text{(C.51)}
$$

Bounds on the volume can now be applied to eq. (C.50) by using the convex hull property, while eq. (C.51) calculates the start volumes of each interval. In addition to an initial volume condition, these relations determine the volume content progression of the reservoir.

C.3.2 Unit commitment constraints

The most typical constraints involving binary variables in a power system operation model are the unit commitment constraints. These constraints replicate the fact that most generators have a minimum production level for safe and efficient operation, and that running the unit between zero and the minimum production level should not occur for prolonged periods of time. Binary variables to signify if the unit is "on" or "off" are used for each time interval to force each generator to either produce above the minimum production level or not produce at all. In a discrete-time model, the constraints may look like:

$$P^{min}u_h \leq p_h \leq P^{max}u_h \qquad \forall h \qquad \text{(C.52)}$$

$$su_h - sd_h = u_{h+1} - u_h \qquad \forall h \neq T \qquad \text{(C.53)}$$

$$u_h, su_h, sd_h \in \{0, 1\} \qquad \forall h \qquad \text{(C.54)}$$

The binary variable u_h is used to constrain the upper and lower bounds of the production variable p_h, while the number of startups and shutdowns are counted by the binary variables su_h and sd_h, respectively. Extra care must be taken to model the behavior of starting and stopping the generator when implementing these constraints in a continuous-time model. If continuity constraints eqs. (C.27) and (C.28) are applied to the production variable $p(t)$, it will be impossible to start or stop the generator if eq. (C.52) is directly translated as

$$P^{min}u_h\mathbf{1} \leq \mathbf{p}_h \leq P^{max}u_h\mathbf{1}. \qquad \text{(C.55)}$$

Since the continuity constraints couple some of the components of $\mathbf{p}_h$ to $\mathbf{p}_{h+1}$, the above implementation will force the commitment variables u_h and u_{h+1} to always be equal. This results in the generator either being on or off for the entire optimization horizon. The solution to the problem is to allow a smooth and continuous startup or shutdown procedure, which requires modifications of the upper and lower bounds of eq. (C.55). Note that the naive formulation in eq. (C.55) is perfectly acceptable if the production variable is not required to be continuous, which is the case in the hydropower formulation used in Papers II, III, and IV.

In a discrete-time model, the binary variable u_h is interpreted as the on/off status of the unit for the whole time interval h. It is useful to think of these variables slightly differently in continuous-time models. The commitment variable now signifies the instantaneous commitment status of the unit at the start of interval h, which can be different from the commitment status at the end of the interval, captured by u_{h+1}. Note that this requires an additional binary variable for the

commitment status at the end of the last interval, u_{T+1}, to be consistent. The unit commitment constraints can now be formulated based on the implications of the continuity constraints and some basic requirements for the upper and lower boundaries for the production variable. Table C.1 shows the desired bounds on the production variable given the commitment status at the start and end of the time interval. If the unit is off at the start and the end of the interval, the unit should be off and not produce anything for the whole interval. In the opposite case where the unit is on at both interval edges, the unit should produce in the legal domain between the minimum and maximum production. Whenever the commitment status is different at the start and end of the time interval, $p(t)$ is allowed to also be in the forbidden region between 0 and P^{min} to make a smooth startup/shutdown possible.

Table C.1: Desired bounds on the production variable $p(t)$ in time interval h given the commitment status of the unit at the start and end of the interval.

Value of u_{h+1} \ Value of u_h	0	1
0	$p(t) = 0$	$0 \leq p(t) \leq P^{max}$
1	$0 \leq p(t) \leq P^{max}$	$P^{min} \leq p(t) \leq P^{max}$

The C^0 continuity constraint eq. (C.27) applied to $p(t)$ reads

$$p_{h,n} = p_{h+1,0} \qquad h \neq T, \tag{C.56}$$

which means that the production at the end of interval h and at the start of interval $h+1$ is the same. The following constraints for $p_{h,0}$ and $p_{h,n}$ will be in line with the requirements in Table C.1 without interfering with continuity:

$$P^{min} u_h \leq p_{h,0} \leq P^{max} u_h \tag{C.57}$$
$$P^{min} u_{h+1} \leq p_{h,n} \leq P^{max} u_{h+1}. \tag{C.58}$$

Similarly, the C^1 continuity constraint eq. (C.28) for $p(t)$ gives rise to the unit commitment constraints

$$P^{min} u_h \leq p_{h,1} \leq P^{max} u_h \tag{C.59}$$
$$P^{min} u_{h+1} \leq p_{h,n-1} \leq P^{max} u_{h+1}. \tag{C.60}$$

The clue to formulating the constraints in eqs. (C.57) to (C.60) is to ensure that the variables related by the continuity constraints are bounded by the same

binary variable. Note that in the common case of using Bernstein polynomials of degree $n = 3$, eqs. (C.57) to (C.60) bound all four vector components of $p(t)$:

$$P^{min}\mathbf{u}_h \leq \mathbf{p}_h \leq P^{max}\mathbf{u}_h \tag{C.61}$$

$$\mathbf{u}_h = \left[u_h, u_h, u_{h+1}, u_{h+1}\right]^\intercal. \tag{C.62}$$

For the general case where $n \geq 4$, the upper and lower bounds for the remaining vector components $p_{h,2}$ to $p_{h,n-2}$ can be formulated as a linear combination of u_h, u_{h+1}, su_h and sd_h. There are several possible formulations that satisfy Table C.1 to different levels of strictness. The least constraining bounds can be formulated as:

$$P^{min}(u_h - sd_h) \leq p_{h,i} \leq P^{max}(u_h + su_h), \qquad i \in \{2, \ldots, n-2\}. \tag{C.63}$$

The use of the startup and shutdown variables allows the middle vector components, which are not implicated in the continuity constraints, to satisfy the description in Table C.1. A stricter formulation would be to extend eq. (C.62) to the appropriate dimension by letting the first half[2] of the vector components be constrained by u_h and the second half by u_{h+1}. Such a formulation leaves the generator with less freedom in how to start up and shut down as it narrows the upper and lower bound trajectories, as shown in Figure C.3. However, the tighter lower bound also pushes the generator to spend less time in the forbidden region between 0 and P^{min}. Both formulations are valid in terms of the continuity constraints as long as eqs. (C.57) to (C.60) are in place, and so choosing the relaxed upper bound and tight lower bound formulations is a possibility. This topic is not explored in the literature since Bernstein polynomials of degree three are commonly used. The unit commitment constraint formulation in continuous-time models is concluded by defining the startup and shutdown variables in the same way as in eq. (C.53).

C.3.3 Tight ramping constraint formulation

The discrete-time and continuous-time ramping constraints formulated in Appendix C.3.1 are potentially problematic, as they do not consider the possibility of $R^{\uparrow/\downarrow}$ being so low that a startup or shutdown is impossible. The formulation is also loose in the sense that it is unnecessary when the unit is off. Therefore, it is

[2]In cases where the degree of the Bernstein polynomials used is an even number, the very center component can be constrained by $\frac{1}{2}(u_h + u_{h+1})$.

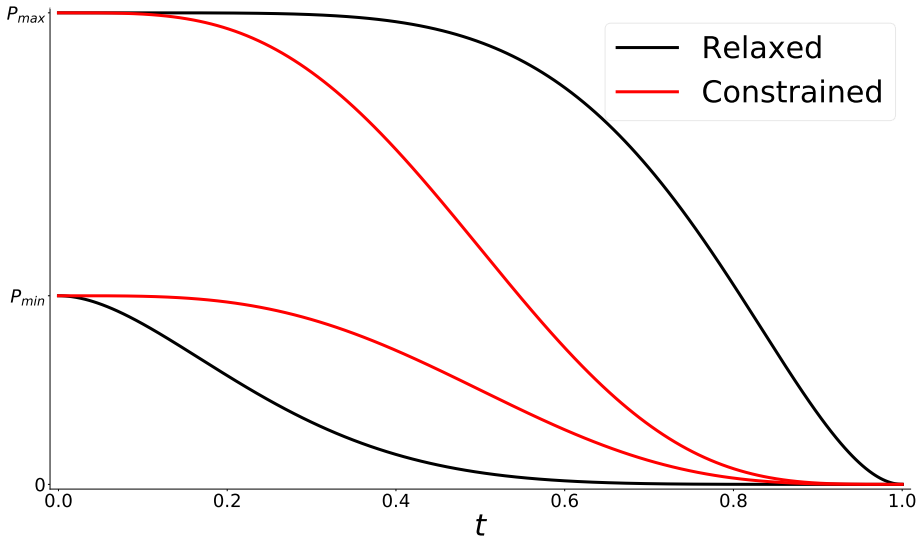

Figure C.3: Two possible choices for the upper and lower generation bounds in a continuous-time model during a shutdown. Bernstein polynomials of degree seven are used in the figure.

common to formulate the ramping constraints by using the binary commitment variables discussed in the previous section to tighten the ramping bounds when the unit is off and relax them when the unit is starting/stopping.

Consider a very slow ramping unit attempting to start up, meaning that $u_h = 0$ and $u_{h+1} = 1$, that follows the generation boundaries set by eqs. (C.57) to (C.60) and eq. (C.63). The ramping constraints in eq. (C.46) can be written in component form as:

$$-R^{\downarrow} \leq \frac{n}{\delta_h}\left(p_{h,i+1} - p_{h,i}\right) \leq R^{\uparrow} \quad i \in \{0, 1, \ldots, n-1\}. \tag{C.64}$$

According to eqs. (C.57) to (C.60), the two first vector components must be zero while the two last must be at least P^{min}. Since $p_{h,1} = 0$, the maximal value for $p_{h,2}$ within the ramping trajectory would be $p_{h,2} = \frac{1}{n}\delta_h R^{\uparrow}$. This logic can be repeatedly applied to the other vector components to find the maximal value $p_{h,n-1} = \frac{n-2}{n}\delta_h R^{\uparrow}$. If $R^{\uparrow}$ is sufficiently small it is possible for the ramping constraints to be in conflict with the unit commitment constraints for $p_{h,n-1}$ during a startup. The break-point is

$$R_h^0 = \frac{n}{n-2}\frac{P^{min}}{\delta_h}, \tag{C.65}$$

where $R^{\uparrow} < R_h^0$ makes it impossible for the unit to start up. The same value is found for the minimal downward ramping capability during a shutdown. Note that eq. (C.65) is only valid for $n \geq 3$, and the simple cases of $n \leq 2$ are left out here. In the case of $R^{\uparrow/\downarrow} < R_h^0$, the ramping constraints must be relaxed to allow startups/shutdowns. A simple way to achieve this is to uniformly give additional upward/downward ramping capability to the unit if a startup/shutdown is occurring:

$$-R^{\downarrow}\left(1+\gamma_h^{\downarrow}sd_h\right) \leq n\,\frac{p_{h,i+1}-p_{h,i}}{\delta_h} \leq R^{\uparrow}\left(1+\gamma_h^{\uparrow}su_h\right). \tag{C.66}$$

Note that only the middle ramping constraints for $i \in \{2,\ldots,n-2\}$ need to be relaxed in this way. The additional ramping capabilities must satisfy

$$\gamma_h^{\uparrow/\downarrow} \geq \frac{R_h^0}{R^{\uparrow/\downarrow}} - 1. \tag{C.67}$$

It is also possible to tighten up the ramping constraints by incorporating the binary commitment variables to change the ramping capability depending on the commitment status. In particular, the upward and downward ramping boundaries can be set to zero when the unit is off. This is fairly simple for the first and last ramping constraints, as the connected production variables are constrained by the same binary variable in the unit commitment constraints:

$$-R^{\downarrow}u_h \leq n\,\frac{p_{h,1}-p_{h,0}}{\delta_h} \leq R^{\uparrow}u_h \tag{C.68}$$

$$-R^{\downarrow}u_{h+1} \leq n\,\frac{p_{h,n}-p_{h,n-1}}{\delta_h} \leq R^{\uparrow}u_{h+1}. \tag{C.69}$$

The middle vector components of $\mathbf{p}_h$ are forced to be zero in eq. (C.63) by the sum $u_h + su_h$. The following ramping constraints are then valid for $i = \{2,\ldots,n-2\}$

$$n\,\frac{p_{h,i+1}-p_{h,i}}{\delta_h} \leq R^{\uparrow}\left(u_h + (1+\gamma_h^{\uparrow})su_h\right) \tag{C.70}$$

$$n\,\frac{p_{h,i+1}-p_{h,i}}{\delta_h} \geq -R^{\downarrow}\left(u_{h+1} + (1+\gamma_h^{\downarrow})sd_h\right). \tag{C.71}$$

The ramping constraint formulation in eqs. (C.68) to (C.71) tightens the upper and lower ramping bounds to zero when the unit is off for the whole period ($u_h = u_{h+1} = 0$), and relaxes the constraints to allow slow ramping units to start up and shut down. An example of the unit commitment and ramping constraints for a slow-ramping unit is given in Figure C.4.

(a) Production

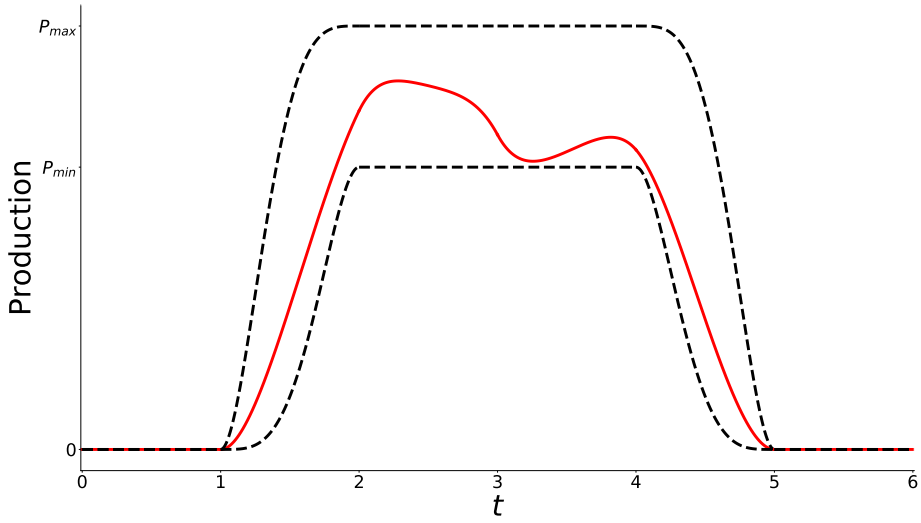

(b) Ramping

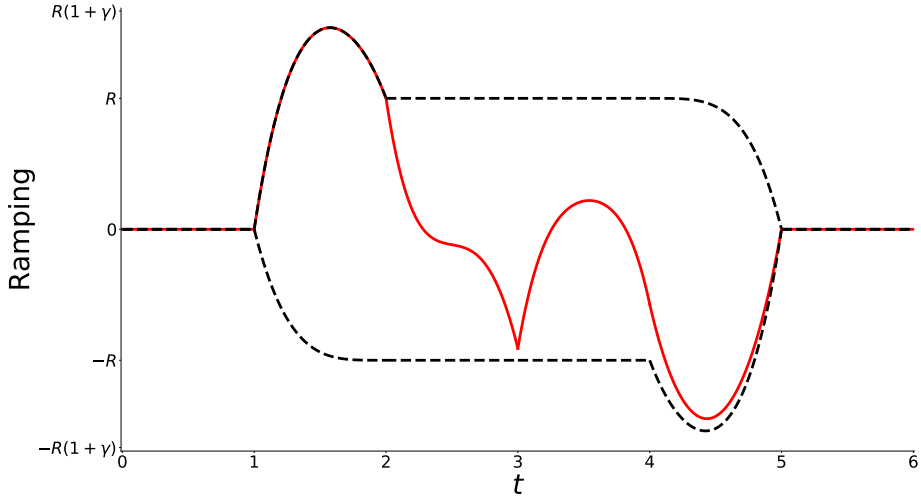

Figure C.4: The top figure shows the production schedule and bounds for a unit starting up and shutting back down. The bottom figure shows the derivative of the production with ramping constraints according to eqs. (C.68) to (C.71).

ISBN 978-82-471-9645-8 (printed ver.)
ISBN 978-82-471-9760-8 (electronic ver.)
ISSN 1503-8181 (printed ver.)
ISSN 2703-8084 (online ver.)

NTNU
Norwegian University of
Science and Technology